Conceptual Design Report

B*ERL*inPro

2012

Editors: Bettina Kuske, Nadine Paulick,
Andreas Jankowiak, Jens Knobloch

Disclaimer:

Written for an evolving project, this report naturally can only reflect a momentary status of the workflow, here the status as of January 2012. Improved solutions, new boundary conditions and technical limitations are continuously being incorporated in the layout. Therefore, little emphasis was placed on the typesetting of this document. The document will evolve to a Detailed Design Report that describes the final technical solutions and the reasoning behind the decisions taken.

Authors:

Michael Abo-Bakr, Wolfgang Anders, Roman Barday, Alexey Bondarenko, Klaus Bürkmann-Gehrlein, Volker Dürr, Stefan Heßler, Andreas Jankowiak, Thorsten Kamps, Jens Knobloch, Oliver Kugeler, Bettina Kuske, Peter Kuske, Aleksandr Matveenko, Atoosa Meseck, Gerd Meyer, Roland Müller, Axel Neumann, Klaus Ott, Yuriy Petenev, Dirk Pflückhahn, Torsten Quast, Joachim Rahn, Susanne Schubert

Table of Contents

List of Figures

List of Tables

1. Project overview

1.1. Next-generation particle accelerators

The application of modern accelerators is extremely multifaceted, ranging from high-energy physics to synchrotron light sources for X-ray production to their use for medical treatment [1, 2]. Today we look back on over 80 years of highly innovative accelerator R&D which continuous unabated, focusing on improving accelerator performance and developing novel ideas to meet future user demands.

While it is impossible to provide an all-encompassing parameter set applicable to all these wide-ranging applications, it is fair to say that there is a trend towards the acceleration of continuous-wave (CW) high-average-current, short-pulse (sub ps) beams of exceptional brilliance and low energy spread. Electron coolers for high energy hadron colliders, electron-hadron colliders, Compton gamma-ray sources, as well as X-ray synchrotron light sources continue to push the already exceedingly challenging beam parameters to new limits. Storage-ring based facilities now operate near to their theoretical limit and only little further improvements may be expected. Their limitation stems from the fact that the beam properties (the six dimensional phase space of transverse emittance, length and energy) are determined by an equilibrium condition dictated by fundamental physics. Many proposed accelerator applications depend on parameters more than an order-of-magnitude beyond the presently achieved and the quest to adjust the parameters for specific application is growing.

To circumvent the limitations of storage rings one turns to linear accelerators (linacs), whose beam properties, in theory, are determined by the electron source and adiabatic damping during the acceleration process. Furthermore, since the beam is in a non-equilibrium state its distribution in phase space can be rearranged using a variety of manipulation techniques. Individual properties, such as bunch length or energy spread, can be adjusted at the expense of other parameters to suit the specific accelerator application. Linear accelerators thus provide a great deal of flexibility and adjustability (and hence adaptability) which largely is lacking with storage rings. At the same time, this concept places a heavy burden on the electron source, which must deliver a beam of extraordinarily high phase space density and, for many future applications, at high average current.

The last requirement also points to one of the main challenges of linacs. Since linacs are designed as single-pass devices, disposal of the beam at high energy requires the average beam current to be low in order to limit the power required to operate them and safely dump the beam. For many applications (e.g., high-energy electron coolers, high-flux X-ray light sources) the average current is therefore too low to merit the use of single-pass linacs.

1.2. Energy Recovery Linac for high-current, high-brilliance operation

Energy recovery linacs (ERLs) hold the promise to circumvent the current limitation of conventional linacs. First proposed by Maury Tigner in 1965 [], the scheme involves re-injecting the spent beam into the linac a second time, but phase shifted by 180°. The

beam is now decelerated and its energy is recouped by the cavities, where it remains available for acceleration of a fresh beam. Subsequently the low energy beam is dumped safely. An ERL thus does not store beam, but rather its energy and therefore combines the efficiency and high-current advantage of storage rings with the superb beam quality and flexibility of a linac. Given their extremely low RF losses, superconducting RF (SRF) cavities operating CW are the enabling technology that allows ERLs to attain a very high efficiency and, due to the cavities' low impedance, accelerate high currents.

As stated above, the concept of ERLs is not new but significant technological challenges have limited their construction so far. More recently, IR facilities (such as the Jefferson Laboratory ERL [4], JAERI ERL [5] and ALICE [6]) have demonstrated experimentally the soundness of the underlying concept. This has sparked many ideas for multi-user X-ray ERLs world-wide, including the Cornell ERL [7], KEK ERL [8], gamma-ray sources [9], as well as electron coolers [10] and electron-hadron colliders [11, 12]. However, all these concepts are early into their development as they require beam parameters that are one to two orders of magnitude beyond those achieved with state-of-the-art ERLs. Prior to the realization of these new projects, a number of vital technological and accelerator-physics advances are required.

1.3. Technology and accelerator physics challenges

Although in principle ERLs can employ pulsed, normal-conducting accelerator technology, energy-efficiency considerations will always dictate that X-ray ERL facilities must be based on continuous-wave (CW) superconducting RF (SRF) technology. ERLs push the accelerator physics and technology on numerous frontiers because of the required extreme beam quality, high current, and CW operation. The demands placed on the electron source, the SRF linac & beam transport, the cryogenics, and the diagnostics are severe. Fortunately, much effort has been invested in developing SRF technology for non-ERL machines such as CEBAF and, more recently, FLASH and the European XFEL. The latter projects have helped to advance electron-source development, albeit for high-charge, low rep-rate operation. Nevertheless these projects have demonstrated the soundness of the overall technology and its *potential* for ERL applications. What remains are numerous ERL-specific challenges and the development of the appropriate expertise. Among the primary issues are:

- Reliable and stable generation of a low emittance (longitudinal and transverse) 100-mA-class CW beam over many hours of continuous operation
- Preservation of the low emittance throughout the ERL, in particular in the injection path from the electron source through to the main linac
- Stable recirculation of the beam without beam breakup
- Operation of SRF cavities at high average currents
- Efficient energy recovery of the beam
- Efficient operation of CW SRF systems to minimize the refrigeration and RF power demands
- Beam manipulation to provide flexible beam parameters for various applications

- Reduction of electron beam loss to well below the 10^{-5} level, radiation protection and demonstration that radiation background/activation can be reliably maintained at levels commensurate with user facilities

To find solutions to these and other challenges, HZB has therefore proposed an ERL-dedicated R&D program designed to pool the existing experience with SRF and linac technology within the Helmholtz Association and internationally. Its goal is to address both the hardware and theoretical aspects of ERLs and to ready the concept for a broad range of applications.

1.4. Resolving the challenges: B*ERL*inPro

Some of the R&D areas can be treated separately. But the majority is intertwined and ultimately can only be analyzed and tested in an integrated demonstration facility. To this end, HZB proposed to build a 100-MeV high-current ERL test facility (B*ERL*inPro) that can put all subsystems relevant to large-scale ERLs to the test and enable the rigorous comparison of theory with the real world. Submitted to the Helmholtz Association in 2008, the project proposal received final approval in October 2010. Following approval and formation of the project team a more detailed layout was then developed, which enabled detailed costing and scheduling of the facility construction. At that point it became apparent that a 100-MeV ERL could not be realized within the fiscal constraints so that a descope to 50 MeV was presented to the newly installed international Machine Advisory Committee (MAC). While this change reduces the number of SRF systems and the required costly radiation shielding, the beam parameters (current, emittance, bunch length) were left unaltered. Hence the scope and relevance of the physics and technology development remains fully intact. The MAC endorsed this approach, which then was used as the baseline for the subsequent development of the conceptual design report (CDR) presented here.

B*ERL*inPro's layout as a single-pass ERL is shown in Figure 1. Its 6-MeV injection line consists of a 1.3 GHz SRF photo injector and a three cavity booster section. The beam is merged into the main linac via a dog-leg merger where it is accelerated by three 7-cell SRF cavities to 50 MeV. Following recirculation via the straight section reserved for future experiments, the decelerated beam is dumped in a 600-kW beam dump at 6-MeV.

Since B*ERL*inPro is a "generic" demonstration facility for accelerator R&D rather than being designed as a specific user facility, its parameter set should be considered flexible. Given HZB's background in the operation of synchrotron light sources, a set suitable for future X-ray light-source applications, as listed in Table 1, has been adopted as the "standard mode." However, the optics design is intentionally flexible to allow future exploration of a wide range of other parameters, including short and low energy spread bunches. Room is also provided in the return arc to install future experiments or insertion devices that can demonstrate the potential of ERLs for various user applications.

The study and minimization of beam loss will be one of the key aspects of the B*ERL*inPro measurement program. Radiation protection must be designed to accommodate a worst-case continuous beam loss scenario. For a cost-effective solution, the accelerator will be housed in a subterranean building with all auxiliary systems placed in a separate, above ground, building. The layout of the accelerator hall provides sufficient room for future

upgrades and could also be extended (e.g. to two-turn recirculation), provided additional funding is secured. Its study can provide valuable results for future large-scale facilities.

Given the long lead time in developing a high-current photo injector, first experiments with an all-superconducting system (SRF cavity, superconducting cathode, superconducting solenoid) commenced in 2009. The focus continuous to be on the injector and a new version that includes a normal conducting cathode capable of generating high currents will be constructed in 2013. In the meantime the ERL optics layout, as presented in this CDR, has been developed so that an application for a building permit ("Errichtungsgenehmigung") will be submitted shortly to German authorities. The goal is to have the B*ERL*inPro building ready for occupancy in 2014. A staged installation of B*ERL*inPro will follow, the primary focus being on accelerating a high (100 mA) current beam by 2016, albeit only up to 6 MeV. Following this, the main linac and recirculation will be installed so that full energy recovery is expected by 2018.

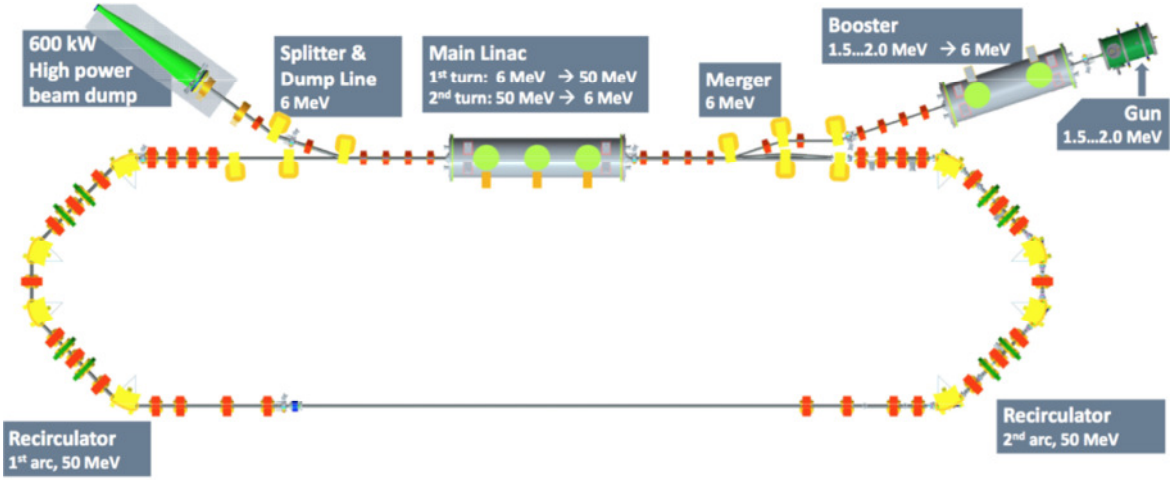

Figure 1: Schematic of B*ERL*inPro

Parameter	Value	Unit
Beam energy	50	MeV
Beam current @ 1.3 GHz	100	mA
Bunch charge	77	pC
Bunch length	< 2	ps
Relative energy spread	0.5%	-
Emittance	< 1	mm mrad
Beam loss	$< 10^{-5}$	-

Table 1: Parameters adopted for the standard mode of B*ERL*inPro

1.5. References

[1] S. Kullander, Accelerators and Nobel Laureates, *Nobelprize.org*, http://nobelprize.org/nobel_prizes/physics/articles/kullander/

[2] R.-H. Menk et al., Proceedings of the 4th International Workshop on Medical Applications of Synchrotron Radiation, Trieste, 2004, *Nuclear Instruments and Methods in Physics Research A*, Volume 548, Issues 1 and 2.

[3] M. Tigner, A Possible Apparatus for Electron Clashing-Beam Experiments, Il Nuovo Cimento Vol. 37, No. 3 (1965).

[4] G. Neil et al., The JLAB High-Power ERL Light Source, *Nuclear Instruments and Methods in Physics Research A*, Volume 557, Issue 1, p. 9-15.

[5] R. Hajima, First Demonstration of Energy-Recovery Operation in the JAERI Superconducting Linac for a High-Power Free-Electron Laser, *Nuclear Instruments and Methods in Physics Research A*, Volume 507, Issues 1–2, 11 July 2003, Pages 115–119.

[6] S. Smith, The Status of the Daresbury Energy Recovery LINAC Prototype, *Proceedings of ERL 2007*, p. 6.

[7] D. Bilderback et al., Energy Recovery LINAC (ERL) Coherent Hard X-ray Sources, *New Journal of Physics* **12** (2010) 035011 .

[8] S. Sakanaka et al, Recent Progress in the Energy Recovery LINAC Project in Japan, *Proc. IPAC 2010*, p. 2338.

[9] R. Hajima et al., Generation and Application of Laser Compton γ-Rays at the Compact ERL, *Proc. 8th Annual Meeting of Particle Accelerator Society of Japan* (2011).

[10] I. Ben-Zvi, The ERL High-Energy Cooler for RHIC, *Proc. EPAC 2006*, p. 940.

[11] V. Litvinenko et al., ERL Based Electron-Ion Collider eRHIC, *Proc. PAC 2005*, p. 2768.

[12] S. A. Bogacz et al., LHeC ERL Design and Beam-Dynamics Issues, *Proc. IPAC 2011*, p. 1120.

2. Subprojects of B*ERL*inPRO

2.1. Building / Infrastructure

B*ERL*inPro will be erected close to the BESSY II storage ring, between the assembly hall and the office building 14.51. Two buildings are planned to host the accelerator and all the necessary technical equipment, as shown in Figure 2.

The dominant requirements and boundary conditions for the basic layout and the location of the B*ERL*inPro buildings are:

- A hall of 13 m x 33 m with a free height of 3 m to host the machine
- 1200 m² to host equipment and laboratory space
- Close vicinity of the cryogenic system and the machine to keep the extremely expensive cryogenic lines as short as possible
- Radiation protection of the cryogenic systems
- Enough shielding to secure the annual dose limit of 1 mSv/a at any accessible uncontrolled area
- Compatibility with environmental contamination requirements (activation of ground water and air)
- Compatibility of the layout with certain future machine developments
- A construction level less than 4m below ground to avoid an environmental impact analysis report

The concept most compliable with these criteria and most cost effective has been identified as

- a subterranean hall to host the machine in order to comply more easily with the radiation shielding requirements (Figure 3)
- an adjacent “gallery” to place the cryogenic cold box, the RF klystrons and the laser systems in close vicinity to the machine (Figure 3)
- a simple industrial hall, the “equipment hall”, built on the ground floor next to the accelerator hall to house all technical subsystems and laboratories, as well as the new conventional infrastructure (Figure 5)

The basement and ground floor are connected by stairs, a freight elevator, the cargo hatchway (Figure 4) and the media bay. The cargo hatchway will be covered by removable concrete T-bars for radiation protection.A crane for the cargo hatchway is required to transport up to 6 t from/to the underground building.

A small mobile crane in the gallery is foreseen for the RF components maintenance.

Several restrictions due to the usage of already existing infrastructure, especially the two cryogenic plants, constrain the placement within the site map, as shown in the Figure 2, where the green rectangle indicates the accelerator hall and the blue rectangle stands for the equipment hall.

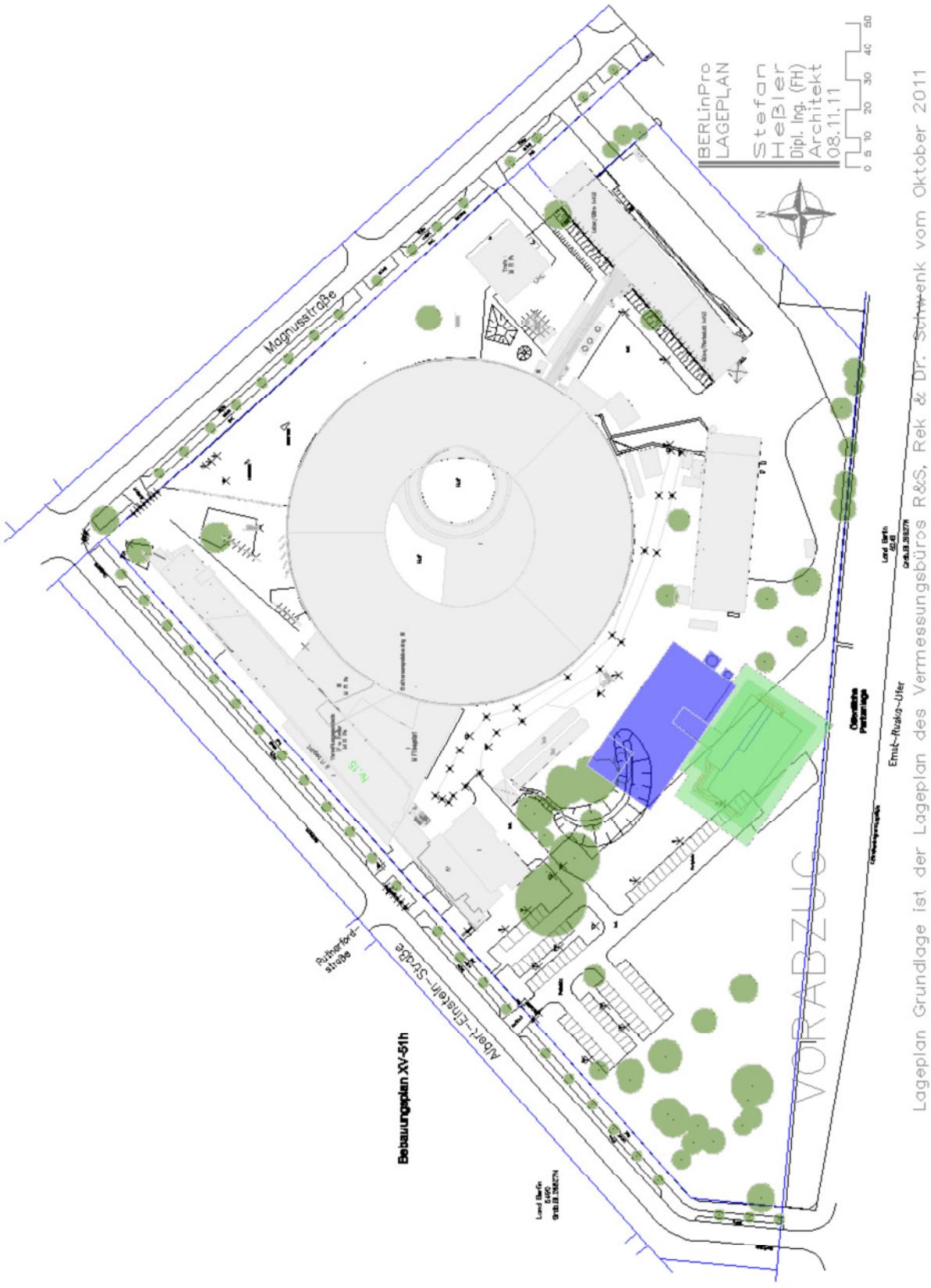

Figure 2: Site map showing BESSY II and the two B*ERL*inPro buildings

2.1.1. Ground water

The construction site lies between 34.67 m and 35.11 m above sea. The centennial ground water level is expected slightly lower, at 33.40 m. Currently, the ground water level is only 32.7 m and the ground water flow rate is 56 m/a to north north-west. The flow rate and direction are determined by the pumping stations of the waterworks in Johannisthal. Without this pumping the natural ground water flow rate changes to 36 m/a to south south-east, in the direction of the Teltowkanal. Due to this low flow rate, ground water contamination is no concern.

While excavation dewatering with fountains is necessary.

An environmental impact analysis report will be requested by the local authority, in case the construction level extends to more than 4 m below surface.

2.1.2. Bundesamt für Bauwesen und Raumordnung (BBR)

First contact with the approving authority has been established in summer 2011 and three unavoidable requirements have been postulated:

- an architectural competition
- a competition “Kunst am Bau”
- compliance with the so called "RZBau“ (Richtlinien für die Durchführung von Zuwendungsbaumaßnahmen)

The envisaged complete date lies in 2014 but depends on the necessity of the architectural competition. A first contact to project consultancies for architecture has been established. The technical building requirements have to be settled to start the request for proposals.

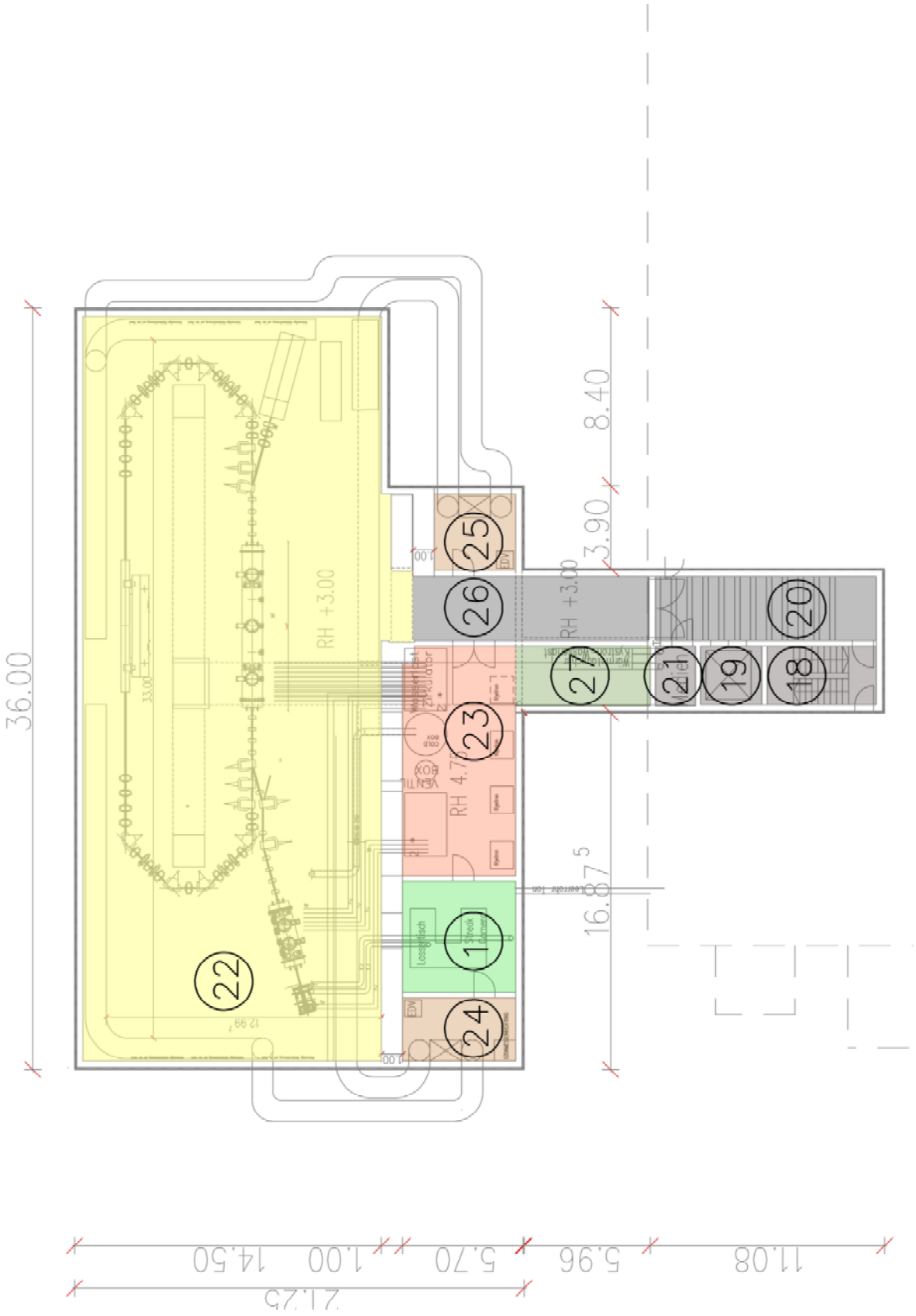

Figure 3: Top view of the B*ERL*inPro accelerator hall and gallery,
The numbers in circles are the room numbers in Table 3

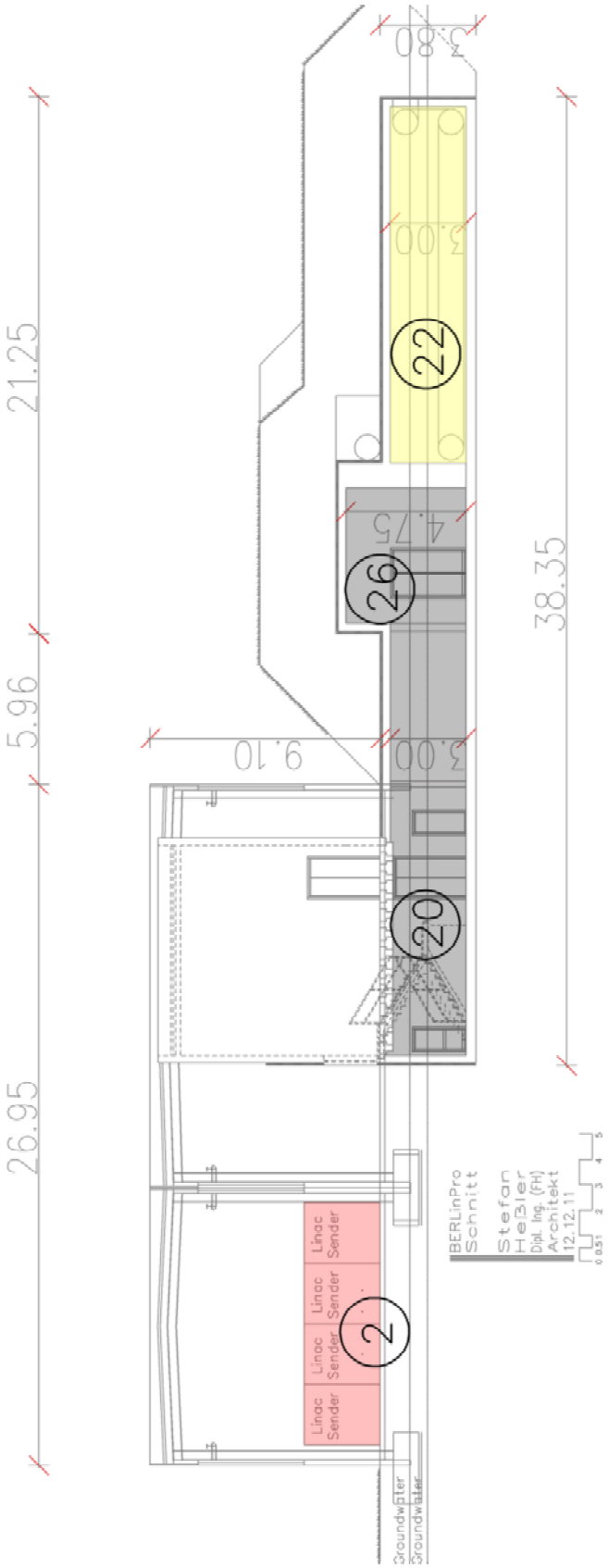

Figure 4: Cut through the equipment hall, the subterranean building and the earth pile for radiation protection, showing the stair case and freight elevator.
The numbers in circles are the room numbers in Table 3

2.1.3. Accelerator hall and gallery

The accelerator hall and the gallery are shown in Figure 3. The foundation will be realized as spread foundation with a plate, walls and ceiling made of waterproof concrete. Due to the expected radiation level water bars will be composed of metal instead of organic materials. Feed throughs are realized by full metal flanges directly installed in concrete.

The basement will be made of waterproof concrete with static walls, ground plate and ceiling.

On the roof of accelerator hall and gallery water barrier and thermal isolation consisting of cement and foam glass will be installed. To fulfill the radiation shielding requirements, the basement will be covered by a 3.6 m layer of sand with the option to increase up to 6m.

The walls of the accelerator hall will be isolated thermally by foam glass. Due to the expected radiation level outside of the walls suitable bonding systems have to be chosen.

The cryogenic cold box, the RF klystrons and the laser systems have to be placed in close vicinity to the machine in the gallery, shielded by 1 m hematite wall. The height of some of these components exceeds the hall's clear height of 3 m, thus the gallery has a clear height of 4.75 m for maintenance.

On top of the hematite wall there will be an infill with L-bricks in different layers with shifted joints to enable the media to be guided through the radiation shielding. The gallery ceiling overlaps the accelerator hall. This enables to guide the cables, wave guides, liquid helium from the gallery to the hall under the restrictions of a radiation shielding. An additional media access to the accelerator hall for the supply with cooling water, electricity data cables and gases will be realized by a tunnel beneath the floor level of the hall and the gallery. This will enable a direct access from the equipment hall via the media bay to the inner area of the machine.

The only personal access to the accelerator hall from the gallery is given by a radiation protection gate, which is moveable in line. This gate has to fulfill the same shielding levels as the hematite wall.

The tubes for air conditioning will run along the outside of the accelerator hall in the soil above ground water level. This reduces the complexity of the transfer of huge transversal sections through the radiation shielding, und saves volume in the accelerator hall itself.

Due to the expected radiation level in the accelerator hall, suitable components and systems for floor coating, and necessary electrical installations have to be chosen. An exact decision will be made by dose by the material list of Landolt-Börnstein.

2.1.4. Equipment hall

The equipment hall, as shown in Figure 5 is a steel frame construction on a reinforced concrete plate, with sleeve foundation. Pillar and bearer will be made out of steel I-beams to a frame. The walls consist of a sandwich structure with expanded polystyrene insulation between metal sheeting, as used for industrial buildings. The roof structure has a trapezoidal sheet steel design with thermal insulation and a film sealing. The roof cladding

will be designed with gas packing foil, drainage and substrate. Arrangements to install solar panels will be made.

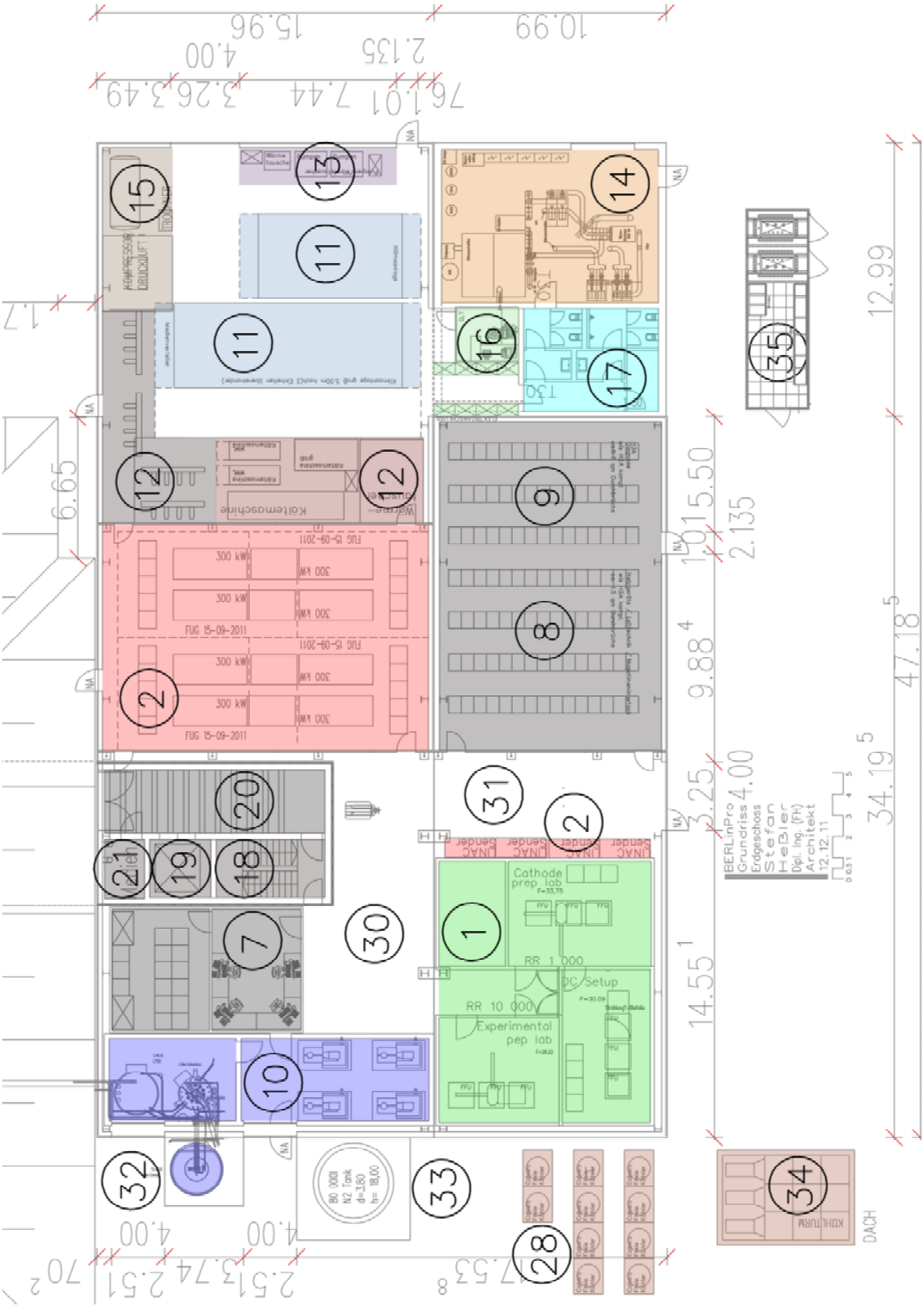

Figure 5: Layout of equipment hall
The numbers in circles are the room numbers in Table 3

Special environmental conditions are required by some of the laboratories, the control room and the computer room. These areas will be separated in different hutches; some are equipped with filter fan units.

Loud sonic sources such as warm cryogenic pumps, water treatment and water cooling system will be encapsulated in sand-lime-bricks.

RF, power supply, diagnostic and all the special electronic units only have to be protected from dust and dirt; they will to be covered by lightweight walls.

So far, there are no special seismic requirements.

B*ERL*inPro overview	area/m²
Total B*ERL*inPro basement	768
Total ground floor	1,197
Total outside	66
Total roof	106
Total	**2,137**

Table 2: Space allocation B*ERL*inPro

2.1.5. Infrastructure

Room number	Room name	Location	Area	Load	Room temperature	Heat dissipation to air	Heat dissipation to cooling water	Flow and return flow	other conditions
			m²	kW	°C	kW	kW	°C / °C	41
1	Labs	gf	160	40	21 ± 0,5	20	20		41
2	RF	gf	176	2270	20 - 30	90	280	28 / 38	
7	Control & computer room	gf	55	50	24	50	0		
8, 9	Diagnostics, control system, power supplies, interlocks vacuum	gf	162	300	20 - 30	80	30	28 / 38	
10	Cryo cold box and pumps	gf	69	131		11	120	28/38	42
11, 12, 13, 15	Technical building equipment	gf	274	360					43
14	Water treatment	gf	74	40					
16	Building control system	gf	22	5					
17	Restrooms	gf	31	5		5	0		
18	Stairs	gf/b	28						
19	Lift	gf/b	16	5					
20, 26	Cargo hatchway	gf/b	98						
		gf	31	5		5	0		
21	Media bay	gf/b	10						
22	Accelerator hall	b	496	140		89	115	28 / 38	
						20	650	31 / 68	44
23	Klystron	b	58	60	20 - 30				44
					20 - 30		810	25 / 35	
					20 - 30		45	28 / 38	
					20 - 30		810	28 / 38	
				10	20 - 30	10	0		
				1	20 - 30	1	0		
						30	60		45
24	Circulating air cooler 1	b	16						
25	Circulating air cooler 2	b	14						
27	Heat exchanger	b	17			10			
28, 34	Air coolers and cooling towers	r	106						
30	Access yard	gf	62						
31	Transportation area	gf	54						
32	LN2 tank	o	26						
33	L He dewar	o	12						
35	Transformer	o	28						
	Storage area	b	43						
	total		**2137**	**3252**		**421**	**2130**		
	b = basement								
	gf = ground floor								
	o = outside								
	r = roof								
	41 = laminar flow, RR 1000; regulated humidity								
	42 = noise insulation, diagonally ventilation								
	43 = modular project								
	44 = activation; additional water circuit								
	45 = from gallery to accelerator hall								
	Gallery are rooms 23, 24, 25, 26, 27								

Table 3: Energy and area requirements for B*ERL*inPro

2.1.6. Technical aspects

Power supply

The total power requirement of B*ERL*inPro is between 4.5 and 5 MVA, therefore a further transformer and a low voltage main distribution station have to be installed in addition to the two existing 1.65 MVA 10/0.4 kV transformers and substation, partly used by the B*ERL*inPro experimental area in the assembly hall. The existing 10 kV power line has been calculated for 5 MVA.

Existing installed load	1200	kW		
Existing installed transformers			3.30	MVA
Additional required power			1.65	MVA
Expected new load	3000	kW		
Total expected load	4600	kW		
Total installed power			**4.95**	**MVA**
Power line is ready for 5 MVA			5.00	MVA

Table 4: Loads and transformers

Cooling water

A cooling water system for process cooling is required. Three different deionized cooling water circuits are foreseen:

- for the electronic units and components in the equipment hall
- for the components placed underground in the accelerator hall and the gallery
- for the high power density units as there are the RF Klystrons, their water loads and the beam dump

A higher (than 45°C) cooling water return temperature can reduce the overall costs of the system. This is to be investigated as well as the ideas of waste heat utilization.

Free capacities of about 350 kW of the existing water cooling system in the assembly hall can be used to reduce new installations for B*ERL*inPro. Potential synergies have to be examined in details. The layout of the new cooling system has to be compatible to the existing one for service and maintenance aspects.

The cooling water has to be demineralized on a low level of conductance (< 10 µS/cm). Acidity as well as the oxygen content has to be controlled and regulated carefully.

Heating

The equipment hall and the accelerator hall will only be equipped with a simple heating system for frost protection. As long as the systems are under operation, the dissipated heat will be sufficient to heat the buildings.

Air conditioning

Although it is essential to dump as much waste heat as possible directly into the cooling water, thermal power losses emitted by electronic equipment or magnets into the air have to be absorbed by air conditioning systems. The necessary cooling power will be provided by cold water units. For the thermal discharge into the atmosphere air coolers or cooling towers have to be installed.

Inside the accelerator hall and the gallery a defined sub atmospheric pressure with a few mbar is to be guaranteed while the accelerator is under operation, due to radiation protection requirements. This area has to be vented with fresh air before access is possible. Specific requirements such as humidity and cleanroom conditions for example in laser room and gunlab will be provided locally.

Compressed air

Compressed air will be supplied by the BESSY II central compressed air.

Security systems

The fire protection system in the equipment hall will be the same as in the existing assembly hall based on smoke detectors installed in two separate lines. An alarm will be send automatically and directly to the fire department when one detector in each line is activated.

In the accelerator hall it is envisioned to install a smoke detection system based on an air sucking system, where the sensors can be installed in the gallery.

The decision between an oxygen reduction and an inert gas system is still pending. Oxygen deficit control sensors will be installed for Nitrogen and Helium gases. The need for an ozone monitoring system and the detection and drain off of spitted hydrogen is yet to be investigated.

Connection to existing conventional services

Services like telephone, building control system, burglar alarm system, video surveillance, access control, will be integrated in existing systems.

2.2. Radiation Protection

2.2.1. Introduction

Due to the potential radiation hazard posed by the tremendous beam power the facility will be placed subterraneous. The basic shielding concepts have been developed. We used the Monte Carlo code FLUKA [1] to calculate the details of the shielding, activations, energy doses for radiation damage and energy spectra for realistic scenarios.

At electron accelerators the photons of the electro-magnetic cascade can produce neutrons by (γ,n) reactions. There are three possible reaction channels: Giant resonance neutrons, whose maximum in the spectrum is 1 MeV, this process starts at photon energies of 10 MeV. Quasi deuteron fission neutrons are produced by the fission of neutron-proton pairs in the nucleus. The threshold energy of this reaction process lies at a photon energy of 30 MeV. If the wave length of the photons is of same size as the diameter of the nucleons, photons can be transformed to quark – antiquark pairs. One of these is exchanged with a quark inside the nucleon. This nucleon is transformed from a proton to a neutron (or vice versa) and the pair of two quarks generates a pion. This pion is then absorbed inside the nucleus and extracts a fast neutron.

The quasi – deuteron fission and photo pion neutrons are high energy neutrons. They have a maximum at 100 MeV in the spectrum or if the electron energy is lower, the neutron spectrum ends at the electron energy. Fast neutrons are more penetrating than the giant resonance neutrons.

Extrapolations of existing formulas valid in the GeV range down to the B*ERL*inPro energy range are not applicable due to the rapidly increasing cross section of the fast neutron production in the range between 50 MeV and 1 GeV. (Above 1 GeV the neutron yield is linear with the electron energy). Formulas valid in the low energy range (< 100 MeV) are not applicable because they do not consider fast neutrons. At 50 MeV the cross section for the fast neutron production is about two orders of magnitude lower than that of the giant resonance neutrons, but because of the shielding thickness and the stronger penetration they determine the dose outside the shielding of B*ERL*inPro.

New analytical formulas for the vertical shielding of B*ERL*inPro have been derived from FLUKA calculations in the 50 MeV to 1 GeV range for a 1 m shielding, due to these aspects and because of the extended computation times. .

The annual dose limit for uncontrolled areas of the facility are set by the German radiation protection ordinance to 1 mSv/a for direct radiation and 0.3 mSv/a for indirect radiation (e.g. activated air) for a 2000 h/a operation. The accelerator hall and the adjacent rooms are exclusion areas during operation. The accelerator hall will be a radiologically controlled area during the time the accelerator is not operated.

2.2.2. Underlying assumptions and basic machine parameters for the radiation protection concept

The intended CW operation with a current of 100 mA requires an electron source with 77 pC/bunch charge at 1.3 GHz repetition rate. The injection linac boosts the energy from the gun to 5 - 10 MeV which corresponds to 0.5 - 1 MW beam power at 100 mA. The electrons are further accelerated to 50 MeV in the linac module. After one turn the electrons are decelerated in the linac module to the injection energy. The energy of the decelerated electrons is stored in the linac cavities and is used to accelerate subsequent electrons (ERL principle). The decelerated electrons are deflected and absorbed in the beam dump.

The electron losses in the recirculator are limited by the RF power of the linac module. 30 kW of RF power correspond to maximum possible losses of 0.6 %. As higher losses due to malfunctioning systems, as well as located losses on apertures, as known from existing ERLs, will cause an interrupt of the machine protection system due to the high current, equally distributed losses can be assumed for the radiation protection concept. We divide the losses into six equidistant point sources (about one for 10 m) with 0.1 % each. For the annual dose an operation time of 2000 h/a has been assumed and for the activations a daily operation pattern of 8 continuous hours. A machine protection system is foreseen (Appendix 3.2) which will stop the machine operation if the losses exceed 5 µA/m. For a circumference of 50 m these losses correspond to 0.25 %. The availability of a machine protection system is not considered for shielding issues because it doesn´t have the required reliability for personal safety.

2.2.3. Derivation of new shielding formulas and first results

FLUKA simulations of the recirculator were performed using one point source of 0.1 % losses. The 50 MeV electrons hit the stainless steel vacuum tube with an angle of 1 mrad. The resulting gamma radiation reaches dose rates up to 1.9E5 Sv/h, Figure 6, about three orders of magnitude higher than the corresponding neutron dose rates, Figure 7, in forward direction.

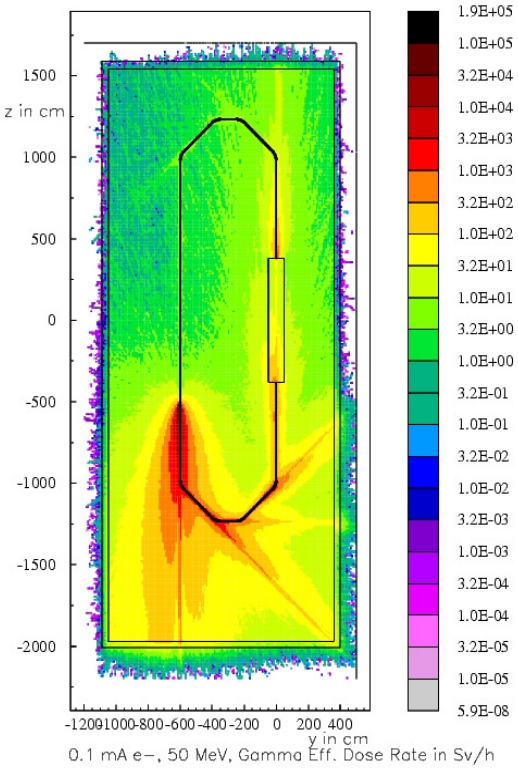

Figure 6: Gamma radiation, 0.1% losses

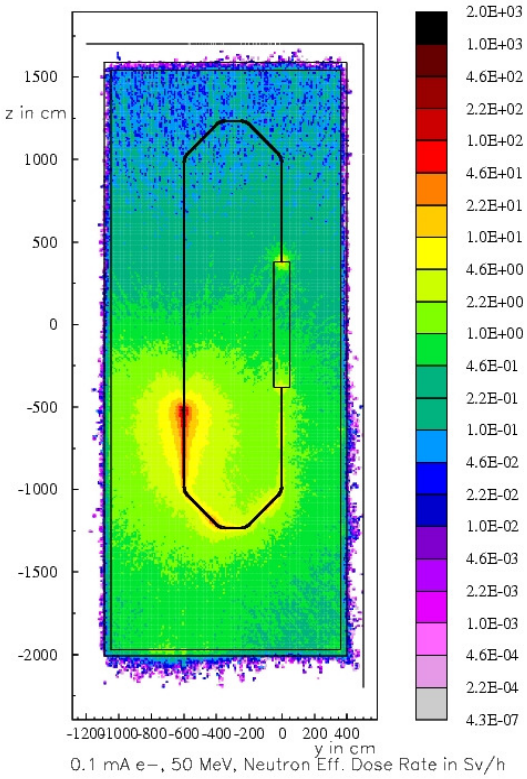

Figure 7: Neutron radiation 0.1 % losses

In the lateral direction, gamma and neutron radiation reach similar levels. Therefore it is favourable to place B*ERL*inPro subterraneous, because the shielding is restricted to the lateral radiation in vertical direction.

The neutron dose rates show the isotropic radiation distribution which is typical for giant resonance neutrons. Additionally there is a contribution in forward direction caused by high energy neutrons (E > 20 MeV). The cross section of the high energy neutron production is about one order of magnitude lower than that of giant resonance neutrons. But the high energy neutrons are far less attenuated in shielding materials, so their tenth value layers are about twice as thick as those of giant resonance neutrons. Therefore it can be deduced that the dose rate outside the shielding will be dominated by high energy neutrons and that several meters of shielding are necessary to hold the annual dose limit of 1 mSv/a above the shielding.

We derived analytical formulas from FLUKA calculations between 50 MeV and 1 GeV with different target and shielding materials in transverse direction [6] starting from [2] and [3] for γ radiation and [4] for neutron radiation. The γ dose in Sv/primary electron is then given by

$$H = 3.45 \cdot 10^{-17} \cdot t^{2.436} \cdot \ln Z \cdot msc \cdot E \cdot \exp((-\rho \cdot x - 75\,g/cm^2)/\lambda)/r^2$$

where Z is the atomic number of the target material, t is the target transmission in radiation lengths, msc = 0.01828 (material scaling factor), E is the energy in GeV, ρ is the density of the shielding material in g/cm³, λ is the attenuation length in g/cm², x is the

thickness of the shielding in cm, r is the distance in m. The dose of giant resonance neutrons (GN) has been determined as:

$$H_{GN} = \eta \cdot 0.24 \cdot A^{2/3} \cdot E \cdot (0.33 + 0.67 \sin(\theta)) \cdot \exp(-\rho \cdot x / \lambda_{GN}) / r^2$$

in pSv/primary electron. η is a target efficiency factor [5],[2], it is 1 for 10 radiation lengths (rl) and 0.3 for two rl. *A* is the atomic mass number, θ the angle of observation in degrees, *r* is the distance in cm, the other symbols have the same meaning and units as above. λ=30.25 g/cm² for concrete and 23.9 g/cm² for sand.

The dose of high energy neutrons (HEN) is:

$$H_{HEN} = K(E) \cdot 23 \cdot A^{-2/3} \cdot E^{1.1} / r^2 \cdot (0.07 + 0.93 \cdot \exp(-\theta / 31°)) \cdot \exp(-\rho \cdot x / \lambda_{HEN})$$

in pSv/primary electron. λ_{HEN} also depends on θ and is 94.4 g/cm² both for concrete and sand at 90°. *K(E)* is a correction factor for high energy neutrons and is given by

$$K(E) = 1 - \frac{1}{\exp(E \cdot 10.52 - 3.59) + 1}$$

First shielding results

The dose rate inside a ceiling consisting of 20 cm concrete and sand has been calculated using the derived analytical formulas, Figure 8. The γ - dose rate (not shown here) is similar to the giant resonance neutron dose rate. A shielding of 20 cm concrete and 3 m sand is sufficient to hold the annual dose limit of 1 mSv/a above the ceiling. At this thickness the dose is determined by fast energy neutrons.

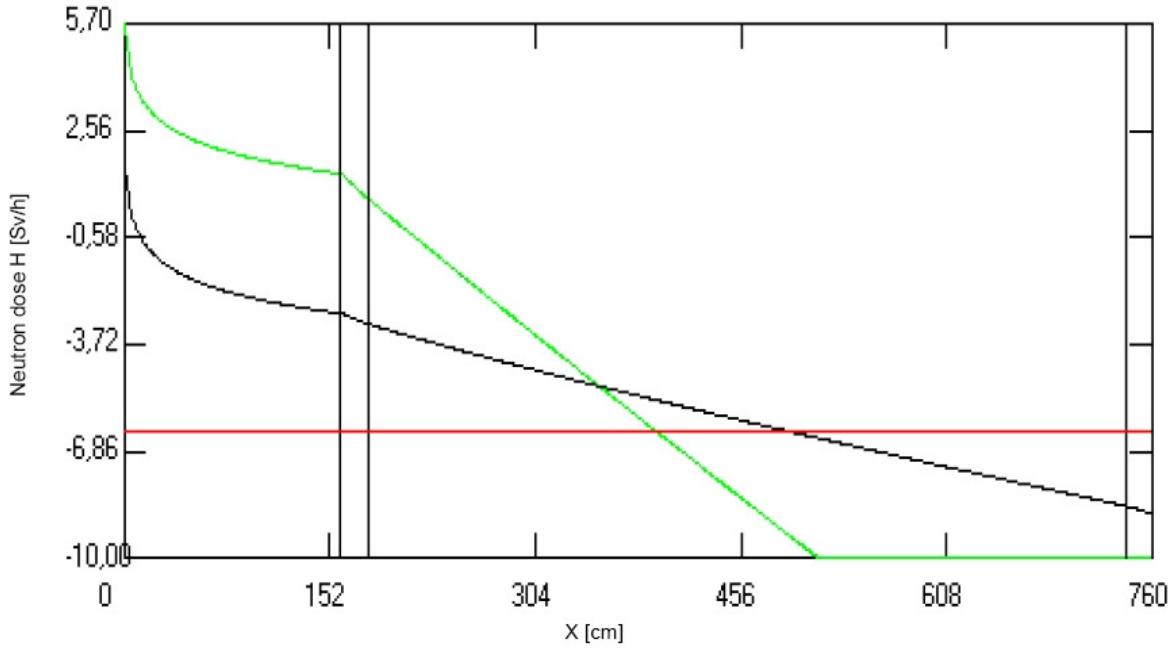

Figure 8: Lg of neutron dose rate in Sv/h
Green: Giant resonance neutrons, black: High energy neutrons, red: 0.5 µSv/h (1 mSv/a for 2000 h/a)

2.2.4. Activations

At electron accelerators most nuclear reactions occur in (γ,n) processes caused by photons, that are produced in electro-magnetic cascades. Other reactions (in much smaller amount) are caused by secondary neutrons (also with thermal energies) and by protons. Because of the pair creation the photon spectrum decreases rapidly at energies > 1 MeV. Threshold energies for (γ,n) reactions are about 10 MeV for the materials usually used for vacuum components. We use FLUKA to calculate the production rates dN/dt of the radio nuclei. The activation was calculated using dN/dt and irradiation/decline cycles of one year. After ν irradiation/decline cycles the activity is [8]:

$$A_\nu = \dot{N} + (1 - \exp(-\lambda \cdot t_I)) \cdot \exp(-\lambda \cdot t_I) \cdot \frac{1 - \exp(-\nu \cdot \lambda \cdot (t_I + t_D))}{1 - \exp(-\lambda \cdot (t_I + t_D))}$$

λ = ln 2/T1/2. For B*ERL*inPro we used ν= 365, irradiation time ti = 8 h, decline time td = 16 h for the calculation of the activation after one year and ν= 1 and ti= 8 h, td = 0 after one irradiation period.

Activation of vacuum components

We compared the activity of three materials used for vacuum components: an aluminium alloy with 97.65 % Al, stainless steel and copper.

Target	**Nuclide 1**	**Nuclide 2**	**Nuclide 3**	**Nuclide 4**
Aluminium	Na22	Na24		
T1/2	2.603 a	14.7 h		
gamma dose rate	318 µSv/h	364 µSv/h		
beta dose rate	1430 Sv/h	1260 Sv/h		
Steel	Mn52	V48	Co56	Fe55
T1/2	5.6 d	15.97 d	77.26 d	2.73 a
gamma dose rate	0.203 Sv/h			-------
beta dose rate	2510 Sv/h			5.32 Sv/h
Copper	Cu64	Co58	Co60	Fe55
T1/2	12.7 h	70.86 d	5.272 a	2.73 a
gamma dose rate		2.93 Sv/h	0.138 Sv/h	-------
beta dose rate		5720 Sv/h	430 Sv/h	7.46 Sv/h

Table 5: Most important radio nuclei from the activation of vacuum components for three different materials after one year of irradiation. γ – radiation in 1 m distance, β – radiation at the surface for the area of one hand.

The γ dose rate in 1 m distance is several 100 µSv/h for Al, few mSv/h for stainless steel and up to Sv/h for Cu. The beta dose rate is calculated as a surface dose directly on the vacuum tube for the area of one hand. It reaches dangerous levels especially for the nuclei produced in copper. We point out, that the calculations have been conducted for a point source with 0.1 % electron losses/turn which is very conservative. Detailed calculations of the dose rate after machine operation are in progress.

After one year of operation the activation of the Al alloy is one order of magnitude lower than the activation of stainless steel, and 20 times lower than copper. The short living nuclei produced in copper (after 1 irradiation period) have very high activities, so that the access to the accelerator hall would have to be restricted. All in all the usage of Al for the vacuum system is most favourable. In the injector and the beam dump the electron energy is below the threshold for the subsequent (γ,n) activation reactions, so steel or copper could as well be used there for the vacuum components.

Activation of air

After 8 hours of irradiation the following radio nuclei are produced in the air of the accelerator hall, where Ca is the activation concentration in Bq/m³.

Target	Nuclide 1	Nuclide 2	Nuclide 3	Nuclide 4
	C11	N13	O15	Ar41
T1/2	20.38 m	9.96 m	2.03 m	1.83 h
Ca	1.72E06	1.67E6	1.92E6	3.08E5

Table 6: Most important radio nuclei due to air activation, half lives and activation concentration, Ca, in Bq/m³ after 8 hours of irradiation.

The degree of activation imposes to control the air given to the environment. Under-pressure is necessary in the accelerator hall (few %) and the exchange of air has to be reduced during operation to hold the limit of 0.3 mSv/a for indirect radiation given to the environment. The air in the accelerator hall will be exchanged after operation with the rate of 1/h.

2.2.5. Current work and outlook

Calculation of analytical neutron formulas

The derived neutron formulas have to be completed by an energy correction term for the giant resonance neutrons at low energies down to the threshold of (γ,n) reactions of 8 MeV, to be applicable for the low energy parts of B*ERL*inPro, especially the beam dump. The neutron yield depends on the material thickness; therefore a target efficiency factor for the high energy neutron term will be determined for different materials as well as the target efficiency factor of the giant resonance term. The analytical expressions will be derived from FLUKA calculations.

Calculations of activations

Detailed calculations of the produced nuclei are necessary to determine the waiting time before access to the accelerator hall after the machine operation. The time depends on the materials used for the vacuum system, the dumps and other machine components. Only for few nuclei radiation constants are available in the literature. The other will be derived from decay schemes and numbers of nuclei produced. Alternatively, the dose rate after irradiation can be calculated with FLUKA. As a bench mark test we compared FLUKA results of the dose rates of Co60 produced by thermal neutrons with our analytical calculations using the decay scheme. The analytical calculations are in good agreement and thus offer a promising new approach.

This approach can as well be used to determine the radiation impact on the environment (activation of earth, ground water and air).

Radiation measurement system

The measurement system will be distributed to eight locations with an ionisation chamber, a neutron detector (BF3 proportional counter) and local electronics each. (Six will be placed above the ceiling, two inside the building). Due to the high bunch repetition rate of B*ERL*inPro in CW operation the radiation is seen as continuous radiation, errors due to pulsed radiation can be neglected. Even operation modes using macro pulses are unproblematic, because the maximum dose rates outside the shielding will be much smaller than at any synchrotron light source. (At synchrotron light sources the annual dose is determined by the short injection periods, at B*ERL*inPro we will have continuous injections). The dose outside the shielding is determined by high energy neutrons (>10 MeV). With the addition of one cm of lead around the moderator the detectors can be enabled to measure the complete neutron spectrum due to a (n,2n´) nuclear reaction. The two emerging neutrons are in the detectable range of the monitors.

We started to simulate those upgraded neutron detectors with FLUKA (high energy proton beam hitting a spallation target) and found an increase of the neutron fluence of thermalized neutrons inside the detector volume by a factor of 3 compared to monitors without lead layer. So this approach is very promising. A lead covered neutron monitor has been built and will be calibrate at the CERN reference field CERF in 2012. Therefore an affordable and well suited measurement system compatible with the radiation measurement network at our campus is within reach.

A measurement system of the outgoing air is in the planning.

Beam dump

The beam dump is one of the technological challenges of this project because of the high beam power of up to 1 MW (6 -10 MeV, 100 mA). The energy has to be extracted from the beam dump while keeping the energy density in the different dump parts below the machine protection limit (< 200 W/cm²).

The current approach is to distribute the energy on the inner surface of a hollow cone of water cooled copper with a widened and divergent (+/- 75 mrad) beam. We conducted FLUKA calculations of the energy deposited in the beam dump by the radiation.

Localized beam dumps for commissioning and diagnostic purposes are under consideration and could be realized by adding additional vertical sand shielding of 60 cm without limitations on location and operation.

Building details

The next goal is to calculate the strayed radiation through entrances and media ducts for a detailed model of the building. The area in front of the accelerator hall has to be shielded to avoid radiation damage of electronics and components. The shielding wall has also to decrease the radiation so that the limit of 1 mSv/a can be held at the entrance of this area, at the door of the stair case and at the entrance of the lifting hole. To complete this work it is necessary to specify the positions of the machine components, the vacuum system, magnets, diagnostic lines and others during the next months.

Licences

To get a *licence of construction* (and later a *licence of operation*) it is necessary to write a report that prognosticates the annual doses, the dose rates, the shielding and safety measures in full detail. An external expert has to write a second report in which the results have to be confirmed and the measures are evaluated. Based on these two reports the state authorities will issue the licence. The complete process will take about six months. The *licence of construction* and the *building licence* are indispensable prerequisites for the ground breaking.

2.2.6. References

[1] G. Battistoni, S. Muraro, P. R. Sala, F. Cerutti, A. Ferrari, S. Roesler, A. Fassò, J. Ranft, Proceedings of the Hadronic Shower, Simulation Workshop 2006, Fermilab 6--8 September 2006, M. Albrow, R. Raja eds., AIP Conference Proceeding 896, 31-49, (2007); A. Fassò, A. Ferrari, J. Ranft, and P. R. Sala, CERN Yellow Report (2005), INFN/TC05/11, SLAC-R-773.

[2] H. Schopper ed., Landolt-Börnstein Vol 10, Springer-Verlag Berlin (1990).

[3] H. Dinter, J. Pang, K. Tesch, Rad. Prot. Dosi. 25,2 (1988).

[4] H. Dinter, A. Leuschner, K. Tesch, D. Dworak, J. Loskiewicz, NIM A 455 (2000).

[5] W. Swanson, IAEA, Wien (1979) and NCRP Report 51 (1977).

[6] M. Helmecke, K. Ott, RADSYNCH'11, Pohang, South Korea, April 2011, Conf. Proc., http://pal.postech.ac.kr/radsynch11

[7] K. Ott, M. Helmecke, IPAC11, San Sebastian, Spain, September 2011, Conf. Proc., http://www.JACoW.org

[8] K. Ott “Sicherheitsbericht für den Betrieb der Speicherringanlage Metrology Light Source”, HZB internal report for the operating licence (2008).

2.3. Optics / Theory / Modelling

One of the mayor advantages of ERL's compared to storage rings is the flexibility in all relevant bunch parameters, providing radiation for diverse applications. As a single pass device, the radiation properties in an ERL, evolving from the repetition rate, bunch charge, bunch length or emittance can be adjusted to demand. In this chapter the 'standard mode' of B*ERL*inPro is described. This is the optics developed in order to show the realization of the project goals. Other operational modes, like the 'low energy spread mode' or the 'short pulse mode' are shortly mentioned as alternative options.

It should be noted, that some options, important for the beam dynamics are not treated here, because, due to the lack of financing, they are not feasible to be implemented in the B*ERL*inPro. These are e.g. a third harmonic cavity and longitudinal laser pulse profiling. The financially driven choice of the number of cavities in the booster is also not optimal due to the resulting strong transversal focusing. Furthermore, if the assumed beam energy of the SRF gun will not be reached, it will definitely lead to a deterioration of the beam quality (emittance).

Optics calculations show that most of the bunch properties are defined at low energy in the injector. This is especially true for the low emittance, but also the successful compression of bunches in the recirculator depends on a keeping the bunch short before the entrance to the booster.

Conservation of the low emittance: Without adequate measures, the projected emittance of the bunch will blow up at low energy due to space charge forces. For a detailed theory see Appendix 3.1. When the bunch is depicted as a longitudinal succession of slices, the transverse emittance blow up can be explained as a misalignment of the transverse phase space ellipses of the single slices either rotationally or transversely or due to a blow up of the individual slice emittance. This effect can be counteracted by adequately setting the transverse focusing in the injector.

The most important emittance diluting effects and the theoretically derived consequences on the design are listed below:

- Transverse space charge: The beam dynamics in B*ERL*inPro is dominated by space charge effects until behind the linac, measures for emittance compensation have to be taken.
- The longitudinal inhomogeneity of space charge density results in oscillations of the x, y size of the slice around a reference value. Using adequate focusing, the oscillations can be minimized at a certain point in the lattice.
- The energy change due to longitudinal space charge is of the order of magnitude of the relative energy spread of the bunch, a few per mill.
- Mismatch of slice centers at the end of a dispersive section results from the energy variation of slices due to longitudinal space charge forces, which leads to horizontal displacement and angle of the slice behind the merger.
- Slice emittance growth due to the inhomogeneity of the energy change in the slices: Due to changes in the direction of motion of the complete bunch (in dipoles) the space charge forces experienced in different parts of a single slices can vary, resulting in different the energy changes within one slice.

- Aberrations in the solenoid lead to emittance growth proportional to the fourth power of the bunch radius and to the fourth power of the solenoid field. Moving the solenoid as close as possible to the gun reduces the bunch radius, and increasing the solenoid length reduces the necessary maximum field.
- Estimations of the over-compression due to RF non-linearity can be used to deduce 'optimal' values for the phase of the bunch center in the booster and the R56 of the merger.

Creation of short bunches: As far as the bunch length is concerned, it can be adjusted in the recirculator by applying an energy chirp to the bunch in the linac and using the R56 of the recirculating arc to compress the bunch. The quality of the compression, though, depends on the linearity of the longitudinal phase space of the bunch. This linearity is limited by the amount of RF curvature experienced by the bunch in the booster. Therefore, short bunches in the recirculator require short bunches in the injector.

For the description of the beam optics and dynamics the machine is split into three parts which are discussed separately:

- the injector including the gun, booster and merger, i.e. the low energy part up to the injection into the recirculator. Physics issues here are the conservation of the low emittance from the gun, longitudinal bunch shaping and the injection into the recirculator.
- the linac straight section with the high energy chicanes including the injection and the extraction dipole, matching quadrupoles and the linac
- the recirculator, i.e. acceleration, beam transport and deceleration of the beam at lowest transmission loss rates
- the dump beam line and the high power beam dump: the necessarily highly effective and secure transport of the 'used' beam into the dump

2.3.1. Beam optics

2.3.1.1. Modes of operation

The difference between the operational modes is dominated by the degree of bunch compression. The compression is controlled by the phases of booster and linac in combination with the fixed R56 of the merger and the adjustable R56 in the arcs.

The higher the compression factor, the higher the demands on the linearity of the longitudinal phase space. Therefore, already at the entrance to the booster the bunch length should not exceed ~6ps to avoid the imprint of the RF curvature on the longitudinal phase space. Restrictions for the bunch length in the linac, for the linac phase and the arc's R56 arise from the energy acceptance of the recirculator.

An rms energy spread of 0.5-1.0 % is required to transport the beam with low losses. Already for on crest acceleration, a bunch length of 9.5 ps results in an energy spread of 0.5 %, only due to the RF curvature. The energy spread increases further with the "off crest" phase of the linac. On the other hand, the higher the phase, the more linear is the chirp on the bunch. Therefore, the merger is used as a first compression stage (6 ps in standard mode, 2 ps in short pulse mode), allowing larger phases in the linac.

	Standard mode	Low energy spread	Short bunch
Bunch charge, pC	77	77	~ 10
Bunch repetition rate, GHz	1.3	1.3	Variable
Max. average current, mA	100	100	≤ 13
Maximum energy, MeV	50	50	50
Beam kinetic energy after injector, MeV	6.0	6.0	6.0-10.0
Transverse norm. emittance, , mm mrad	< 1	< 1	1-5
Minimal bunch length, ps, rms	2	5-10	<0.1
Bunch length behind injector ps, rms	4-5	5-10	1-2

Table 7: Envisaged parameters for typical operation modes

2.3.1.2. Injector design considerations

A technical drawing of the injector layout is shown in Figure 15.

The gun is described in detail in 0.1 and the booster is described in the 2.5.2.2.

The merger section between the booster and the entrance to the recirculator is designed to merge the low energy beam from the injector and the high energy beam from the recirculator, in order to bring both beams onto the linac axis. It is designed as a 'dogleg' with three identical, parallel faced dipoles. Two quadrupoles are necessary to suppress the linear dispersion behind the merger. Four quadrupoles behind the booster are foreseen for the emittance compensation. Four quadrupoles in front of the linac allow the beam matching into the linac.

The following criteria motivated the positioning of the elements in the injector

- move the solenoid as close as possible to the gun cavity in order to keep the bunch size and the emittance small
- move the booster module as close as possible to the gun module to keep the bunch length under control, while providing enough space for the higher order mode couplers for the gun. A bunch length of < 2mm in front of the booster is crucial to prevent too much RF curvature imprinted on the bunch in the booster.

- keep the distance between the merger dipoles as short as possible while still providing enough space to accommodate the quadrupoles without interference with the high energy branch, in order to keep the dispersion small and achieve an R56 of 10cm
- provide enough drift space (40cm each) between the quadrupoles to separate their functionality

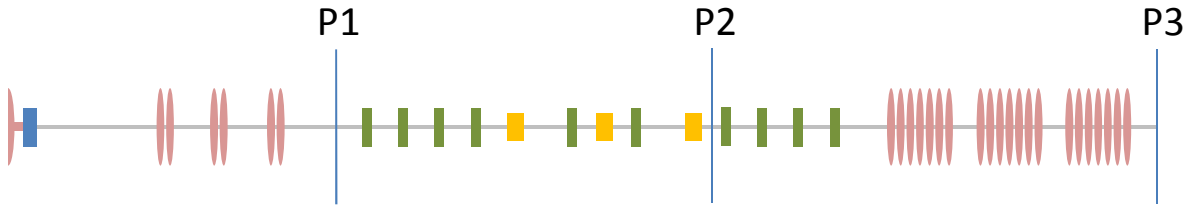

Figure 9: Schematic of the injector, including the linac
P1-P3 indicate the three separated parts for the calculations: P1: ASTRA – round beams, P2: ASTRA – 3D space charge routine, downstream of P3 – ELEGANT

Figure 9 shows the schematics of the injector. The following tables list the position of the components in the injection path, as used in the calculations, the magnetic elements in the injector and the most important geometrical features and beam properties.

	Position in m from cathode
Cathode plane	0.00
Solenoid center	0.35
Center booster cavity 1	2.435
Center booster cavity 2	3.223
Center booster cavity 3	4.088
Quadrupole 1, center	5.461
Quadrupole 2, center	6.011
Quadrupole 3, center	6.561
Quadrupole 4, center	7.111
Dipole 1, start	7.586
Quadrupole 5, center	8.594
Dipole 2, start	8.897
Quadrupole 6, center	9.426
Dipole 3, start	10.226

Table 8: Position of injector elements in m from the cathode

	No.	Length[m]	Strength [T], [T/m]
Solenoid	1	0.21	<0.1
Merger dipole (parallel faced)	3	0.25	<0.03 Bending radius = 0.8m Deflection = 18°
Merger quadrupole	2	0.15	<0.1
Quadrupoles	8	0.15	<0.25

Table 9: Magnetic elements of the injector section; the field strength is for the standard optics and 6 MeV.

Merger length (path length)	2.95 m
Max. dispersion	0.34 m
R56	0.10 m
Bunch length	1.9 - 1.3 mm
Horizontal beam size	0.1 - 2 mm
Vertical beam size	0.4 - 1 mm

Table 10: Geometrical and beam properties in the merger for the standard mode

2.3.1.3. Linac straight section

The low energy beam from the injector has to be merged with the recirculated, high energy beam to pass both beams on axis through the superconducting main linac. The linac is composed off three 7-cell cavities, for a detailed description see 2.5.2.3.

Depending on the average RF phase of the bunch in the linac cavities, it can be accelerated or decelerated. The 6 MeV beam from the injector is accelerated to the recirculation energy of 50 MeV, while the recirculated beam is decelerated from 50 MeV to 6 MeV to recover the invested energy. The linac is usually operated on crest, or close to it ($\phi_0 < 15°$) if the bunches have to be compressed in the recirculator.

To separate the decelerated 'spent' beam from the accelerated 'fresh' beam downstream the linac a splitter composed of two dipole magnets similar to the merger is used, guiding the high energy beam into the recirculator and the low energy beam into the dump line. To compensate the deflection of the 50 MeV beam in the merger/splitter dipoles located in the recirculation path, two additional dipoles each form the injection and the extraction chicane in the recirculator.

	No.	Length [m]	Deflection angle [°]
Merger dipole (parallel faced)	3	0.25	18
Injection (merger)	1	Common with merger	
	1	0.25	$36 * {E_{inj}}/{E_{rec}}$
	1	0.25	$18 * {E_{inj}}/{E_{rec}}$
Splitter dipole (parallel faced)	2	0.25	18
Extraction chicane (splitter)	1	Common with splitter	
	1	0.25	$36 * {E_{inj}}/{E_{rec}}$
	1	0.25	$18 * {E_{inj}}/{E_{rec}}$

Table 11: Parameters of the injection and extraction chicane dipoles including merger and splitter. The field is set by the injection energy, and is the same for all dipoles, except the central chicane magnets who have twice the field.

The field of the outer chicane dipoles is set by the injection/extraction angle (18°) of the low energy beam. The deflection angle and the offset of the beam in the central chicane dipole depend on the ratio between the injection and the recirculator energy. The deflection angle of the outer dipoles will lie between 2.1° and 3.6° for the high energy beam. The beam offset at the center lies between 4 cm and 7 cm (assuming 90 cm drift space between the dipoles). The field of these dipoles is low, <<100 mT and their task merely is to keep the high energy beam on axis.

Up- and downstream the linac four weak quadrupoles magnets focus the low energy beams in both case: The beam from the injector into the linac and the recirculated and decelerated beam into the dump line.

The strengths of these quadrupole magnets are set to

- adjust for small beam sizes in the linac, which eases the matching into the recirculator
- perform the final stage of emittance compensation
- match the decelerated beam effectively into the dump line

Despite the small gradients of “low energy beam” quadrupoles in front and after the linac, the high energy beam is affected by the quadrupole fields. Low beta function values help to reduce this effect.

2.3.1.4. Injector simulations

For the optics calculations the program ASTRA [1] is used. The beam at the cathode is modeled with a uniform distribution in the transverse plane; the distribution has a hard edge profile. The initial longitudinal distribution is defined by the form of the laser pulse and cathode response time. In the model we assume a 7 ps rms laser pulse with the

Gaussian profile. The initial bunch distribution is defined by the parameters listed in Table 12.

No. of particles	100.000
Charge per bunch	77 pC
Longitudinal profile	Gaussian, 7 ps rms, cutoff: 2.5 sigma
Longitudinal energy distribution (isotropic)	0.43 eV (green laser / 1.9 eV work function)
Laser spot	Flat top, 0.8mm radius

Table 12: Parameters of the initial bunch distribution

The transverse focusing strength of the RF field, the longitudinal beam dynamics and the correlated energy spread of the bunch behind the gun depend on the phase of the gun field with respect to the laser pulse. In the case of the standard mode 15˚ is an optimum. The transverse beam size behind the gun increases with smaller phases, therefore aberrations in the following solenoid have to be minimized.

The phases in the booster cavities are set to -90˚, -3˚, and -3˚ respectively. The first booster cavity is used to compensate for the energy chirp from the gun and create the necessary chirp for compression in the merger section. The amplitudes are 7.0, 19.0 and 19.0 MV/m (amplitude of the on-axis accelerating field). The amplitude in the first booster cavity (7 MV/m) is set to the maximum value possible with the planned 20 kW transmitter. 19 MV/m corresponds to the beam loading of app. 200 kW per 2-cell booster cavity by on-crest acceleration.

The strengths of the four quadrupoles between the booster and the merger are adjusted to provide emittance compensation. Two quadrupoles inside the merger are adjusted to compensate the linear part of the space charge dispersion. Four quadrupoles between the merger and the linac optimize the bunch size at the beginning of the linac. Aberrations in the linac are visible, if the transverse rms beam sizes in the linac exceed 1 mm.

To calculate the initial quadrupole gradient values a self-written code is used. The code tracks individual slices in Kapchinsky-Vladimirsky approximation. An algorithm for minimization of an objective function is also implemented in the program. The objective function is composed of the weighted projected transverse emittances and the beam sizes behind the linac. Further optimization was pursued with ASTRA.

The main ‘knobs’ accessible to tune the optics, their set value, functionality and tuning range are listed in the following table, again the settings are for the standard mode at 6 MeV.

	Setting for standard mode	Tuning range, function
Laser pulse length	7ps rms	Tunable between 3 ps and 10 ps for a YLF laser
Laser spot size on cathode	Flat top, radius 0.8 mm	Fully adjustable
Gun phase	15°	>10° to extract full current; the higher the gun phase the longer the bunch and the larger the energy spread
Max. gun field on axis	39 MV/m	Critical to keep bunches short
Solenoid	0.071 T	Emittance compensation solenoid. The strength depends on the bunch charge.
Booster cavity 1	-90°, -7 MV/m	Application of an energy chirp for bunch compression or additional acceleration at low average current
Booster cavity 2	-3°, -19 MV/m	Acceleration to 6 MeV
Booster cavity 3	-3°, -19 MV/m	
Quadrupoles before merger	< 0.02 T/m	Emittance compensation
Quadrupoles in merger	< 0.1 T/m	Dispersion suppression
Quadrupoles behind merger	< 0.2 T/m	Emittance compensation and fitting of Twiss conditions for linac

Table 13: The main 'knobs' accessible to tune the optics, their set value in the standard mode, functionality and tuning range

The most important bunch parameters are listed in Table 14 at three locations: Behind the booster module, behind the last merger dipole and behind the linac. The following pictures show the development of the emittance, the transverse beam sizes and the bunch length between the cathode and until behind the linac. The transverse and longitudinal phase space plots are taken at locations close to those of the bunch properties.

Parameter	Unit	Behind booster	Behind merger	Behind linac
Distance from cathode	m	4.986	10.689	17.4641
Energy	MeV	6.1	6.1	49.4
Energy spread (projected) abs. / rel.	keV / -	30 / 4.9e-3	22 / 4.4e-3	251 / 5.1e-3
Correlated energy spread	keV	-29	-21	249
Bunch length	mm / ps	1.8 / 6	1.3 / 4.3	1.3 / 4.3
Trans. emittance x, y	π mm mrad	0.83 / 0.83	1.09 / 0.86	0.82 / 0.82
Long. emittance	π keV mm	11.1	8.0	38
Beam size x,y	mm	0.68 / 0.68	0.63 / 1.14	0.21 / 0.28

Table 14: Bunch properties behind the booster, behind the merger and behind the linac

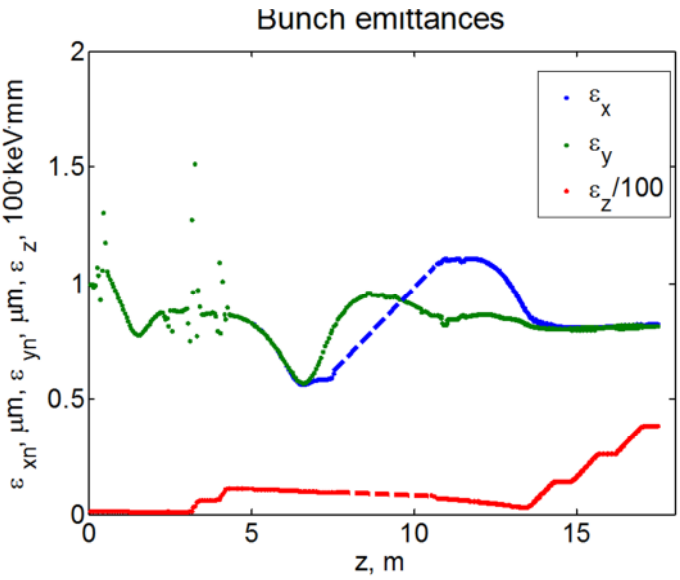

Figure 10: Development of the emittances (x – blue, y – green, z – red) from the cathode until behind the linac.
Dashed line parts (x- and z- emittance) in the merger replace unphysical values given by the ASTRA postprocessor in the field of dipoles and/or in a rotated coordinate system. The longitudinal emittance (ε_z) grows in the booster and linac cavities due to the cos(ωt) non-linearity of the accelerating field.

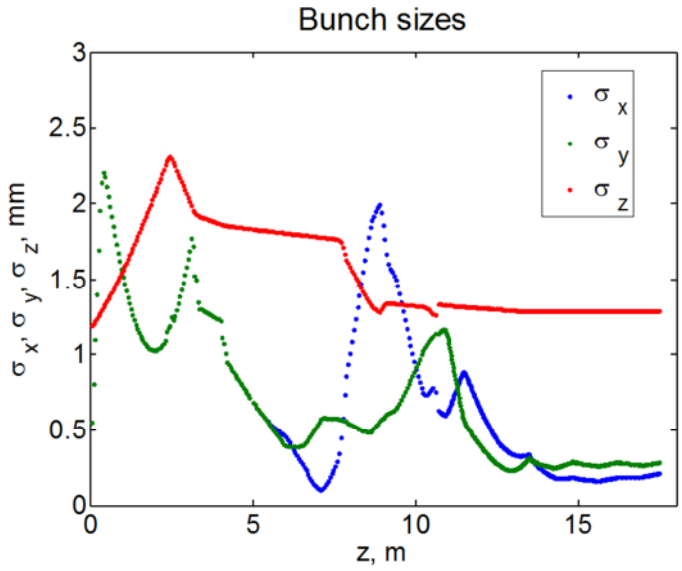

Figure 11: Development of the bunch sizes (x – blue, y – green, z – red) from the cathode until behind the linac.
The beam is round until the first quadrupole behind the booster. The compression in the first booster cavity and in the merger is clearly visible. The final bunch length is 1.33 mm rms.

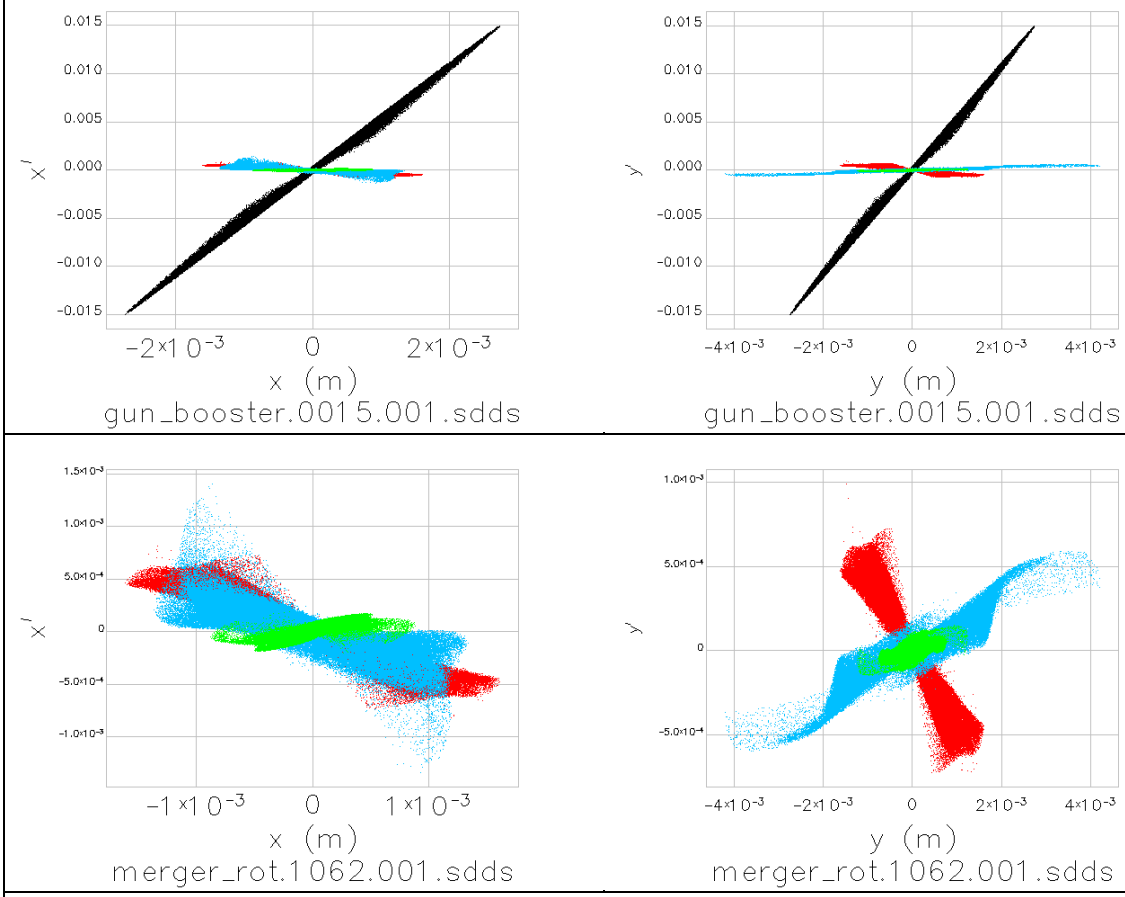

Figure 12: Horizontal (left) and vertical (right) phase spaces
Black @ s=0.15 m, behind the gun cavity; red @ s=5.00 m, behind the booster (P1); blue @ s=10.62 m, behind the merger (P2) and green @ s=17.46 m, behind the linac (P3)

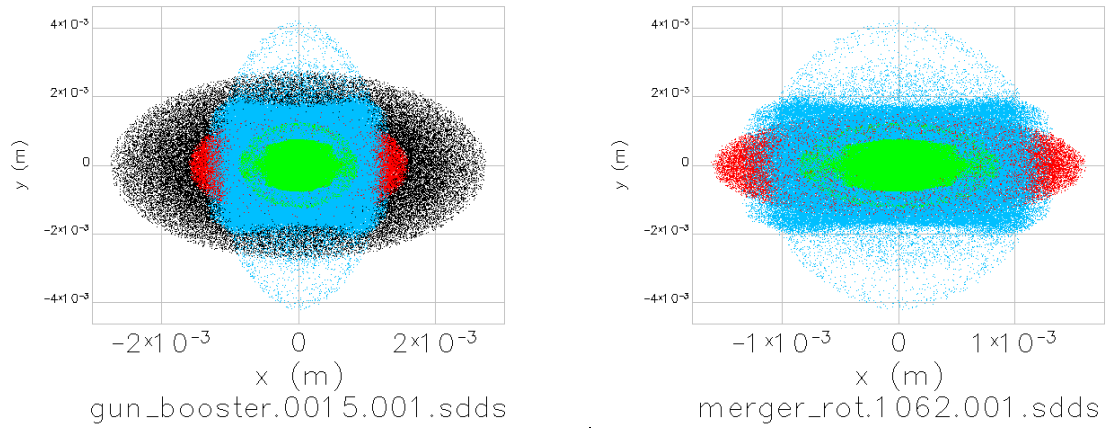

Figure 13: X, Y phase spaces
Black @ s=0.15 m, behind the gun cavity; red @ s=5.00 m, behind the booster (P1); blue @ s=10.62 m, behind the merger (P2) and green @ s=17.46 m, behind the linac (P3)

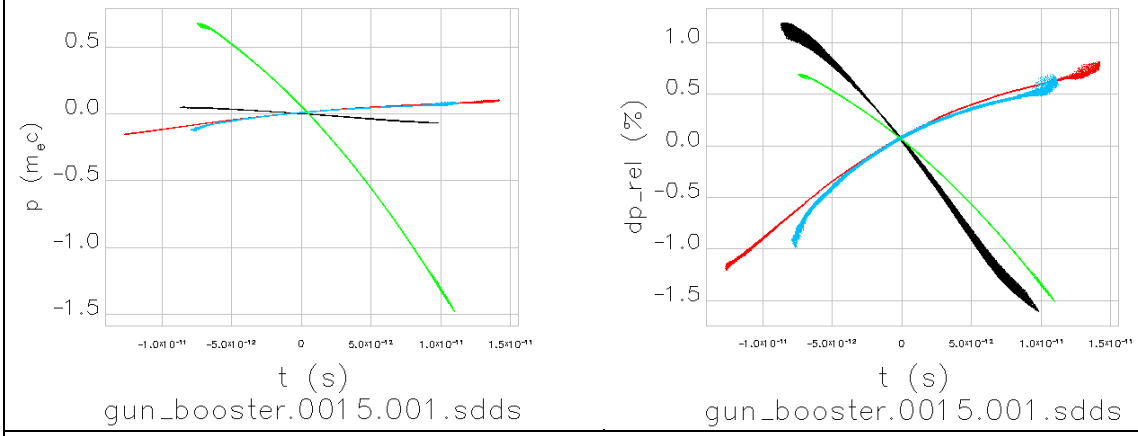

Figure 14: Longitudinal phase spaces in absolute (left) and relative (right) values
Black @ s=0.15 m, behind the gun cavity; red @ s=5.00 m, behind the booster (P1); blue @ s=10.62 m, behind the merger (P2) and green @ s=17.46 m, behind the linac (P3)

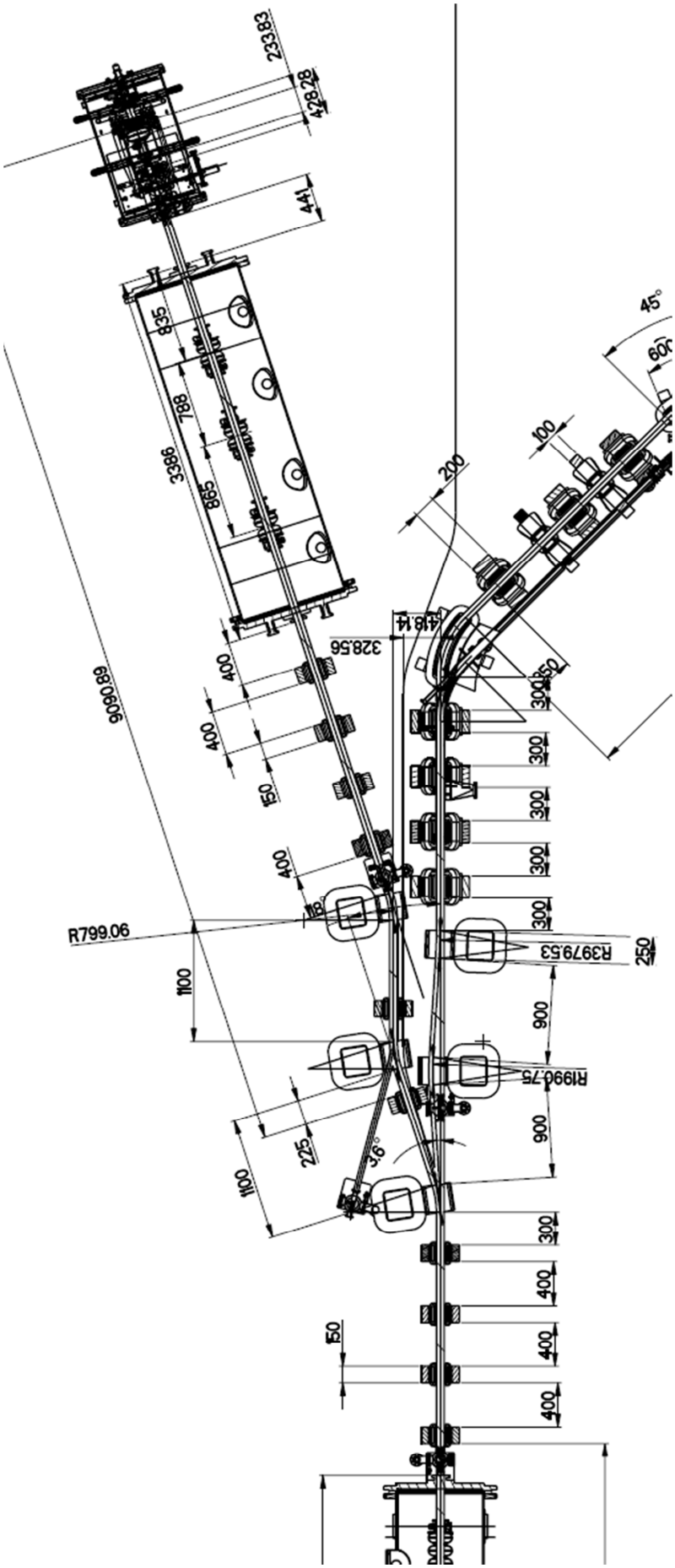

Figure 15: Technical drawing of the injector

2.3.1.5. Recirculator optics requirements

The recirculator transports the accelerated beam from the linac exit via a potential experiment back to the linac entry, where it is decelerated to recover the beam energy. The primary goal for its layout is a beam transport without significant losses while conserving the excellent quality of the beam. The recirculator will be designed to have also compressor capabilities, as an optional feature of B*ERL*inPro is the generation of short (100 fs-range) pulses. Various beam physics aspects determine the layout of the recirculator:

- High transmission: In order to minimizing the loss rate a large transverse acceptance is required. Together with a sufficiently large vacuum chamber this is achieved by tuning the optics to moderate β-functions of a few tens of meters. A large longitudinal acceptance is realized by minimizing the dispersion function inside the achromatic arcs, by using four 45° dipoles.
- Variable R_{56}: For the low energy spread mode we plan to keep the bunch length unchanged from the injector and benefit from a small energy spread in the recirculator (R_{56} = 0 m). In the short pulse mode bunch compression in the recirculator is mandatory. Therefore the R_{56} is tunable over a broad range -0.25 m < R_{56} < 0.25 m, for the standard mode R56=+/-0.14m.
- Betatron phase advance: It determines the character of the interference between the linac's higher order modes (HOM) from the accelerating and decelerating passage of the beam and can be used to maximize the BBU limited current threshold.
- Coherent Synchrotron Radiation (CSR): CSR power is emitted in the arc dipoles and widens the energy spread of the beam. This results in emittance dilution even at 50MeV. The amount of emitted CSR power is practically independent of the Twiss parameters. The CSR induced emittance growth though can be minimized by either tuning the Twiss parameter values in the bending magnets or by a suitable phase advance between CSR emitting bends so that the energy modulation leading to emittance dilution cancels out.
- Non-linear beam transport properties: Non-linear effects like T566, the RF-curvature or fringe fields can limit the compression capabilities of the arc (e.g. T566). Higher order multi-poles can be used for non-linear corrections and to linearize the longitudinal phase space. Moreover, multi-pole magnets might be required to optimize the transport of beam halo. Whenever implemented in the magnet lattice they require well separated Twiss parameters to be effective.
- Matching: To be able to tune the optics in arcs and in the straight sections independently, sufficient matching quadrupoles are foreseen, four each before and behind the two arcs.

The linear optics with the Twiss parameters presented later is a weighted tradeoff between all these requirements.

Guiding the beam from the linac exit back to its entry could be achieved by a ring segment like a storage ring but the most compact shape is a racetrack structure. It consists of two

180° arcs connected by two straight sections: one accommodates the linac, the beam injection and extraction and in the other an experiment could be placed.

Various designs exist for 180° arcs: a single 180° bend, two 90° bends, three times 60°, four times 45° or the bates arc [2]. The 60° and 45° options were studied in detail. The 45° solution benefits from a lower maximum dispersion and better tuning properties due to the reduced vertical edge focusing of the dipoles and an additional quadrupole introduced between the central dipoles. The spatial requirements of the 45° arc lie only insignificantly above the 60° arc.

In order to suppress the dispersion outside the arcs and simultaneously to adjust a specific value of R56 at least two quadrupole families are required. A third one is introduced to adjust the Twiss parameters. Simulations show, that all quadrupoles are focusing in the horizontal plane, due to the implicit vertical focusing of the parallel faced dipoles. That's why a fourth quadrupole is placed between the central dipoles to introduce variable vertical focusing. In this configuration the R56 can be tuned over a range much wider than required with respect to bunch compression issues, while keeping the arc achromatic at a low maximum dispersion and at acceptable beta function values.

To match the Twiss parameters between the arcs and the straight sections four individually powered quadrupoles are placed up- and downstream of each arc. Due to the limited drift space in between these quadrupoles their efficiency is limited. Investigations on reducing the number of matching quadrupoles are ongoing.

Four sextupole magnets per arc are foreseen to counteract for non-linear beam transport effects as described above.

Two achromatic dipole chicanes, composed of three dipole magnets each, are placed up- and downstream the linac. They compensate the deflection that the high energy beam experiences in the dipoles needed for the low energy beam for the injection into and the extraction out of the recirculator. The last dipole of the injector chicane is shared with the merger; the first one of the extraction chicane is shared with the beam splitter, guiding the 'spent' beam into the dump line. The deflections of the high energy beam are closed (no residual horizontal offset) so that the injection and extraction beam energy can be changed independent of the recirculator optics, except for the bump amplitude inside the chicane, which scales with the ratio between injection and recirculator energy. Between each chicane and the linac four short quadrupoles are placed to match the low energy beam into the linac and adapt to the BBU conditions. The effect of these quadrupoles on the high energy beam is not negligible.

2.3.1.6. Recirculator simulations

Linear optics calculations as well as optimizations and tracking studies have been performed using ELEGANT [3].

In Figure 16 the Twiss parameters of the B*ERL*inPro recirculator optics in the standard mode are shown. The R56 in the arcs is tuned to +/-0.14 m, corresponding to a bunch length of 2 ps in the straight section. The maximum dispersion is about 60 cm (absolute) and tuned to zero outside the arcs and the chicanes. The size of the beta function in the recirculator strongly depends on its values inside and behind the linac. They are moderate

for the standard mode, but can grow largely if the conditions in the linac are changed, e.g. due to BBU requirements.

	No. / fam.	Length[m]	Strength
Dipole magnets (parallel faced)	8 / 1	0.6 (45°)	B = 0.22 T, rho = 0.76 m
Quadrupole magnets - inside each arc - outside the arcs	 7 / 7 16 / 16	 0.2 0.2	 $\|k\| < 10$ 1/m² $\|k\| < 10$ 1/m²
Sextupole magnets	8 / 4	0.1	not used in standard mode

Table 15: Magnetic elements of the recirculator, operated in the standard mode

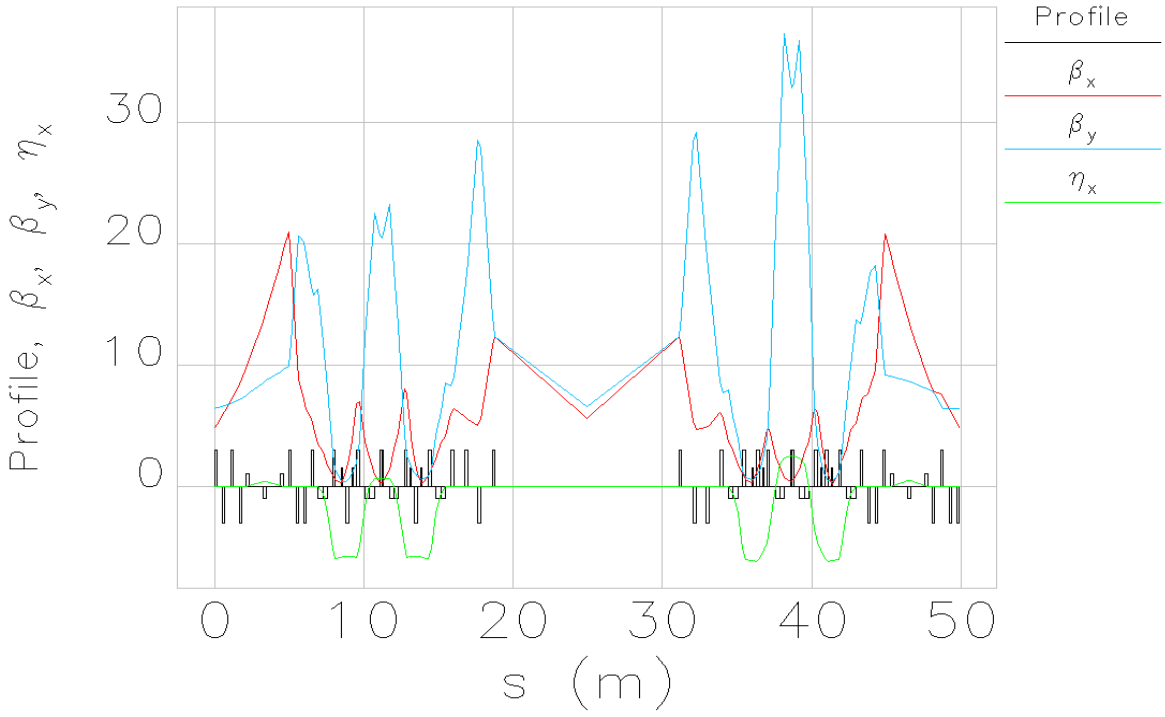

Figure 16: Twiss parameters
Red: horizontal, blue: vertical beta function [m] and dispersion, green, [dm] of the B*ERL*inPro recirculator for the standard mode, R_{56} tuned to +/- 0.14 m in the arcs.

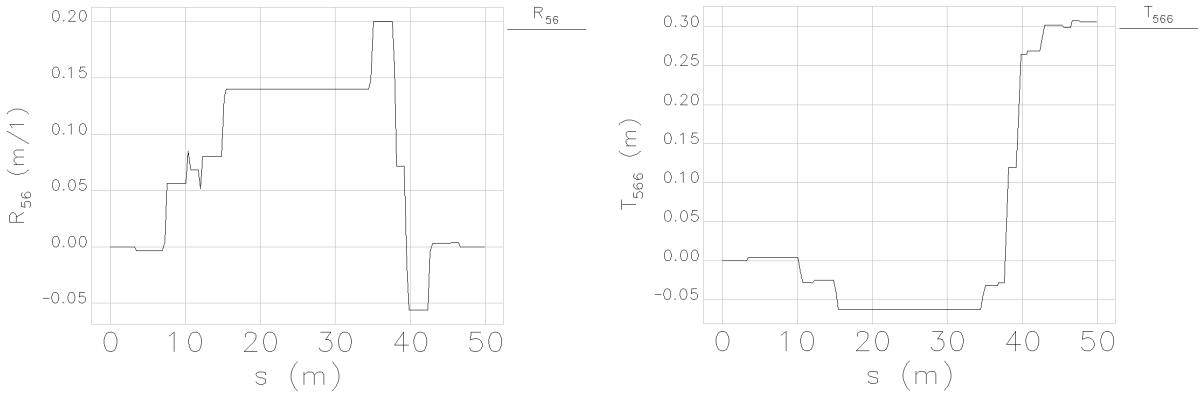

Figure 17: Evolution of R56 and T566 in the recirculator for the standard mode.

In Figure 17 the evolution of R56 and T566 is shown. Up to the end of the first arc (~20m) R56 reaches the value required to compress the bunch to the required 2 ps. In the second arc it is reduced again to enable a highly efficient energy recovery in the second linac passage. The intrinsic increase of the R56 in the first bend of the second arc in combination with the unavoidable energy spread of the bunch leads to even shorter bunches. Enhanced CSR probably is the reason for the emittance growth in the second arc. The T566 plot shows generally small values not capable to significantly influence the bunch length.

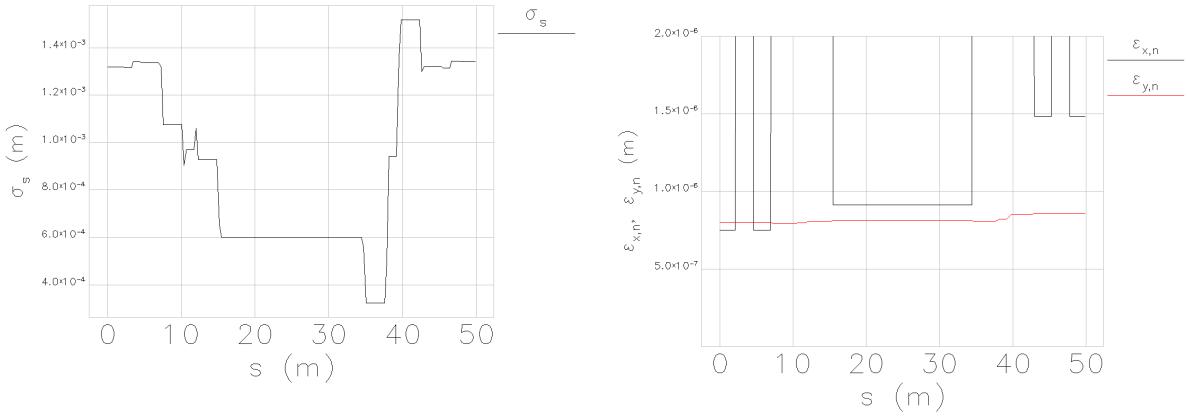

Figure 18: Evolution of bunch length (left) and emittance (right) in the recirculator for the standard mode.

In Figure 18 the development of bunch length and the emittance in the recirculator are drawn. The bunch length clearly corresponds to the R56. The emittance in the straight section is almost conserved: In the horizontal plane it grows by about 20%, in the vertical by below 5%. Due to the inevitable compression at the beginning of the second arc the horizontal emittance is further increased by about 60% as already mentioned.

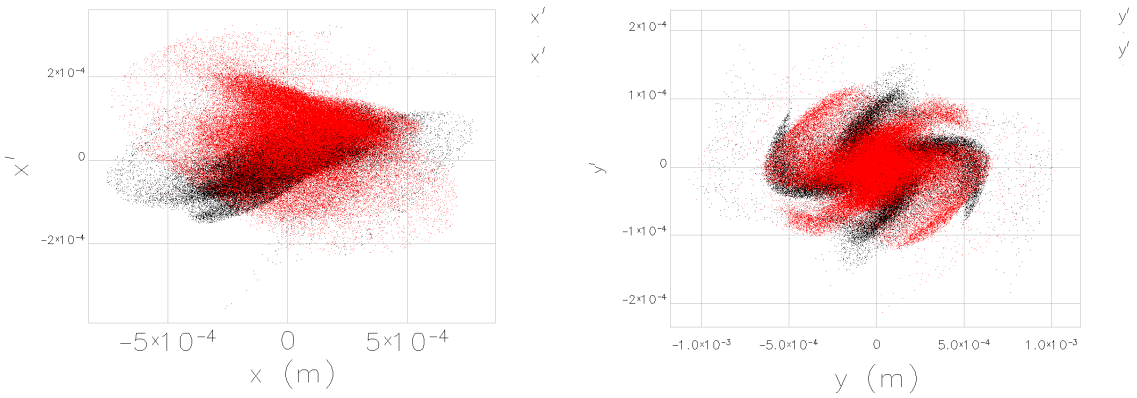

Figure 19: Horizontal and vertical phase space behind the linac (black dots) and at recirculator end before the second entrance to the linac (red dots).

In Figure 19 the horizontal (left) and vertical (right) phase space is depicted at the exit of the linac (red dots) and after recirculation before the second entrance to the linac (black dots). The deformations of the phase space are adopted from the injected beam and transported through the recirculator. Further investigations of the injector will investigate this and search for improvements.

In Figure 20 the transverse beam dimensions along the recirculator and the longitudinal phase space are plotted. The pattern of the horizontal beam size is clearly dominated by the linear dispersion inside the arcs. Maximal values of about $\sigma_x \approx 3$ mm arise from the linac phase and corresponding momentum chirp. The longitudinal phase space at the end of the recirculator resembles that of the beginning quite well so that an efficient energy recovery and a decelerated beam with moderate energy spread can be expected.

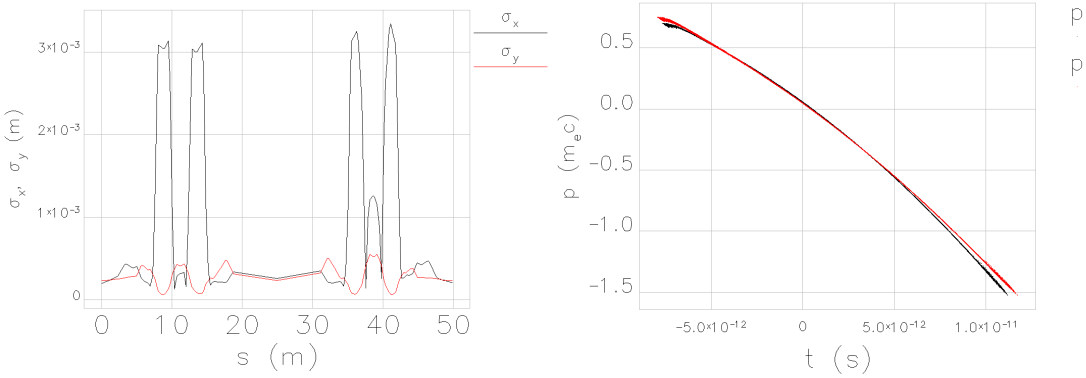

Figure 20: Left: Transverse beam size over the recirculator, right: Longitudinal phase space behind the linac (black dots) and in front of the linac (red dots).

2.3.1.7. Path length adjustment

In order to the recover the energy, the accelerated beam passes the linac a second time with a phase shift of 180°. This ensures not only the balance of invested and recovered energy but also the cancelation of the momentum chirp, imprinted in the accelerating linac passage. The phase shift is achieved by setting the recirculator path length to $(n+\frac{1}{2})\lambda_{rf}$.

Due to the limited alignment accuracy of the recirculator magnets a path length adjustment knob is mandatory. The required adjustment range can be derived from the expected alignment tolerances and from the foreseen injection energy variation between 5 and 10 MeV, where the bump amplitudes in the high energy chicanes define the path length. A value of about 10 mm is expected to be sufficient. Such a range can be covered by shifting the two central bending magnets in the second arc longitudinally by about 2 cm each. The quadrupole in between has to adjusted horizontally to avoid steering by an off axis passage. A draft of this scheme is shown in Figure 21.

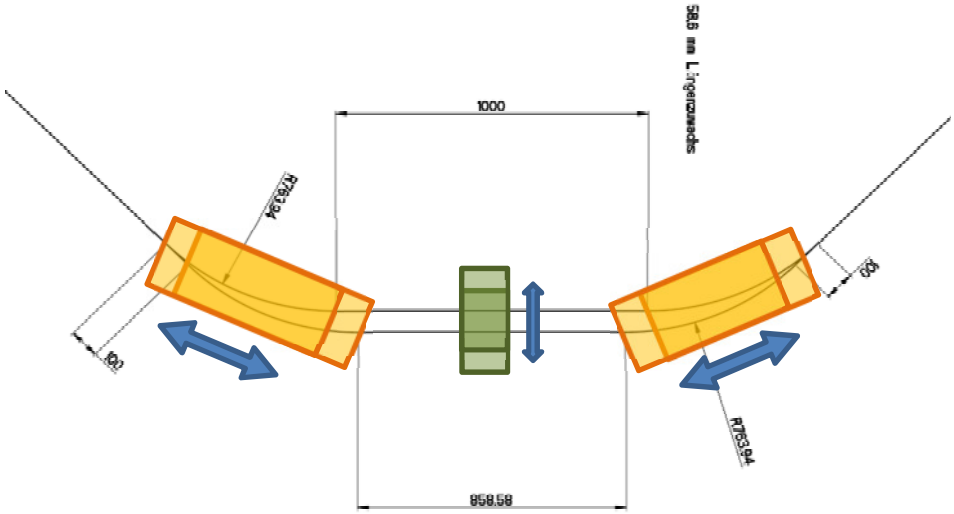

Figure 21: Principle of the path length adjustment
The two central bending magnets are shifted longitudinally in the arcs and the position of the quadrupole is adjusted transversely.

2.3.1.8. Trajectory correction

No trajectory correction system has been developed so far. A basic layout for the distribution of beam pick up's is described in 2.6.3. Additional coils integrated in the main magnets will be used for steering whenever possible: Horizontal: Dipoles and sextupoles, vertical: Sextupoles. It has to be investigated if also the quadrupoles can be used in this way – saturation effects in the iron and limited field homogeneity might inhibit such an operation. In this case dedicated steerer magnets are necessary, which have not yet been implemented in the current magnet lattice.

2.3.1.9. High power beam dump

The decelerated beam is separated from the accelerated high energy beam in the first dipole of the extraction chicane. The magnets forming this chicane are of the same kind as those of the injector chicane. Two options for the first part of the dump line have been investigated:

- no additional dipole in the dump line: In this case the dispersion can reach large values. Since the beam's energy distribution is hard to predict reliably this might limit the beam line transmission to the dump.
- a second dipole and a quadrupole are used to build up an achromatic arc. Here large horizontal beam sizes due to linear dispersion are avoided. This requires a little more space and hardware.

At the moment the second option is favored. To reduce the power per square unit in the dump, the transverse beam size has either to be statically widened by quadrupole or solenoid magnets until the corresponding limit is undercut. Alternatively the small beam spot could be swept by a pair of steering magnets, to distribute the power over the whole dump surface. Both options have reliability limits, which possibly can be extended by applying a mixture of the methods.

2.3.2. High current

2.3.2.1. Beam breakup instability

One challenge for ERLs is the transverse beam breakup instability (BBU), which may limit the beam current. The severances of this problem has been revealed in early experiments at the recirculating SRF accelerators at Stanford [4] and Illinois [5], where threshold currents of this instability occurred at a few microamperes average beam current. In the works of Rand and Smith [6] higher order dipole modes were identified as drivers of this instability. In the late 80's a detailed theoretical model and simulation programs were developed [7, 8]. Nowadays the interest in this problem is renewed. The demands for a more detailed theory and for adequate simulation programs [9-11] are posted by the needs of high current (~100 mA) ERLs.

When an electron bunch passes through an accelerating cavity it interacts with dipole modes (e.g. TM110) in the cavity. It exchanges energy with the mode and it is deflected by the electro-magnetic field of the mode. After recirculation the deflected bunch will interact again with the same mode in the cavity. If the net energy transfer from the beam to the mode is larger than the energy loss due to the mode damping the beam becomes unstable.

The threshold current for the transverse beam breakup may be estimated for the case of a single cavity and single mode as [10]

$$I_b = -\frac{2pc^2}{e\omega\left(\frac{R}{Q}\right)_d Qm_{12}\sin(\omega T)}, \qquad (1)$$

where p – is the beam momentum, ω – the HOM frequency, $(R/Q)_d$ – the HOM impedance, Q – quality factor, m_{12} –element of recirculator transfer matrix, T – recirculation time and c, e – fundamental constants.

Another approach [11] gives estimation for multi-pass ERLs in the form

$$I_b \approx I_0 \frac{\lambda\!\!\!^{-2}}{Q_a L_{eff} \sqrt{\sum_{m=1}^{2N-1} \sum_{n=m+1}^{2N} \frac{\beta_m \beta_n}{\gamma_m \gamma_n}}}, \qquad (2)$$

where I_0- Alfven current, Q_a is the quality factor of HOM, $\lambda\!\!\!^{-} = \lambda/2\pi$, λ is the wavelength corresponding to the resonant frequency of the TM_{110} mode, γ_m is the relativistic factor at the m-th pass through the cavity, β_m – is the Twiss parameter, L_{eff} – is the effective length of the cavity. This expression shows that it is preferable to have small β-functions at low energies.

With Eq. (1) we may roughly estimate that for a stable beam and 100 mA, dipole modes have to be damped stronger than

$$f\left(\frac{R}{Q}\right)_d Q < \frac{pc^2}{\pi e m_{12} I_b} \sim 10^7\ \Omega \cdot GHz, \qquad (3)$$

where $f=\omega/2\pi$, I_b =100 mA and m_{12} ~ 1 m were taken for the estimation.

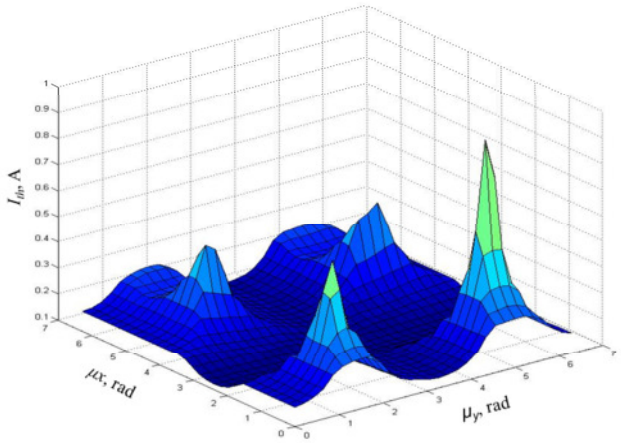

Figure 22: The results of 2D phase scan.

The BBU instability has been simulated for a 50 MeV linac based on three standard TESLA-type cavities [12, 13] using the GBBU code [14]. The TESLA-type cavities were used in the modelling because the cavities planned to be used in B*ERL*inPro are still in the design stage, but they are expected to have better (smaller) HOM impedances. The frequency spread of the dipole modes due to fabrication accuracies is expected to be of the order of 10 MHz. In the modelling we set the differences between the frequencies of the dipole modes for different cavities to 1 MHz. The recirculator optics was modelled using the transfer matrix from the end of the linac after acceleration to the beginning of the linac before deceleration and it was assumed to be adaptable to BBU needs. First we set the transfer matrix to have independent betatron phase advances in the x and y plane and

scanned over the phase advances using 30x30 points. The Twiss parameters of the beam were taken from recirculator simulations, as listed in Table 16. The results of the modelling are presented in Figure 22. The threshold current varies from ~110 to ~930 mA.

α_x	-3.528e-02
β_x	1.249 m
α_y	-1.458e-02
β_y	2.092 m

Table 16: Twiss parameters of the beam used in the simulations, behind the linac

f, GHz	R/Q, Ohm	Q
1,713	86	40000
1,739	118	32000
1,865	42	21000
1,873	58	27000
2,578	90	19000

Table 17: The most relevant polarized HOM modes for TESLA cavities used in the modelling. Both polarizations of the modes have nearly equal parameters.

The modelling results show, that for the assumed HOM parameters (see Table 17) 100 mA is feasible at all betatron phase advances in the recirculator. However, the smallest value of the threshold current is ~110 mA. If the quality factor R/Q of some modes will be higher than expected or if the frequencies of some HOMs in different cavities overlap (frequencies difference is smaller than the bandwidth of the mode) [9, 15, 16], then the beam might become unstable. Therefore it is suggested to have addition quadrupoles in the beam line to adjust the phase advances by $\pm\pi/2$ independently in the x and y planes.

2.3.2.2. CSR effects

The expected incoherent synchrotron radiation in B*ERL*inPro is low due to the low beam energy and does not affect the particle dynamics in the machine. Coherent synchrotron radiation, on the other hand, is independent of the beam energy and its effect on the performance has to be studied.

Following [17], the characteristic transverse distance in a dipole, i.e. the transverse offset between the bunch position and its own radiation after a distance σ_z, is given by $L_\perp = 2\sqrt[3]{9\sigma_z^2 R}$, where R is the bending radius of the dipole. For the standard optics of B*ERL*inPro with a bunch length of 0.6 mm (2 ps) and a bending radius of 0.8 m, $L_\perp = 2.8\ \mathrm{cm}$, smaller than the horizontal vacuum chamber dimensions. Therefore, shielding of the radiation by the vacuum chamber can be neglected. As the transverse beam size is

much smaller than $L_\perp$, the one dimensional model is valid and the energy lost in the arcs can be estimated by e.g. [18]:

$$P_{CSR} = \frac{f_0 Q^2 R^{1/3}}{4\sqrt[3]{2}\varepsilon_0 \sigma_z^{4/3}} \left\{ 1 + N \frac{2\sqrt[3]{2}}{3\pi\sqrt{3}} \frac{\sigma_z^{1/3}}{R^{1/3}} \left[\ln\left(\frac{\sqrt{12}\sigma_z \gamma^3}{R}\right) - 4 \right] \right\}, \quad \frac{1}{\gamma} << \left(\frac{48\sqrt{3}\sigma_z}{R} \right)^{1/3} \leq \frac{2\pi}{N}.$$

$$P_{CSR} \approx 4.4kW$$

where f_0 is the bunch repetition rate, Q the bunch charge, and N the number of dipole magnets.

Modelling with the code ELEGANT [3] shows, that the total energy loss in the standard mode with an average current of 100 mA is about 3.5 kW, which is in agreement with the analytical estimation.

Due to high amount of radiated CSR power precautions for the vacuum chamber cooling should be made.

The maximum of the spectral power density is at the wave length of $\lambda_{csr} \approx 2\pi\sigma_z$, the corresponding frequency is of the order of 80 GHz. Since the metal vacuum chamber wall has high reflectivity in this frequency range, the collimation of the radiation can be important for the cryo modules.

The CRS power in the short pulse mode will be an important limitation factor of the average current. For a rough estimation we assume the same average power as in the standard mode to be the limit, and take the bunch length of 100 fs. The CSR power is proportional to

$$P_{CSR} \sim \frac{f_0 Q^2 R^{1/3}}{\sigma_z^{4/3}}$$

At 1.3 GHz repetition rate the bunch charge will be limited then to

$$Q_{0.1ps} = Q_{2ps} \left(\frac{0.1}{2} \right)^{2/3} \sim 10pC$$

2.3.2.3. Resistive wake

Total power losses in the vacuum chamber due to resistive wake fields can be estimated as [19]:

$$P = \frac{\Gamma\left(\frac{3}{4}\right)}{4\pi^2\sqrt{2}} \frac{cQ^2 L \sqrt{Z_0 \rho}}{r\sigma_z^{3/2}}$$

where L is the total length, Z_0 the vacuum impedance, ρ the resistivity of the vacuum chamber material and r the vacuum chamber radius.

The estimation shows that in the standard mode P=17 W for aluminum (in case of stainless steel P=50 W). The roughness of the vacuum chamber further increases these

values. As long as the loss power due to resistive wakes is much smaller than the expected CSR power no special considerations are required.

There are other impedance sources generating wake fields and causing losses, which influences on the beam are to be investigated still.

2.3.2.4. Ion accumulation

The rest gas pressure in the beam pipe of B*ERL*inPro is assumed to be about 10^{-9} mbar. In the vicinity of the electron beam this residual gas is rapidly ionized. The ionization time for molecules around the electron beam is less than 100ms (assuming the collision cross-section given in [20]). In the case of high repetition rate machines, such as B*ERL*inPro, no ion escapes the electron beam potential. The ions accumulate around the beam trajectory or may even get trapped in the electron beam, thus neutralizing the beam. A full neutralization due to the ions reduces significantly the space charge effects in the electron beam. In such a case in addition to the optical errors, acceleration issues and the ion-electron-scattering can increase the emittance to unacceptable levels. The maximum beam energy, where the neutralization by ions causes a significant reduction of the space charge forces is given by [20]:

$$E_{\max} = 511keV / \sqrt{1-\beta_{\max}^2} \quad with \quad \beta_{\max}^2 = 1-\sqrt{2\pi}\sigma_z / 2\Delta L ,$$

where σ_z is the rms bunch length and ΔL is the bunch separation. For different bunch lengths along the injector and main accelerator of B*ERL*inPro, the corresponding maximum beam energy varies from 5 to 9 MeV, clearly indicating that this effect should be addressed in future simulation studies for the injector section.

However, even a partial neutralization can lead to an intolerable error in betatron phase, and to emittance growth [20]. For instance, a neutralization fraction of 0.1% causes a relative phase error of 5% for the nominal operation mode of the B*ERL*inPro. Therefore, it is mandatory to fight the ion accumulation. Clearing electrodes with a voltage sufficiently high to draw ions away from the beam is the best tool. The potential of a round uniform electron beam of radius a in a round grounded beam pipe of radius r_0 is given by [20]:

$$V_0 = \frac{I_{av}}{2\pi\varepsilon_0\beta c}\left(\ln\left(r_0/a\right) - 1/2\right),$$

where I_{av} is the average current. The beam pipe of the B*ERL*inPro is only partially round. It varies in diameter from 4 cm to 7cm for round sections and has an elliptical shape with 4x7cm in the arcs. The beam size varies according to the betatron function. Thus, the beam potential varies from 18V to 38 V along the accelerator. According to [20] the voltage on the clearing electrodes needs to be much higher. It varies from 100 V for locations with high betatron amplitude and small round beam pipe to 2000 V for the section with low betatron amplitude and an elliptical beam pipe.

In order to determine the number and exact location of the clearing electrodes, a further impact of the accumulated ions has to be taken into account: The fast ion instability. This instability arises with higher ion densities around the beam causing a fast amplification of the random centroid oscillations of the electron beam. The characteristic time scale for this instability is given by [20]:

$$\tau = \frac{1}{n^2} \frac{\gamma \sqrt{3(\sigma_y(\sigma_x + \sigma_y))^3} \sqrt{A_{ion}}}{4\rho_{gas}\sigma_{col} r_e c \beta_{x,y} \sqrt{n_e^3 r_p \Delta L}},$$

where r_e is the classical electron radius, r_p is the classical proton radius, n_e is the electron density, ρ_{gas} is the gas density, σ_{col} is the collision cross-section and n is the number of the bunches. For B*ERL*inPro, the characteristic time can be made sufficiently long by placing the electrodes sufficiently close to each other. For instance, to obtain $\tau = 3\,ms$ the electrodes have to be placed such that the average time needed by ions to move to the clearing electrodes is about 0.4 μs (corresponding to n=520).

2.3.2.5. Halo and collimation

Dark current in the accelerating cavities usually grows exponentially with the field amplitude and limits the accelerating gradient. However, dark current particles are usually well separated in energy from the core of the beam and can be collimated in dipole magnets. Only those generated from the cathode region can overlap in energy with the core of the beam.

Beam halo, on the other hand, is one of the most important factors limiting the average current in high power ERL's. We call halo the particles in the "tails" of the bunch (3-10 σ_{rms}). As an important source of the halo particles in the beam we identify

- cathode and plug system
- strongly non-linear fields (aberrations)
- collimators

The cathode is the most natural source of the halo. Stray laser light, surface structure (geometrical and QE non-flatness, craters, etc.) and field emission of cathode and cathode insert edges with enhanced electrical fields are considered as probable causes.

Aberrations and non-linear fields must be controlled. For example, too strong solenoid fields used for the emittance compensation can over focus low current slices in the bunch and produce transverse diffusion. On the other hand, low solenoid strength in the current injector geometry leads to large transversal beam size and aberrations in the booster cavities.

Collimators used to clean the halo are themselves sources of multiple scattered particles which are partially transported further with the main beam.

Beam halo diagnostic and a collimation system are thus indispensable for the successful operation of B*ERL*inPro. A first absorber scheme is under consideration in the B*ERL*inPro merger section.

2.3.3. References

[1] K. Floettmann, ASTRA user manual, http://www.desy.de/~mpyflo/Astra_dokumentation

[2] J. B. Flanz, S. Kowalski, C. P. Sargent, An Isochronous Beam Recirculation Magnet System, IEEE Transactions on Nuclear Science NS-28 (1981) 2847.

[3] M. Borland, “elegant: A Flexible SDDS-Compliant Code for Accelerator Simulation", Advanced Photon Source LS-287 (2000).

[4] C. M. Lyneis, M. S. McAshan, R. E. Rand, H. A. Schwettman, T. I. Smith and J. P. Turneaure, The Stanford Superconducting Recyclotron, IEEE Transactions on Nuclear Science, Vol. NS-26, No. 3, June 1979.

[5] P. Axel, L. S. Cardman, H. D. Graef, A. O. Hanson, R. A. Hoffswell, D. Jamnik, D. C. Sutton, R. H. Taylor, and L. M. Young, Operating Experience with MUSL-2, IEEE Transactions on Nuclear Science, Vol. NS-26, No. 3, June 1979.

[6] R. E. Rand and T. I. Smith, Beam optical control of beam breakup in a recirculating electron accelerator, Particle accelerators, Vol. 11, pp. 1-13 (1980).

[7] J. J. Bisognano, R. L. Gluckstern, in Proceedings of the 1987 Particle Accelerator Conference, Washington, DC (IEEE Catalog No. 87CH2387-9), pp. 1078-1080.

[8] G. A. Krafft, J. J. Bisognano, in Proceedings of the 1987 Particle Accelerator Conference, Washington, DC (IEEE Catalog No. 87CH2387-9), pp. 1356-1358.

[9] G. H. Hoffstaetter, I. V. Bazarov, „Beambreakup instability theory for the energy recovery linacs”, Phys. Rev. ST AB 7, 054401 (2004).

[10] E. Pozdeyev, et al., “Multipass beam breakup in energy recovery linacs”, NIM A 557 (2006) 176-188.

[11] N. A. Vinokurov et al., Proc. of SPIE Vol. 2988, p. 221 (1997).

[12] http://tesla.desy.de/oracle/6i/CavityDB/GUI/ view?config=app_hom_meas

[13] L. Xiao et al., “Modelling imperfection effects on dipole modes in TESLA cavity”, Proceedings of PAC07, pp. 2454-2456.

[14] Generic Beam BreakUp (GBBU) by E. Pozdeyev.

[15] E. Pozdeyev, “Regenerative multipass beam breakup in two dimensions”. Phys. Rev. ST AB 8, 054401 (2005).

[16] Y. Petenev, A. N. Matveenko, A. V. Bondarenko, “Modelling of the beam breakup instability for B*ERL*inPro”, Proceedings of IPAC11, pp. 718-720.

[17] Ya. S. Derbenev, V. D. Shiltsev, “Transverse Effects of Microbunch Radiative Interaction”, SLAC-PUB-7181, 1996.

[18] E.L. Saldin, E.A. Schneidmiller, M.V. Yurkov, NIM A 398 (1997) pp. 373-394.

[19] A. Chao, M. Tigner, Handbook of Accelerator Physics and Engineering, World Scientific, 1998.

[20] G. H. Hoffstaetter, M. Liepe, NIM A 557(2006) 205-212.

2.4. Cold Systems – SRF Gun

2.4.1. SRF Gun

The ultimate performance of the ERL depends on the ability of the electron gun to deliver high brightness, high average power electrons to the main accelerator complex. For B*ERL*inPro this means an average current of 100 mA, a normalized beam emittance of better than 1 mm mrad and < 20 ps fwhm long electron pulses (upper limit to minimize RF curvature contributions to the transverse emittance). Furthermore, the electron gun should have the flexibility to generate pulses of higher charge at lower repetition rates or shorter pulses with less charge to meet specific experimental needs.

The beam energy from the gun has to be larger than 1 MeV to be able to capture the electron bunches from the gun directly into an $\beta = 1$ accelerating section and to minimize space charge driven beam dilution. The goal for B*ERL*inPro is to reach up to 2 MeV beam energy out of the gun.

We decided on a laser-driven SRF gun, as full control over the electron pulse properties (transverse and longitudinal pulse shape) can only be realized with photo-emission sources. Operation of an injector at high gradient and at 100% duty cycle is only possible using superconducting radio-frequency (SRF) technology. Hence the SRF gun combines the advantages of photo-emission sources and high-gradient, low-loss CW operation of a superconducting cavity. The main challenges for such a system are to achieve high average current and high beam brightness.

2.4.1.1. High average current

For any linear photo-emitter the average current, $I_{avg,}$ is given in practical units by

$$I_{avg} = q_e * \frac{P_L}{h\nu} * Q_E$$

with the photocathode drive laser photon energy $h\nu$ and average power P_L, the electron charge q_e, and the photo-emitter quantum efficiency $Q_E = N_e/N_\gamma$ at the drive laser photon energy. In order to reach an average current of 100 mA a combined laser power times quantum efficiency of $P_L * Q_E$ = 23.3W% is required in the right transverse and longitudinal pulse shape on the cathode. Materials which exhibit high QE are usually normal-conducting alkali antimonides or other positive (or negative) electron affinity semiconductors. Cornell, JLAB (both DC guns) and Boeing (with a normal-conducting RF gun) demonstrated Q_E for CsK_2Sb in excess of 10% at 352 nm and 1% at 532 nm [1].

CsK_2Sb is not a superconductor and thus needs to be thermally and electrically insulated from the SRF cavity. Issues emerge from the cathode/cavity interface, and the operation of a room temperature cathode inside an SRF cavity with high accelerating field. For this reason a special cathode insert and a procedure for cathode changing need to be developed. For average beam loading power levels in the 200 kW region minimum disruptive high power RF feeds must be implemented.

2.4.1.2. High brightness

For any photoelectron-source the minimum achievable emittance depends on the space charge limited emission for a bunch with charge q for a given launch field E_l :

$$\varepsilon_{scl} = \sqrt{\frac{q(h\upsilon - \phi_W)}{12\pi\varepsilon_o E_l m_o c^2}}$$

with the photocathode work function ϕ_W of the cathode material and the vacuum permittivity ε_o. This is the static limit where the surface charge field induced by the electron bunch equals the launch field. Operation at this limit results in severe decompression of the electron bunch. That is the reason why photoelectron guns, NCRF and SRF alike, usually operate at least three times away from the space charge limited emittance [2] or up to six to ten times away [3]. For an emittance of 1 mm mrad at 77 pC bunch charge and allowing for some emittance degradation in the passage from gun to linac the sliced emittance goal for the gun is ε_{gun}= 0.6 mm mrad. Therefore launch field levels between E_l = 7-20 MV/m have to be reached. Depending on the cavity design specific E_{pk}/E_{acc} ratio and cathode recess, the peak field on the cathode area should not exceed 25-30 MV/m. Beyond this level generation of dark current from field emission might be problematic. The exact barrier needs depends strongly on the local work function, field level and surface morphology of the cathode and cathode substrate and needs to be investigated.

To conserve the emittance, the first focusing element, usually a solenoid, should be placed as close as possible to the cathode. At the same time any additional magnetic field needs to be avoided on any superconducting material of the cavity. The solenoid magnet poses a risk to the operation of the SRF cavity as residual magnetic fringe fields might be trapped inside the superconducting material leading to a degradation of the surface resistance of the cavity material and in a worst case to a quench. At the same time, flexible transverse laser pulse shaping must be included to minimize the impact of space charge on the emittance.

2.4.1.3. Baseline design

For the baseline design we propose an SRF gun with a 0.6-cell SRF cavity operating at 1.3GHz with an embedded CsK_2Sb photocathode illuminated with short laser pulses from a high repetition rate drive laser. The number and shape of the gun cavity cells will be discussed in Section 2.5.2.1.

Figure 23 shows the schematic layout of the SRF gun consisting of a gun cryogenic vessel with the gun cavity and a superconducting solenoid. The RF power is fed into the gun cavity with two fundamental power couplers (FPC) to symmetrize the coupler kicks. A magnetic shield protects the gun cavity from residual fringe fields of the solenoid. A higher order mode (HOM) load is located inside the cryo vessel. A laser input port and a diagnostics port are located in the section between gun and booster.

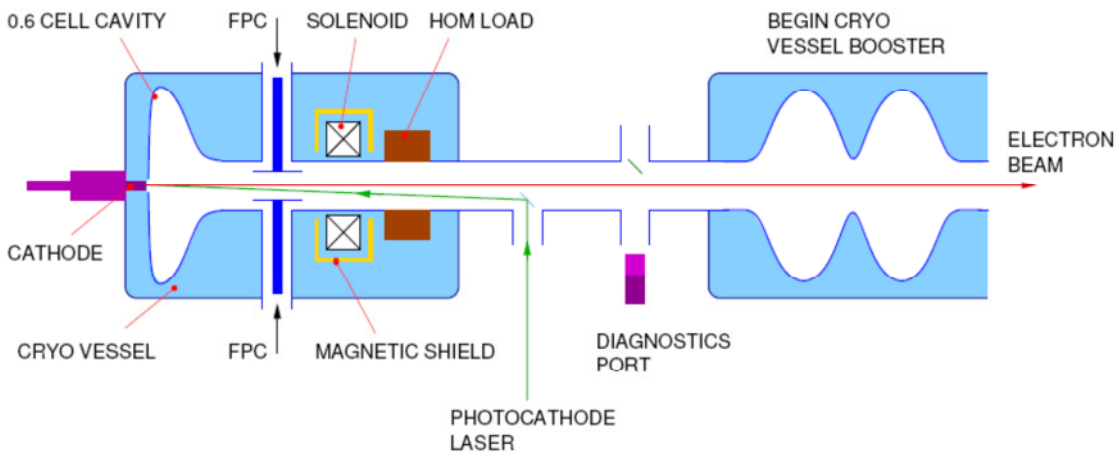

Figure 23: Schematic baseline layout of the B*ERL*inPro SRF gun section
The minimum distance between cathode plane and exit of the gun cryo module is roughly 1.0m, the minimum distance of the warm region between gun and booster cryo module is 0.6m.

The beam pipe radius inside the cryo module is 106 mm to allow propagation of the higher order modes into the HOM load. The radius will be reduced after the HOM load in the warm section at the laser input port.

Beam diagnostics in the warm section between gun and booster will be minimal and allow only for setting up the gun with phase scans and beam based alignment. This can be done with a view screen, a Faraday cup and steering coils. Detailed measurements of the beam parameters will happen in the beam line section following the booster module.

All gun subsystems like cavity, cathode, solenoid and coupler need to be integrated into a single cryogenic vessel. The vessel should facilitate changing of the cathode during operation of the gun in a revolver type way from a barrel holder. Furthermore it is envisaged to change complete barrels of cathodes to be replenished in a preparation chamber. The operation of semiconductor cathodes poses stringent requirements on the warm and cold parts of the cryogenic vessel. Especially the operation of CsK_2Sb cathodes requires vacuum levels in the 10^{-11} mbar range.

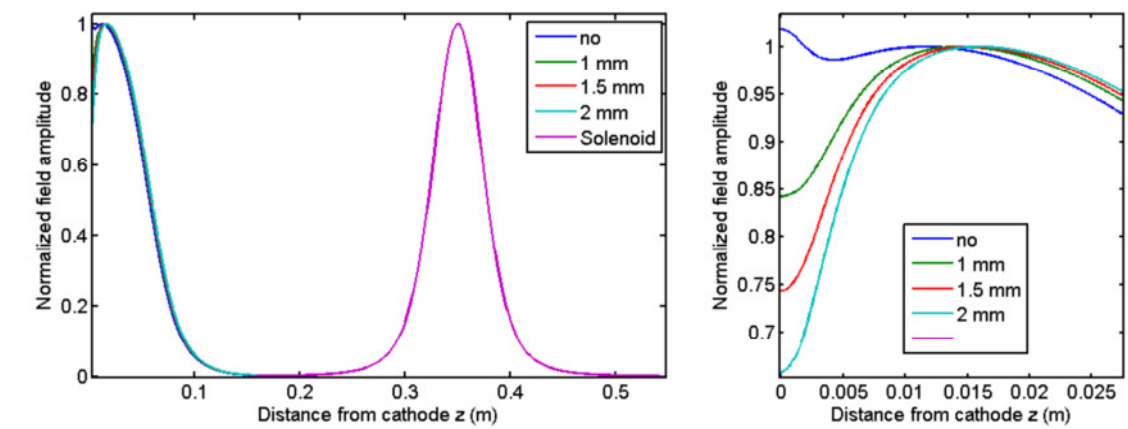

Figure 24: Left: Cavity electric field on axis and solenoid magnetic field profile for the baseline design. Right: Zoom into the region close to the cathode plane. The cavity field is shown for various levels of cathode recess.

Figure 24 shows the fields of the SRF cavity and the solenoid. The cathode in the SRF cavity can be recessed to yield radial RF field for transverse focusing during emission. Initial studies showed that a cathode recess of 1.5 mm results in the best overall emittance performance [4]. The solenoid is located 0.35 m away from the cathode plane, which is a lower limit set by vacuum components and the size of the fundamental power coupler.

2.4.1.4. Staged approach

The gun for B*ERL*inPro is developed in three stages. The first stage, Gun0, avoided the issues connected to the integration of a normal-conducting cathode into the SRF cavity by using a superconducting Pb cathode. The Pb cathode film was directly coated on the back wall of the cavity. Gun0 has been completed in 2011 with first beam achieved in April [5], and the measurement of all fundamental beam parameters [6, 7].

The main goal of Gun1 is to show that space charge and RF induced emittance growth can be controlled in an SRF gun system and to develop a cathode insert system for high quantum efficiency normal-conducting cathodes.

For Gun2 the goal is to accelerate 100 mA of current to 2 MeV, so the development of suitable high average power RF couplers is the main focus of R&D activities in this stage. Gun2 will be the operating gun for B*ERL*inPro.

The goals and parameters for each stage at summarized in Table 18.

	Gun0	Gun1	Gun2
Goal	Beam Demonstration (First beam April 2011)	High brightness R&D gun (2014)	High average current operating gun (2015)
Cathode material	Pb (SC)	CsK_2Sb (NC)	
Cathode QE_{max}	1*10^-4@258 nm*	1*10^-2@532 nm	
Drive laser wavelength	258 nm	532 nm	
Drive laser pulse length and shape	2..3 ps fwhm Gaussian	≤ 20 ps fwhm Gaussian (flat-top)	≤ 20 ps fwhm Gaussian
Repetition rate	8 kHz	54 MHz/25 Hz	1.3 GHz
Electric peak field	20 MV/m*	≥ 10 MV/m and ≤ 25 MV/m	
Operation launch field	5 MV/m*	≥ 10 MV/m	
Electron energy	1.8 MeV*	≥ 1.5 MeV	
Bunch charge	6 pC *	77 pC	
Electron pulse length	2-4 ps rms*^{o}	≤ 20 ps fwhm	
Average current	50 nA*	4 mA/40 µA	100 mA
Normalized emittance	2 mm mrad*	0.6 mm mrad	

Table 18: Tentative beam parameters for the SRF gun R&D program

*Results for Gun0 are preliminary, ^{o}: the value describes the emission time of the electron pulse.

2.4.1.5. Gunlab

All SRF guns for the B*ERL*inPro programme will be commissioned, characterized and optimized in Gunlab, a surface radiation protection hall connected to the SRF cavity test facility HoBiCaT. Gunlab will be equipped with an electron beam diagnostics line allowing 6D phase space measurements, with a transverse deflecting RF structure and electron beam energy spectrometer. Due to constraints from the radiation shielding only beam average currents below 50 µA at 2 MeV beam energy may be generated. For this reason we are planning to run the gun system at high average macro-pulse current with low duty cycle (54 MHz micro-pulse rate at 25 Hz macro-pulse rate). This operation mode is compatible with current laser technology developed for photo guns. Only inside the B*ERL*inPro accelerator hall it will be possible to generate and accelerate average currents approaching 100 mA at 1.3 GHz repetition rate.

2.4.1.6. Cathode preparation system

The successful operation of an ERL requires a photocathode which can provide high average current and low emittance. Currently, mainly alkali-antimonide and multi-alkali systems as well as II-V III-V semiconductor cathodes activated to negative electron affinity are investigated. GaAs:CsO is the photocathode material most commonly used in DC electron guns since the material combines low emittance and high quantum efficiency with the possibility to obtain a highly polarized beam. Recently, CsK_2Sb has been rediscovered as the photocathode material of choice for high average current guns. The system was used at the Boeing RF gun and could deliver average currents of up to 32 mA [8]. CsK_2Sb is the envisaged cathode material for B*ERL*inPro. Lifetimes over several days and extracted average current of 20 mA at JLAB [9] and even exceeding 25 mA at Cornell [10] have been demonstrated recently, only a factor of four away from the B*ERL*inPro parameters. The system has never been operated inside an SRF gun, though.

Within the B*ERL*inPro project we want to establish a research platform at HZB to investigate the issues from the integration of CsK_2Sb and other advanced photocathodes into an SRF guns and verify the beam properties such systems can deliver.

The characterization of the cathode materials by state-of-the-art surface and material science techniques is important. The determination of the materials emissive behavior and the photoelectron transport within the material is useful for the overall understanding of these materials and the improvement of the cathode performance.

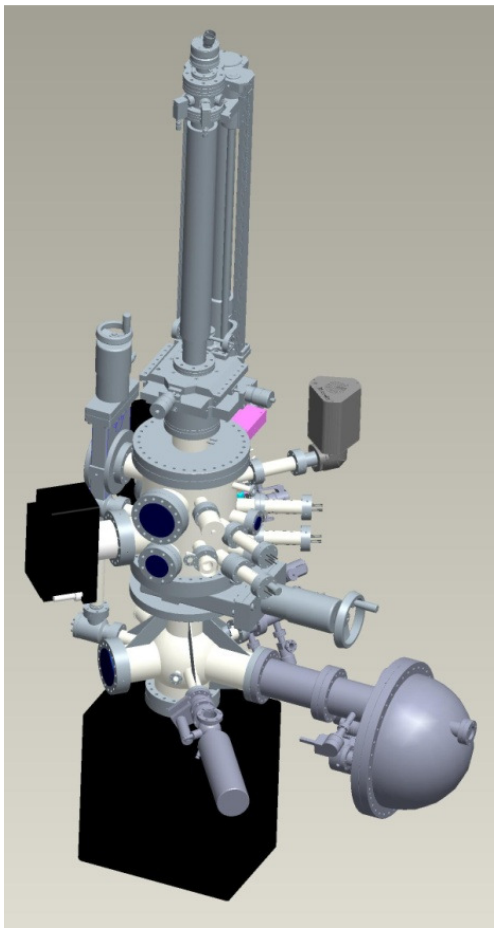

Figure 25: UHV System for cathode preparation

The cathode preparation system shown in Figure 25 for the growth of CsK_2Sb has been designed and ordered. The system will be divided into two parts: A preparation chamber on top and a chamber for the analysis of the films below. Due to the sensitivity of the electron/ion energy analyzer towards alkali metal adsorption the analysis chamber must be separated by a valve. The preparation chamber offers the possibility to adsorb one or two materials at the same time with a controlled co-adsorption process. After preparation the sample can be transferred to the analysis chamber without any manipulation risks. The analysis chamber provides several experimental possibilities: The stand-alone X-ray tube enables state of the art XPS measurements at 1487 eV (Al) or 1253 eV (Mg) photon energy. The integrated ion source will be able to produce a focused, moveable ion beam of high current density. This instrument enables depth profiling and LEIS (low energy ion scattering) measurements. Depth profiling is useful to determine the homogeneity of the films; ISS offers the possibility to determine the chemical nature of the top layer as well as a precise growth rate. The analysis chamber also offers the possibility to measure quantum efficiency and holds spare flanges for further measurements, yet to be developed e.g. the planned compact analyzer for emittance measurements.

It will be possible to mount the analysis chamber onto existing beam lines at the Bessy II facility and/or transfer the cathodes samples into existing end-stations. The project will make extensive use of the unique possibilities offered by the Bessy II infrastructure, e.g. photoemission, pump probe and diffraction experiments.

2.4.1.7. DC gun setup

For better understanding of the photoemission and field emission processes affecting the beam parameters a compact photocathode DC gun test facility at several kV bias voltage with a variable field gradient at the photocathode surface will be constructed. Field strengths up to 20 MV/m can be achieved by introduction of the intermediate electrodes with a variable operating voltage. The measurements at the DC setup will be focused on field emission studies and homogeneity of the efficiency over the photocathode area.

2.4.2. Laser

The development of the B*ERL*inPro gun is split into three stages (Gun0 to Gun2), each having different goals and milestones (2.4.1.4). Consequently, the different stages need different laser systems. While the laser for Gun0 with its metallic Pb photocathode is emitting in the UV (258 nm), the laser for Gun1 and Gun2 are emitting in the green spectral region around 530 nm.

The project goal of 100 mA average current inevitably requires a green emitting photo cathode with high quantum efficiency (QE). With CsK_2Sb as a cathode material a QE in the range of 10% and higher has been routinely obtained. This material eases the demands on the laser since it emits already in the green spectral range and a second (rather inefficient) frequency conversion stage is obsolete.

2.4.2.1. UV laser for Gun0 (review)

The laser for Gun0 has been developed in cooperation with the Max-Born-Institute in the group of Ingo Will. It was delivered end of 2010.

It consists of a Yb:YAG passive mode locked oscillator and a Yb:YAG regenerative amplifier followed by a frequency quadrupling stage.

The laser emits pulses at 258 nm with a length of 2.5 ps (fwhm). The energy per pulse is 0.15 µJ in the UV; the repetition rate can be adjusted stepwise from 120 Hz to 30 kHz.

In first experiments this laser system has been successfully operated during measurements of the fundamental beam parameters of Gun0.

2.4.2.2. Green laser for Gun1 (Laser1)

By using a CsK_2Sb cathode in Gun1 the requirements for the photocathode laser are significantly different. With the high QE of CsK_2Sb cathodes, emitting in the green spectral region already a moderate laser power of a few Watt will allow for a high average current in the order of up to 100 mA. (2.3 W at 532 nm for 100 mA with a QE of 10%)

The goal for Gun1 is the production of 77 pC bunches at a “medium” repetition rate of 54 MHz. This would result in an average current of 4 mA. Gun1 will be operated in the HoBiCaT bunker which can only handle up to 40 µA due to radiation shielding regulations.

The laser therefore is designed as a pulse train laser with a macro pulse repetition rate of up to 25 Hz. The laser system runs at a basic repetition rate of 54 MHz (oscillator frequency, micro pulse frequency). The baseline mode will be an operation with 400 µs long pulse trains with a train repetition frequency of 25 Hz corresponding to a 1% duty cycle. The average current is thus reduced from 4 mA to 40 µA.

The operation of a pulse train laser not only allows for operation of Gun1 in the HoBiCaT bunker, it also provides more flexibility in diagnostics. The number of micro pulses within a train can be reduced stepwise down to 1 single pulse. This allows for operation at full bunch charge but low average beam current.

Specification of the laser

The desired laser produces pulses of green light at 54 MHz repetition rate with a minimum pulse length of 3-4 ps (fwhm, Gaussian shape). The pulse length can be lengthened to 20 ps (fwhm) by a small modification inside of the laser. The suitable energy of the pulses is 18nJ. This is 10 times more than the pulse energy that is actually needed at the photocathode. This factor is to compensate for losses at the beam shaping elements in the optical beam line as well as for aging of the photocathode.

The pulse energy of 18 nJ corresponds to an average power of 1 W during the bursts (green light, $\lambda = 527$ nm wavelength). Assuming a conversion efficiency of 33-50%, this requires a laser power in the infrared of 2-3 W during the bursts.

The pulses of 54 MHz repetition rate should be arranged in bursts of 0-4 ms duration at an adjustable repetition rate of 1-25 Hz, thus the number of pulses in these bursts will be programmable between 1 and ~ 200 000.

Finally, the laser will be synchronized to the RF of the linac with better than ~1 ps synchronization accuracy.

2.4.2.3. Basic concept for the 54 MHz burst-mode laser

The proposed laser system that fulfills the parameter set above consists of the following components:

1. a diode-pumped Nd:glass oscillator that generates the initial pulses with 54 MHz repetition rate
2. a fiber preamplifier, with stretcher and compressor for chirped-pulse amplification
3. a "burst-mode unit" containing an appropriate pulse generator and a Pockels cell for selection of the bursts from the CW output signal of the fiber amplifier
4. the pulsed Nd:YLF multi-pass amplifier that boosts the energy of the laser pulses to 2-3 W average power during the bursts
5. the wavelength converter for generating green light
6. a control computer for remote control of the laser
7. an RF synchronization system for synchronizing the Nd:glass laser oscillator to the electronic RF master oscillator of the linac

The scheme of the laser is shown in Figure 26. In this approach, the pulse duration is mainly determined by the gain narrowing in the final Nd:YLF power amplifier. Since the fiber preamplifier reduces the gain required in the final amplifier to ~25, the expected pulse duration at the output is between 3 and 4 ps (fwhm). In order to further simplify the system, one could omit the fiber preamplifier at the cost of somewhat longer pulses of 5-6 ps duration (Anyway, the calculations for the standard mode operation assume a 7 ps rms Gaussian pulse). However, besides the longer pulse duration, this simplified system cannot be extended with an optional pulse shaper (see below).

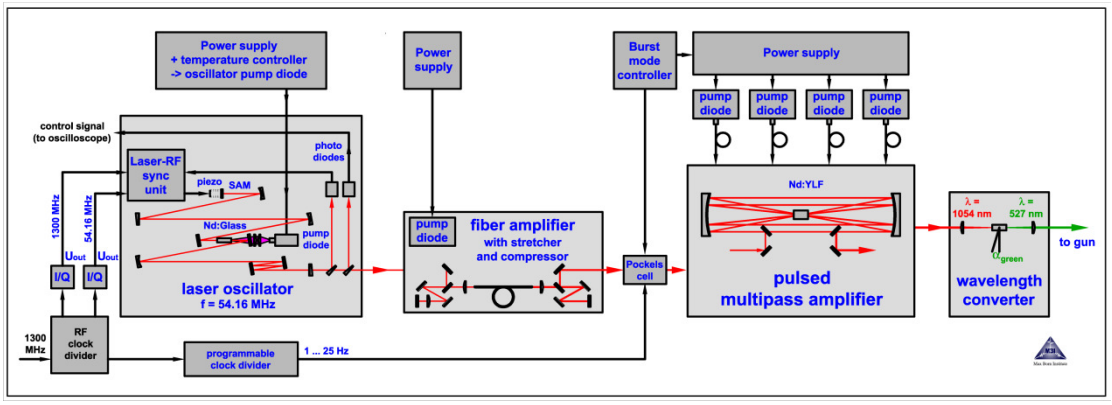

Figure 26: Conceptual scheme of the burst-mode photocathode laser

Laser option #1: 1.3 GHz repetition rate

The system can be extended to produce pulses with 1.3 GHz repetition rate. This requires the following extensions:

- replacement of the 54 MHz laser oscillator by a laser oscillator that produces pulses with 1.3 GHz repetition rate
- modification in the RF and in the control system to synchronize and stabilize the laser oscillator
- changes in the wavelength converter to adapt the intensity in the conversion crystal appropriately

These extensions will increase the average power of the laser only to a limited extent. An increasing to more than several Watt of green light requires a redesign of the last amplifier stage of the laser.

Nevertheless, this opens up a possible way of a staged extension from 54 MHz toward the final 1.3 GHz required for the B*ERL*inPro.

Laser option #2: CW operation

The laser can be extended to CW operation with moderate effort, provided that the average power needed can be limited to several Watt of green light.

Laser option #3: Pulse shaping

Generation of flat-top pulses can be accomplished by adding the following components to the laser system:

1. the multicrystal birefringent pulse shaper [11]
2. an XFROG[1] system for measurements of the pulse shape
3. a broadband laser amplifier with a built-in fast-scanning optical delay line for generating the short sampling pulses for the XFROG.

The components (2) and (3) enable the user of the laser to align the pulse shaper appropriately. The laser can also be equipped with an additional control system that permits complete automatic alignment and stabilization of the pulse shape. This technology is currently being developed at the MBI for the photo injector drive laser of the upcoming European XFEL.

The Figure 27 shows the shape of a flat-top pulse obtained with a Nd:YLF photocathode laser built at the MBI in 2008/2009. The duration of the flat top can be varied by changing the number of birefringent crystals in the shaper.

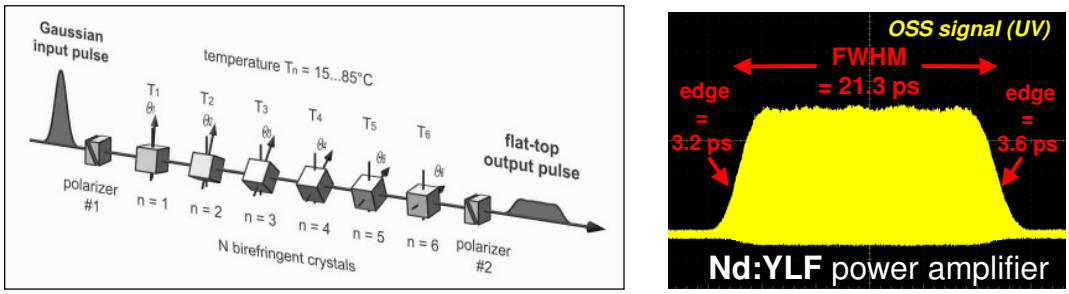

Figure 27: Pulse shaper (left) and cross correlation signal (right) showing the shape of the flat-top pulses generated at the MBI with a similar Nd:YLF laser.

2.4.2.4. The B*ERL*inPro 1.3 GHz Laser (Laser2)

With the options described above Laser1 can be upgraded to the 1.3 GHz system.

The building blocks of Laser2 are mostly conceptually independent and can be tested with Gun1. The beam shaping setup described as option 3 for example can be tested within the 54 MHz system and then be moved to the final 1.3 GHz system with only minor changes.

The 54 MHz CW option could be useful for B*ERL*inPro operation with a 4 mA average current at full bunch charge. It therefore allows for commissioning with reduced current.

The final 1.3 GHz system incorporates a multi-pass amplifier that has to deliver 2-3 times more power than the one described above. Though the concept seems to be clear, still some development work has to be done.

[1] XFROG: Cross-correlation Frequency Resolved Optical Gating

This is also true for a diagnostic mode laser for B*ERL*inPro. A laser with reduced repetition rate at full bunch charge will be needed for machine diagnostic. At present it is not clear whether one could cut out bunches from a 1.3 GHz train fast enough to clearly separate two succeeding micro pulses.

Alternatively a second oscillator with a lower repetition frequency (e.g. the 54 MHz oscillator) has to be implemented for the diagnostic mode.

Again the components of Laser1 can be used, reused or simply copied for this purpose.

The B*ERL*inPro laser concept offers high flexibility allowing for changes in the time schedule of the project.

2.4.3. Synchronization

With a projected electron bunch length of a few ps (RMS) the required precision for a timing and synchronization system is still within the range of a conventional RF distribution. This RF system will serve as a day zero solution and will provide a well understood and reliable solution for the first commissioning of B*ERL*inPro. In a later stage of the project the bunch length will be reduced to about 100 fs and a more precise synchronization system will be necessary. With the aim of understanding as much of the underlying physics of the machine as possible, a comprehensive diagnostic of the bunch parameters is essential. Also with respect to the use of the short pulses in a future experiment at the ERL, it is necessary to have knowledge of pulse length and arrival time at the experimental station.

2.4.3.1. Layout / Components

A stability of a few 100 fs can be achieved by carefully choosing the components and by running them under well stabilized environmental conditions. The low phase noise oscillator as well as the RF distribution components will be placed in temperature stabilized racks near the accelerator hall. The layout of the components will take care for short distances of the signal distribution path in general.

Expertise about stabilizing the environmental conditions is available from other labs (e.g. Cornell (Figure 28), DESY). Low phase drift RF-cables are installed inside a plastic tube that is ventilated with air of constant temperature. Tests are underway at HoBiCaT.

Figure 28: Low drift RF cables are passed inside a plastic tube that is ventilated with air of constant temperature. Photo taken at Cornell University.

2.4.3.2. Optical distribution for diagnostic

While the precision of a conventional RF based synchronization/signal distribution system seems to be sufficient for a first day operation of B*ERL*inPro, any optimization will need a precise and reliable diagnostic.

A high precision optical synchronization system consisting of a quartz stabilized fiber laser as a master oscillator, a stabilized fiber link and a fiber laser at the diagnostic stage is capable to reach an accuracy in the order of a few 10 femtoseconds.

Utilizing electro optical techniques a bunch arrival time measurement as well as an electron bunch length measurement can be implemented. The stabilized fiber link therefore can serve as a reference distribution which allows for benchmarking the conventional RF distribution.

The infrastructure for this optical reference will be foreseen. Space will be reserved in the photocathode laser room as well as tubes for the fibers to be blown in later.

A large scale timing distribution system based on short pulse fiber lasers has been developed at DESY for the XFEL Project. Many of the DESY developments will be given to industry for mass production, which enables us to buy well designed products needed for an optical synchronization.

2.4.4. References

[1] B. Dunham et al., Proc of ERL2011, see for a summary D. Dowell et al., NIM A 622 (2010) 685-697.

[2] LCLS and FLASH, D. Dowell and S. Schreiber private communication.

[3] UCLA Pegasus, P. Musumeci private communication.

[4] T. Kamps, Proc. of HBHAP 2009.

[5] T. Kamps et al., Proc. of IPAC 2011.

[6] A. Neumann et al., Proc. of SRF 2011, IPAC 2011.

[7] R. Barday et al, Proc. of PST 2011.

[8] D. H. Dowell, et al., Appl. Phys. Lett. 63 (15) (1993) 2035.

[9] J. Smedley, et al., Proc. of IPAC 2011.

[10] B. Dunham, et al., to be published in ERL2011.

[11] Will, Klemz, "Generation of flat-top picosecond pulses by coherent pulse stacking in a multicrystal birefringent filter", Optics Express **16**, 14922-14937 (2008).

2.5. Cold Systems

The acceleration of electrons in B*ERL*inPro is performed by superconducting radio frequency systems (SRF-systems).

B*ERL*inPro will have three different superconducting acceleration sections each with an own cryogenic module:

- a gun module containing one 0.6-cell cavity for electron generation and first acceleration
- a booster module containing three 2-cell cavities to gain the energy up to 6-10 MeV, depending on the bunch charge
- a main linac module accommodating three 7-cell cavities to accelerate the beam to the final energy using the energy recovery principle

The use of SRF systems in the main linac is indispensable. The beam loading in this section is nearly canceled by the energy recovery principle. To gain from this reduction of RF transmitter power, the losses by the accelerating RF field in the cavity walls should be minimized. This leads directly to the use of superconducting cavities. The characteristic design features of the SRF linac section are given by:

- generating high accelerating fields with low cryogenic losses
- using strong higher order mode (HOM) damped cavity structures
- moderate RF power level for the fundamental input coupler (FPC)

In the gun and booster section, the full beam loading has to be covered, because the ERL principle is not applied in this part of the accelerator. This leads to RF power levels of several hundred kW. The design of the modules is dominated by the requirements of the high power FPC.

The SRF gun approach was chosen for having the highest potential for high current, low emittance applications.

For the booster section it is not obvious to use SRF technique. High power RF transmitters are needed to cover the beam loading. But having all needed components at hand, such as the high power FPC of the gun and the cryogenic environment, using SRF technique for the booster section is a cost effective solution as well.

2.5.1. High power RF

The high-power RF systems of an ERL are responsible for feeding adequate power with the required stability into the accelerating RF cavities. It amplifies a signal in the milliwatt power range from the master oscillator to a typical power level, from kilowatts to a few hundred kilowatts, which is fed to the fundamental power couplers of the accelerating cavities. Its main components are the preamplifier, the tube- or solid-state-based high power amplifier, with the corresponding power supplies and the RF-transmission line,

including a circulator. All RF systems of B*ERL*inPro are operated in continuous wave (CW) mode.

2.5.1.1. Power requirements

The power requirements of the RF systems depend on the main design parameters of the corresponding cavity and the beam current I. Closer attention has to be paid to the coupling strength of the fundamental power coupler (FPC) of the cavities.

The coupling strength, in the absence of the beam, given by the ratio between external and intrinsic quality factor, Q_{ext} and Q_0 respectively, gives the half-bandwidth, $f_{½}$, of the system

$$f_{½} = \frac{f_0}{2\,Q_L}$$

with f_0 the cavities resonance frequency and Q_L, the loaded quality factor given by

$$Q_L = \left(\frac{1}{Q_{ext}} + \frac{1}{Q_0}\right)^{-1}$$

where

$$Q_{ext} = \frac{\omega_0\, U}{P_{ext}}$$

and ω_0 the cavity's angular resonance frequency. Q_{ext} is the ratio of stored energy in a cavity U and the power P_{ext} leaking through the coupler in every RF period ω_0. Three factors drive the choice of Q_{ext}: The current to be accelerated, the expected cavity detuning Φ_b and the available power. The optimum setting for Q_{ext} using the beam current I and the geometric shunt impedance (R/Q) of the cavity is given by

$$Q_{ext} = \frac{V_{cav}}{\frac{R}{Q} I \quad \cos\Phi_b}$$

The required power to establish a given accelerating field V_{cav} at a given Q_L and an accelerating phase Φ_b is given by

$$P_f = \frac{V_{cav}^2}{4\left(\frac{R}{Q}\right)Q_L} \cdot \left(\left(1 + \frac{\left(\frac{R}{Q}\right)Q_L I}{V_{cav}} \cdot \cos\Phi_b\right)^2 + \left(\frac{\Delta f}{f_{1/2}} + \frac{\left(\frac{R}{Q}\right)Q_L I}{V_{cav}} \cdot \sin\Phi_b\right)^2\right)$$

Besides the beam loading, the necessary RF power is determined by the cavity's (micro phonic) detuning, Δf, over the cavity's half-bandwidth, $f_{½}$.

2.5.1.2. Injector transmitter

The power level of the four cavities in the injector, the gun cavity and the three booster cavities, is dominated by beam loading. There is no energy recovery in this part of B*ERL*inPro. For an energy gain of 6.5 MeV and a beam current of 100 mA the beam loading is 650 kW.

Each cavity will be powered by an individual transmitter. To reduce costs, only the gun cavity and two of the booster cavities will be equipped with high power transmitter of 270 kW_{CW}. One booster cavity will be powered by a medium power transmitter of 15 kW. This cavity can be used during machine studies at low currents to boost the energy higher than the nominal value or to introduce an energy chirp on the beam at nominal current.

The three 270 kW_{CW} high power transmitters are klystron based. At the nominal power the incremental gain is 0.5 dB/dB, a value where the low level RF control system (LLRF) is in a good working order. The klystrons have a special internal tuning of their cavities to provide a high linear output level at high efficiency of 52 %. This tuning prohibits operation in saturation, as the beam will be defocussed and might hit the klystron walls, destroying the tube.

The transmitter for the klystron is a set of different power supplies. The main power supply for the klystron beam is built by a matrix of 30 switched power supply units (Figure 29) resulting in 65.2 kV voltage and 9.2 A current to achieve 270 kW RF output power. It is designed to have a certified switch off to be integrated in the radiation interlock system.

Initially, the number of modules is reduced to 20 to reduce the investment costs while the gun has not achieved its design current. This reduces the voltage and maximum current of the power supply to an equivalent of about 160 kW RF power (Figure 30). Each transmitter is prepared to be upgraded to its full power later.

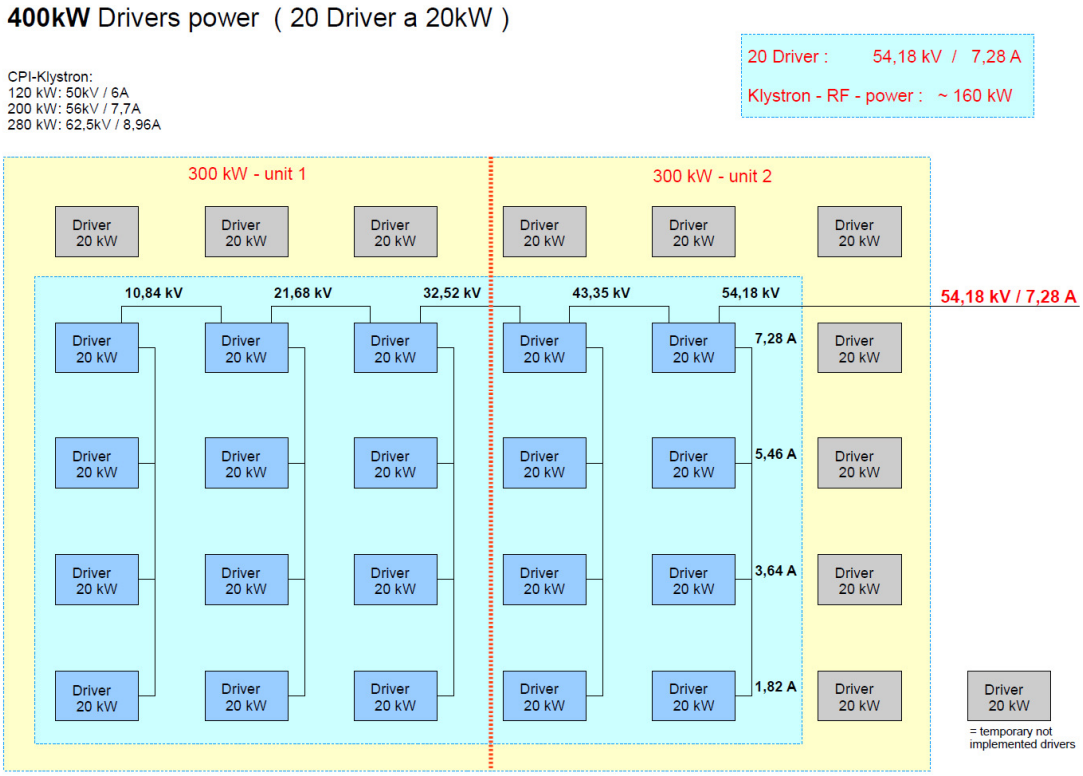

Figure 29: Matrix of the power supply modules for the anode voltage of the klystrons

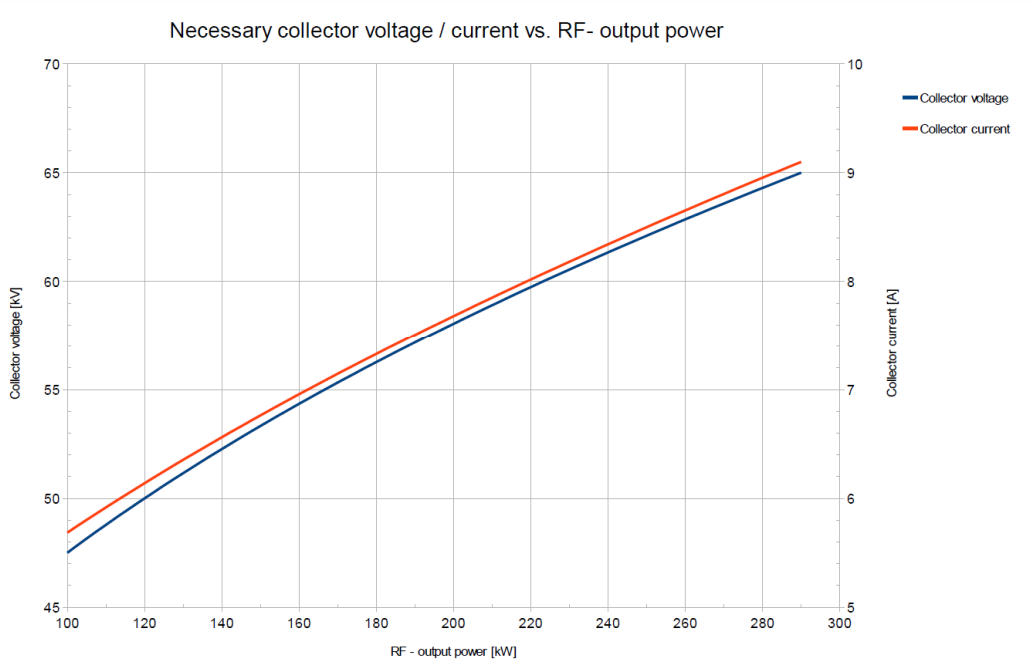

Figure 30: Maximal RF output of the klystron in dependence on the collector voltage and current.

One 270 kW transmitter at the gun and two 270 kW transmitter at the booster are sufficient to accelerate the beam to the desired energy but provides no overhead, as discussed later in 2.5.2.2. Booster cavity number one will be equipped with one linac transmitters (2.5.1.3.) to cover beam loading at low currents and to allow for using all three cavities for acceleration of the beam up to an energy of 10 MeV. Three-stub tuners in the waveguide shift the coupling strength of the fundamental power coupler by about a factor three to achieve high cavity voltages (Table 22).

The RF transmission lines will be water cooled waveguides of type WR650 for each injector transmitter. They have losses of 1 dB/100 m. In each line a circulator protects the klystron from reflections of the cavity. The losses of the circulator are 0.15 dB.

Assuming a waveguide length of 50 m, the losses of the waveguide are 0.5 dB. Including the circulator losses, the attenuation of the complete transmission line is 0.65 dB or about 15 % power loss. Including 5 kW safety margin the klystron power of 270 kW will end up to 225 kW usable RF power at the input couplers of each cavity (adequate 160 kW/130 kW).

In summary, the injector RF transmitter will be set up in 3 stages (Table 19):

1. Transmitter with reduced power limiting the beam current to a few 10 mA
2. Transmitter with full power to cover 100 mA beam current
3. Optionally, enhanced transmitter power in the first booster cavity, if advantageous from beam dynamics aspects

	base design		upgrade option
	stage 1	stage 2	
	transmitter power		
Gun cavity	160 kW	270 kW	270 kW
Booster Cavity 1	15 kW	15 kW	80 kW
Booster Cavity 2	160 kW	270 kW	270 kW
Booster Cavity 3	160 kW	270 kW	270 kW

Table 19: Transmitter upgrade stages

2.5.1.3. Main linac transmitter

In the main linac beam loading plays only a minor role for the RF power requirement due to the energy recovery principle. The power level for the transmitter is dominated by micro phonic detuning of the cavities operated with a bandwidth of only 13 Hz (2.5.1.4). A 15 kW transmitter is foreseen for each cavity. Solid state technology is the most reliable, maintainable and economic solution in this power range. The circulators are included in the transmitter modules. A 3" coaxial line with losses of 1.7 dB/100 m will be used as RF transmission line with internal air cooling being a cost-effective and “easy” to install solution. Assuming a cable length of about 100 m the remaining power at the cavity input coupler is 10 kW.

2.5.1.4. Low Level RF

The LLRF system is responsible for controlling the amplitude and phase *via* feedback loops and provides the input signal for the high power RF system. The feedback loops in digital technology is based on field programmable gate-array processors.

2.5.2. SC cavities and modules

Dimensions and design of the modules are mainly dominated by the size of the cavities, the adjustability of the cavities, the HOM dampers and the dimensions of the fundamental power couplers for the RF.

2.5.2.1. SRF gun

The general description of the SRF gun is given in 2.4.1, while this chapter describes the SC cavity cell and the cryo module.

Gun cavity

The design criteria of a gun cavity differ from the approach towards any other superconducting accelerating cavity. Besides optimizing the design for the typical SRF parameters affecting its performance as peak surface fields, multipacting regimes, accessibility for surface chemical treatment and mechanical stiffness, and the influence of the field distribution on longitudinal and transverse beam dynamics is of crucial importance. Furthermore, a normal conducting high-quantum-efficiency cathode must be inserted in the back plane and thermally isolated from the superconductor. The gun cavity will operate at high beam current and beam power, therefore might require strong HOM damping and high power fundamental couplers delivering hundreds of kilowatt of power to the beam in CW mode while avoiding emittance diluting coupler kicks.

As the beam leaves the cathode at a few electron volt kinetic energy, gaining about 1-2 MeV in the accelerating gaps of the cavity, it is subject to strong velocity effects. The longitudinal geometry of the cavity affects the transit time of the electron bunches and thus the phase with respect to the field when it leaves the cavity. This timing not only affects the longitudinal phase space and energy gain, but also the strength of the RF focusing by the radial field component.

Longitudinal focusing may be achieved by aiming for a positive slope of the extraction phase in the energy-phase diagram of the cavity. The energy-to-phase relation depends on the effective accelerating length of the cavity, including field penetration into the beam pipe and recess of the cathode tip.

To avoid space charge driven inflation of the beam the electric field component during beam extraction at the cathode has to be as high as possible. This favors high emission phases and a flat back wall of the cathode half-cell to achieve the highest field level at the cathode position. This means to maximize the ratio of the field at the cathode to the field anywhere on the surface and high emission phases to transform the high field at the cathode most effectively to field level during emission. This will further minimize the danger of high dark current levels.

Longitudinal beam stability depends on high field stability in the resonator. In CW mode the field stability is mainly affected by mechanical detuning of the cavity. Considering micro phonics and Lorentz-force detuning the back wall has to be constructed under some angle to improve its stiffness to achieve good field stability.

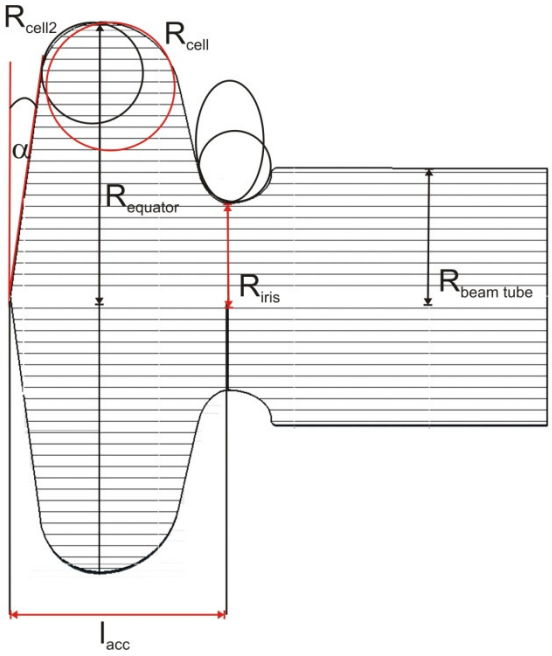

Figure 31: Sketch of a half-cell gun cavity showing the variable geometric parameters

Figure 31 shows a sketch of a half-cell gun cavity under investigation, including the geometric parameters which can be optimized to achieve the performance goals. First studies of a half-cell design for various effective accelerating lengths are listed in Table 20:

Parameter	0.6 cell	0.5 cell	0.45 cell	0.4 cell	0.4 cell
Iris radius (mm)	30	30	30	30	35
R/Q (Ω) (Linac definition)	143.2	126.5	119	111	106
l_{acc} (m)	0.069	0.058	0.051	0.047	0.047
E_{peak}/E_{acc} (β=1)	1.21	1.44	1.86	1.57	1.59
H_{peak}/E_{acc} (mT/(MV/m))	2.85	3.56	3.8	3.23	3.16
V_{acc} at 1 J stored energy (MV)	1.08	1.02	0.99	0.95	0.93
E_{launch} (MV/m) [1]	4.5	6.9	7.6	10.4	8.7
E_{kin} (MeV) [1]	1.43	1.35	1.28	1.22	1.23
Opt. phase (degree) (Optimized for energy gain)	10	15	17.5	23	19

Table 20: Parameters of gun cavities with different accelerating length

[1] For optimal launch phase with respect to kinetic energy and E_0=30 MV/m

For the given field values the following definitions apply: E_{acc} is the mean accelerating field gradient of the whole cavity, E_0 is the maximum field amplitude along the beam trajectory, E_{launch} the field level at which the particle beam is emitted from the cathode – thus depending on the launch phase –, $E_{cathode}$ the field level at the cathode's position and E_{peak} the maximum electric field anywhere on the cavity surface. Thus the energy gain in the cavity of an accelerating length l_{acc} is given by:

$$\Delta E = E_0 T(\beta(t)) \sin \varphi \, l_{acc}$$

where T is the beam energy dependent transit time factor which changes within the gun cavity along the accelerating gap and $E_0 T = E_{acc}$.

Reducing the effective length of the half-cell shifts the launch phase for maximum energy gain to higher values (Figure 32) for the small iris case. This coincides with an increased field level during emission, eventually improving the transverse emittance due to space charge effects compensation. The optimum phase is also a function of the field gradient in the half-cell, that also the constraints by the power coupler limiting the maximum field level act back on the cavity design.

An iterative approach of cavity design calculations and ASTRA beam dynamic simulations is applied to develop a design which fulfills the aspects of RF superconductivity, high beam current operation and a low emittance beam. Further the constraints of the coupler power limit have to be considered which will restrict the choice for the number of cavity cells. Still, a 1.x cell option might be advantageous over a half-cell design and is subject to ongoing calculations.

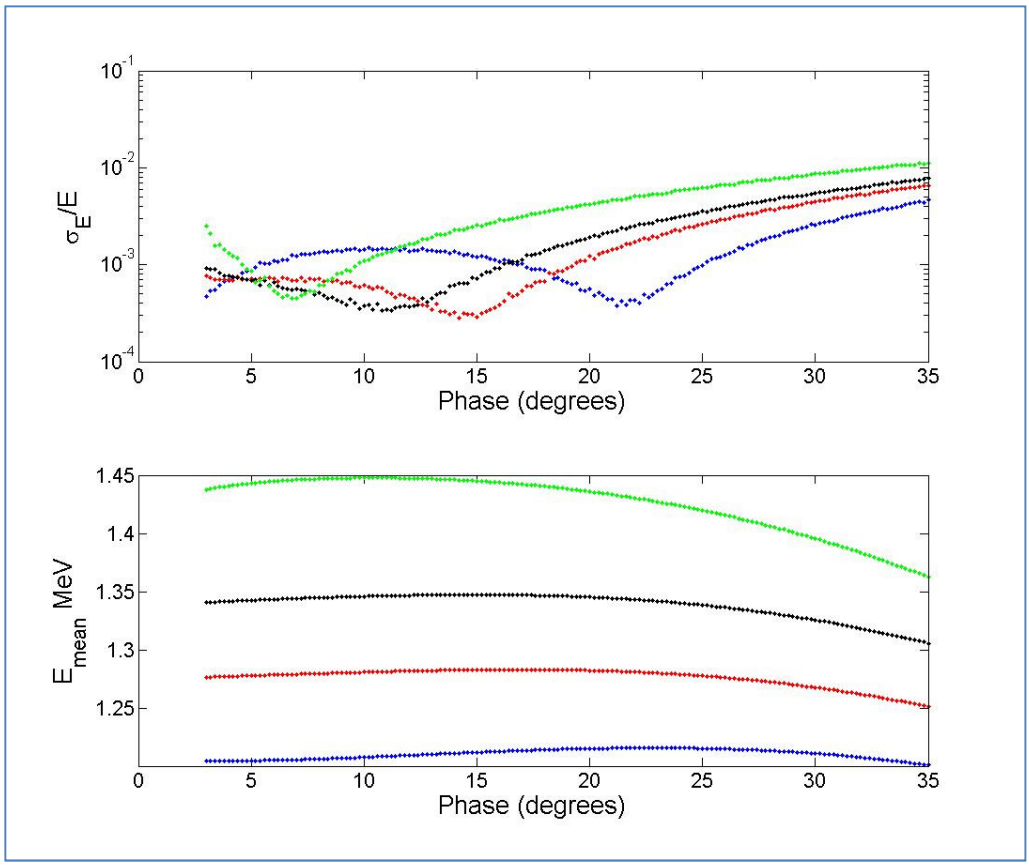

Figure 32: Energy spread and kinetic energy versus launch phase for different cavity designs
Green: 0.6 cell, black: 0.5 cell, red 0.45 cell and blue 0.4 cell operated at the same on axis peak field

Besides studying the RF properties of the gun cavity itself, a choke filter has to be introduced with the cathode insert to suppress RF field propagation along the normal conducting coaxial insert geometry. Figure 33 shows an example of a choke filter attached to a 0.6-cell cavity. At the moment studies are underway to adapt the HZDR choke filter design to the cavity and insert.

The beam pipe section of the gun cavity has to be adapted to house two KEK type fundamental power couplers with strong coupling to compensate the beam loading. The beam pipe diameter is also dictated by the propagation of higher-order modes as the KEK couplers omit the installation of further HOM couplers, so that a beam pipe absorber is planned.

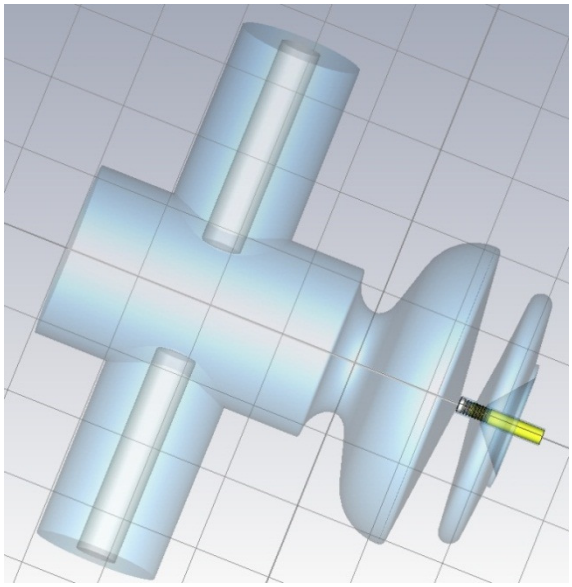

Figure 33: Sketch of a 0.6 cell cavity showing the attached cathode insert with the choke cell band pass filter and coupler assembly

Gun module

The main impact on the mechanics of the gun module is given by the large cathode insert attached to the gun cavity cell. A choke cavity cell prevents RF field leaking out of the cavity to the cathode holder.

Assuming an accelerating field of up to 2 MeV in the gun and a beam current of 100 mA, the beam loading in the gun cavity is 200 kW. Therefor high power fundamental power couplers for the RF are required. By using two adverse couplers the demanded power capability is reduced to 100 kW each and the effects of the coupler kicks on the beam are reduced. KEK (cERL) type couplers were chosen, for being the only tested FPC at this power level and frequency.

Caused by the high beam current, up to 30 W of HOM power is expected in the gun cavity. Ferrite (ceramic) beam pipe absorbers are best choice fitting to the mechanical restrictions in the module.

A solenoid magnet has to be mounted close to the cavity to focus the beam. The emittance of the beam is very sensitive to its position, so it is foreseen to be able to adjust the position of the solenoid as well as the position of the avity during operation.

The main components and design criteria of the gun module are given by:

- size of the 0.6-cell cavity including a choke cell
- the requirements for the cathode insert
- the ferrite beam pipe HOM load
- position and size of a SC solenoid
- independent adjustability of the solenoid and the cavity under cryogenic conditions
- the tuner system

- the size and cooling requirements of the fundamental RF power couplers
- the cryogenic distribution

Figure 34 show the actual status of construction of the B*ERL*inPro gun module. The gun cavity including the blade tuner is hanging on an adjustable support structure. Two horizontal KEK type FPC (Figure 35) can be seen as well as the cathode insert at the rear side of the cavity. In the beam pipe there is space for a SC solenoid and the ceramic beam pipe HOM absorber (Figure 36).

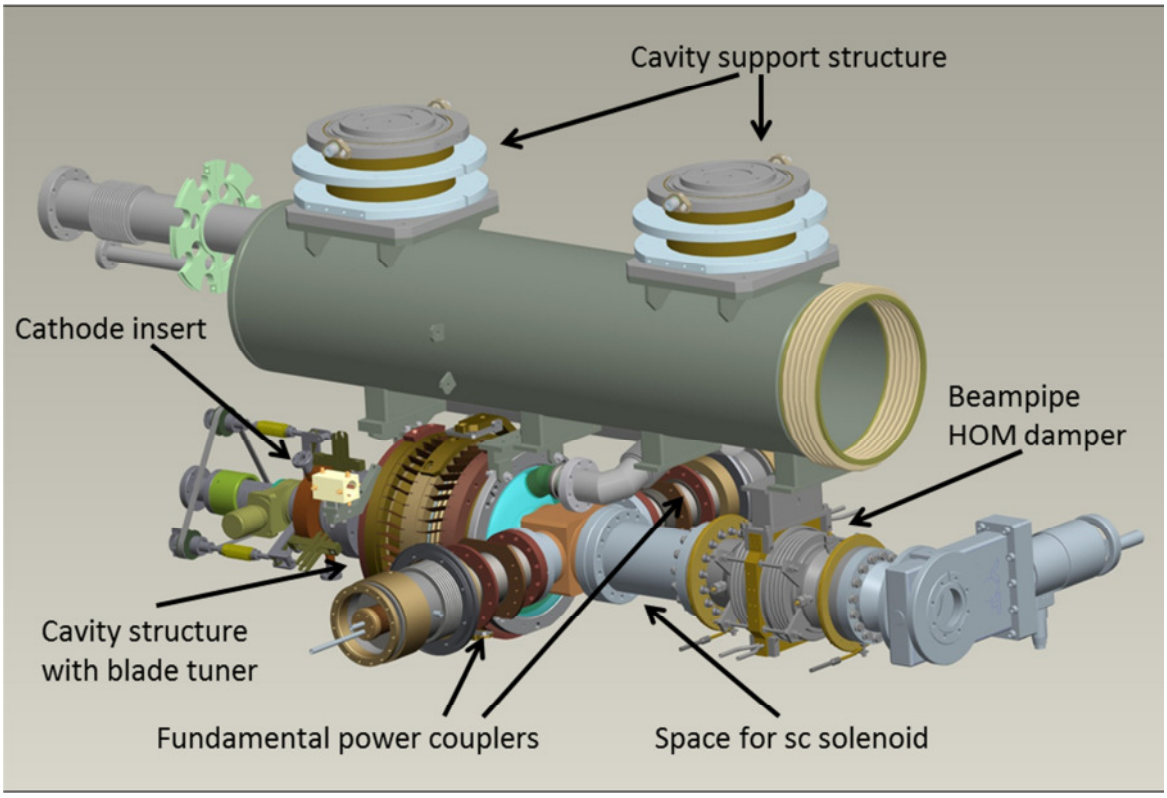

Figure 34: Gun module

Figure 35 : KEK type fundamental power couplers (courtesy E. Kako)

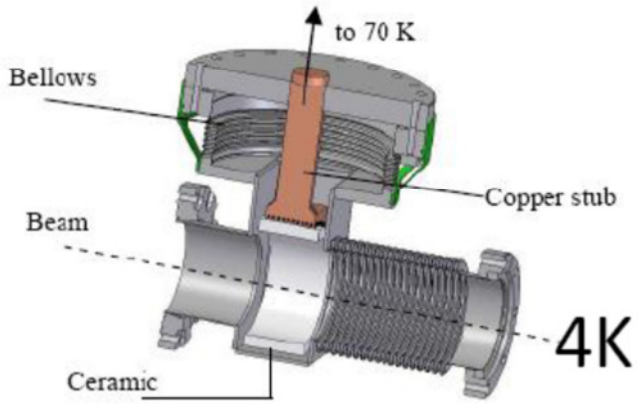

Figure 36: Ferrite beam pipe HOM absorber [courtesy J. Sekutowicz)

The estimated cryogenic loads of the gun module based upon [1], [2], [3] are listed in Table 21:

V_{cav} = 2 MV Q_o = 2E9		1.8 K		4.5 K		80 K	
	Quantity	Static load	Dynamic load	Static load	Dynamic load	Static load	Dynamic load
Cavity	1	--	14 W	--	--	--	--
Coupler	2	1 W	1 W	4 W	4 W	10 W	15 W
HOM load	1	< 0.1 W	--	3.5 W	--	--	45 W
Subtotal		2 W	16 W	11.5 W	8 W	20 W	75 W
Beam pipe	1	< 0.1 W	--	2 W	--	10 W	--
Others	1	5 W	--	20 W	--	100 W	--
Module total		**7 W**	**16 W**	**34 W**	**8 W**	**130 W**	**75 W**

Table 21: Cryogenic losses of the gun cryo module

2.5.2.2. Booster

In the booster the electrons are accelerated from 1.8-2 MeV to about 6.5 MeV. The booster has to cover the full beam loading of 100 mA beam resulting in an RF power requirement of 450-470 kW. Using two cavities each equipped with a pair of KEK type RF couplers (Figure 35) with a power capacity of >150 kW each (> 300 kW/cavity) and installing two 270 kW RF transmitter these requirement can be handled.

The optimum number of cells per cavity results from the field gradient. The maximum accelerating field is 2.3 MeV/cavity. The resulting field gradient in a cavity would be 20 MV/m in a 1-cell structure, 10 MV/m in a 2-cell and 6.7 MeV/m in a 3-cell cavity. A 2-cell cavity is the best choice to minimize cavity length and having moderate field gradients.

In order to reach higher energies at reduced currents the use of a third cavity is indispensable, therefore three 2-cell cavities will be installed in the booster module.

Booster cavities

The performance of the Cornell 2-cell booster cavity design is well proven, so this cell geometry will be adapted for the B*ERL*inPro booster. The ratio of the peak field on axis and the accelerating field is E_{peak}/E_{acc} = 1.94. Figure 37 shows the results of the booster cavities operated in the Cornell module demonstrating a field gradient limit of 12.5 MV/m, sufficient to meet the B*ERL*inPro requirement.

As in the gun, pairs of KEK type couplers will be used instead of the Cornell couplers. Calculations concerning coupler kicks are ongoing.

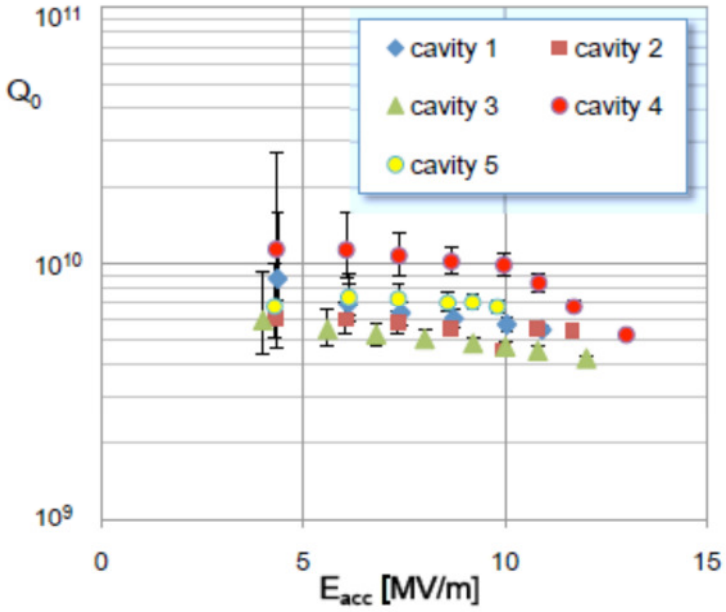

Figure 37: Intrinsic quality factor Q vs. accelerating field E_{acc} at 1.8 K of the SRF cavities of the Cornell booster module after rework of the cryo module [4].

KEK type couplers employ a fixed coupling to achieve the high power level. The coupling factor is chosen to provide zero reflection at full beam current at the operating voltage for acceleration to 6.5 MeV.

The transmitter for the first booster cavity will be only a 15 kW (linac-) transmitter to reduce investment cost. At this power level the coupling factor can be adjusted by a factor of three using waveguide three stub tuners. The cavity will be used to imprint an energy chirp on the beam at full current or to increase the injection energy for reduced currents.

The second and third booster cavities will be used for acceleration to maximum energy limited by the RF power at nominal beam current or up to maximal energy given by the gradient limit at low currents in beam physics study mode.

Table 22 summarizes the coupler settings for the booster and the resulting accelerating parameters.

Cavity number	Coupling strength	V_{acc} MV	V_{max} MV	Accelerating gradient MV/m	Beam current mA	RF power at FPC kW	Comment
1	1.1E5	0.95	1.84	4	1	10	3-stub tuner
1	3.7E4	0.8	1.55	3.4	100	80	Upgrade option
2 and 3	1.0E5	2.25	4.37	9.5	100	225	RF Power limit
2 and 3	1.0E5	3.0	5.82	12.5	1	100	Gradient limit

Table 22: Coupling strength of the fundamental power couplers of the booster cavities.
Note, that the coupling of the first cavity has different settings due to beam dynamics requirements.

Booster module

The construction of the B*ERL*inPro booster module is greatly influenced by the use of KEK-type FPC. It is an open item, if the orientation of the FPC will be horizontal or vertical.

Cornell University developed and operates the booster module shown in Figure 38. This well-proven design consists of five 2-cell cavities. Each cavity is equipped with two Cornell type couplers with a power capacity of 61 kW each (122 kW/cavity). Ferrite beam pipe absorbers are used to damp the HOM modes of the cavities. The beam line string of the Cornell booster module including three 2-cell Cornell type cavities and the ferrite based beam pipe HOM couplers can probably be inherited. It is under evaluation, if more mechanical parts of the Cornell booster module can be adopted.

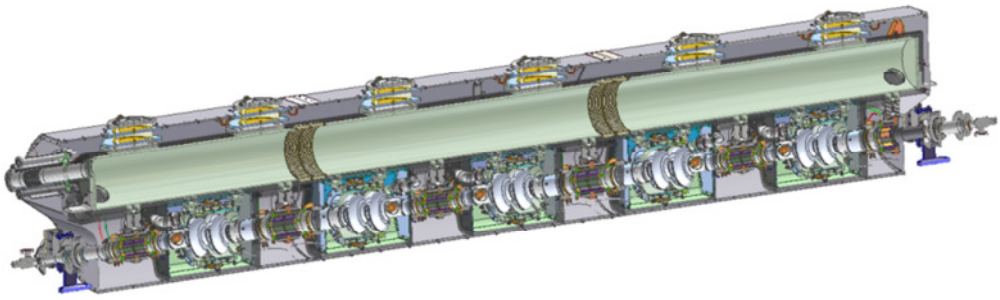

Figure 38: Cornell booster module

The lengths of the module components are added up in Table 23:

Device	**Length**	**Position**
Beam entrance spool	160.25 mm	0 mm
Gate valve	075.00 mm	160.25 mm
1/2 HOM load	321.31 mm	235.25 mm
106mm beam tube	168.91 mm	556.56 mm
Cavity #1	218.64 mm	725.47 mm
78mm beam tube	150.90 mm	944.11 mm
78mm HOM	268.00 mm	1095.01 mm
78mm beam tube	150.90 mm	1363.01 mm
Cavity #2	218.64 mm	1513.91 mm
106mm beam tube	168.91 mm	1732.56 mm
106mm HOM	308.10 mm	1901.47 mm
106mm beam tube	168.91 mm	2209.57 mm
Cavity #3	218.64 mm	2378.48 mm
78mm beam tube	150.90 mm	2597.12 mm
78mm HOM	268.00 mm	2748.02 mm
78mm load-gate spool	159.99 mm	3016.02 mm
Gate valve	075.00 mm	3176.01 mm
Exit spool	135.08 mm	3251.01 mm
Total length booster module		**3386.09 mm**

Table 23: Expected length of the booster cryo module

The module has a cryogenic shield at a temperature level of 80K. The estimated cryogenic loads of the booster module based upon [1], [2], [3] are listed in Table 24:

		1.8 K		4.5 K		80 K	
Q_o = 3E9	Quan-tity	Static load	Dynamic load	Static load	Dynamic load	Static load	Dynamic load
Cavity 1 V_{cav} = 1 MV	1	--	3 W	--	--	--	--
Cavity 2+3 V_{cav} = 2.25 MV	2	--	15 W	--	--	--	--
Coupler	6	1 W	1 W	4 W	4 W	10 W	15 W
HOM load	4	--	--	3.5 W	--	--	45 W
Subtotal		6 W	39 W	38 W	24 W	60 W	270 W
Beam pipe	2	< 0.1	--	2 W	--	10 W	--
Others	1	5 W	--	20 W	--	100 W	--
Module total		**11 W**	**39 W**	**62 W**	**24 W**	**180 W**	**270 W**

Table 24: Cryogenic loads of the booster module

2.5.2.3. Linac

In the main linac the beam will be accelerated from 6.5 MeV to the final energy of 50 MeV and will be decelerated back to 6.5 MeV to recover the energy. The beam will pass the linac twice, so highly HOM damped cavities are required.

Linac cavity

The goal of the main linac cavity design is to deliver an energy gain of 43.5 MeV at a beam current of two times 100 mA for the accelerated and decelerated beam respectively using three SC cavities. Thus, the cavity design has to be a carefully evaluated compromise between achieving a fairly high CW field gradient of nearly 20 MV/m omitting high peak fields at the metal surface on the one hand and good coupling and thus propagation of higher order modes out of the structure on the other hand. A less important design feature is the reduction of cryogenic losses, which has to be taken into account for future large scale ERLs. Unlike the booster system, beam loading is not an important consideration, thereby relaxing the coupler design. Consequently, though, the weak coupling yields a small bandwidth so that microphonics and electro-mechanical modelling take on a prominent role.

The first choice taken was the number of cells per cavity. A higher number increases the real estate gradient and lowers the field gradient of the accelerator section, but depending on the cell-to-cell coupling increases the probability of strongly localized higher order modes which cannot be damped by means of HOM couplers or beam pipe absorbers.

The main linac cavity will feature a 7-cell structure. As a baseline design two different cell shapes were considered, the high current JLAB 1.5 GHz 5-cell cavity scaled to 1.3 GHz and the 1.3 GHz 7-cell cavity by Cornell University [5] [6].

A comparison of the cavity cell shapes of both designs for a inner cell is shown in Figure 39.

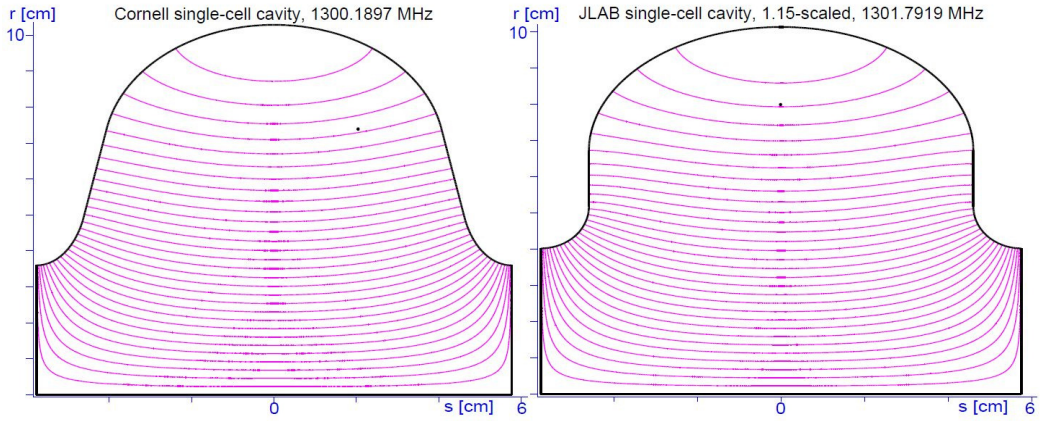

Figure 39: Comparison of Cornell (left) and scaled JLAB based cells (right) with TM_{010}-mode electric field lines calculated by Superfish [7].

Table 25 summarizes the most important electro-magnetic parameters of these cavities. Note that these values will vary slightly for the end-cells due to the attached beam tubes and the tuning for field flatness and frequency. Both designs feature a similar transit time factor and normalized shunt impedance *R/Q* for the fundamental TM_{010} π-mode. The Cornell design, given by the smaller iris opening and the smoother slope of the sidewalls, has an improved ratio of maximum surface to accelerating field value. This is favorable for operation at 19 MV/m minimizing the probability of field emission. The JLAB design was optimized to improve the propagation of higher order modes out of the cavity by the increased iris opening. This is reflected by the increased cell-to-cell coupling. However, its ratio E_{peak}/E_{acc} of 2.5 is unacceptably high. The cavity design studies concentrate on comparing the high current performance of both structures with respect to beam breakup instabilities by the excitation of higher order modes while trying to reduce the peak field.

Higher order mode damping will be achieved by strongly coupled waveguides attached to the beam tube next to the cavity's exit iris. In contrast to beam pipe absorbers waveguides allow a broadband damping independent of an absorber material's frequency response spectrum. Further it minimizes the danger of dust particles emitted by the absorber material on the niobium surface and saves beam tube space. The cutoff to reject the fundamental mode is naturally given by the lowest TE mode cutoff frequency. Finally, they allow dissipating the HOM power in loads located at ambient temperature.

The original symmetry of the JLAB design of 6 waveguides separated by 60° each is broken in order to implement the TTF-III fundamental power coupler that offers a higher variability in the coupling and to compensate for the polarization angles of higher order modes [8].

Figure 40 shows the current geometry and waveguide assembly under investigation.

	Cavity electro-magnetic parameter	
Parameter for β=1	JLAB design scaled (inner cell)	Cornell design (inner cell)
R_{iris} (mm)	40.25	36.0
R/Q (Ω) per cell	104.2	111.1
Transit time factor	0.77	0.77
Geometry constant G (Ω)	278.9	272.8
E_{peak}/E_{acc}	2.44	2.06
B_{peak}/E_{acc} (mT/(MV/m))	4.14	4.02
Cell-to-cell coupling (%)	3.2	2.2
Q_{ext} operational range	$3{\cdot}10^7$-$1{\cdot}10^8$	$3{\cdot}10^7$-$1{\cdot}10^8$

Table 25: Comparison of cell shapes developed by Cornell and JLab

A modified TTF-III-type fundamental power coupler is positioned such that an external quality factor of $5{\cdot}10^7$ is feasible which corresponds to a cavity bandwidth of 13 Hz. Recent CW LLRF tests at HZB showed a stable operation at this high external Q, allowing field stabilities of better than 0.01 degree in phase and a relative amplitude error of $1{\cdot}10^{-4}$ [9].

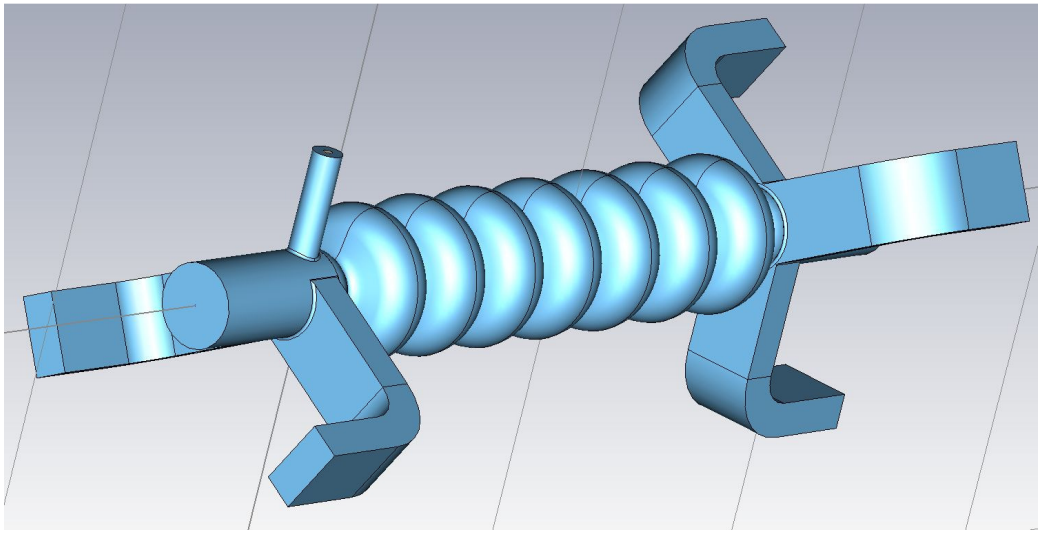

Figure 40: Current cavity design using the Cornell cell shape and JLAB style waveguide HOM couplers. The fundamental power coupler is a coaxial TTF-III coupler.

While the three-waveguide end group will maintain its 120 degree symmetry to couple to all possible polarization angles of excited higher order modes, the fundamental power end group aims at optimizing the asymmetry further to damp polarization angles provoked by that asymmetry and to compensate coupler kicks by the coaxial power coupler. The impact of coupler kicks on the beam quality still has to be determined.

HOM spectrum: Transverse R/Q calculations

The HOM damping efficiency is the most important aspect of a high current cavity design. The threshold current above which the beam breakup instability occurs for a cavity with a single deflecting mode is inversely proportional to the normalized transverse shunt impedance times the external quality factor of that mode. According to the Panofsky-Wenzel theorem the transverse shunt impedance may be expressed by integrating the transverse gradient of the longitudinal fields:

$$\frac{R_\perp}{Q} \equiv Z_0 \frac{c^3}{\omega_D^3} \frac{\left| \int \frac{\partial E_z}{\partial x} e^{j\omega_D z/c} dz \right|^2}{\int E^2 dV}$$

This relationship may be approximated by calculating the longitudinal shunt impedances at two different offset positions x_1, x_2 and to calculate the difference quotient:

$$R_{\perp x} \approx \left| \frac{c}{\omega} \frac{\sqrt{R_\parallel(x_2)} - \sqrt{R_\parallel(x_1)}}{x_2 - x_1} \right|^2$$

Figure 41 depicts the transverse R/Q evaluated for different angles with respect to the given coordinate system allowing to distinguish dipole modes from other higher order modes and to determine the polarization angle which has to be implemented into BBU calculations.

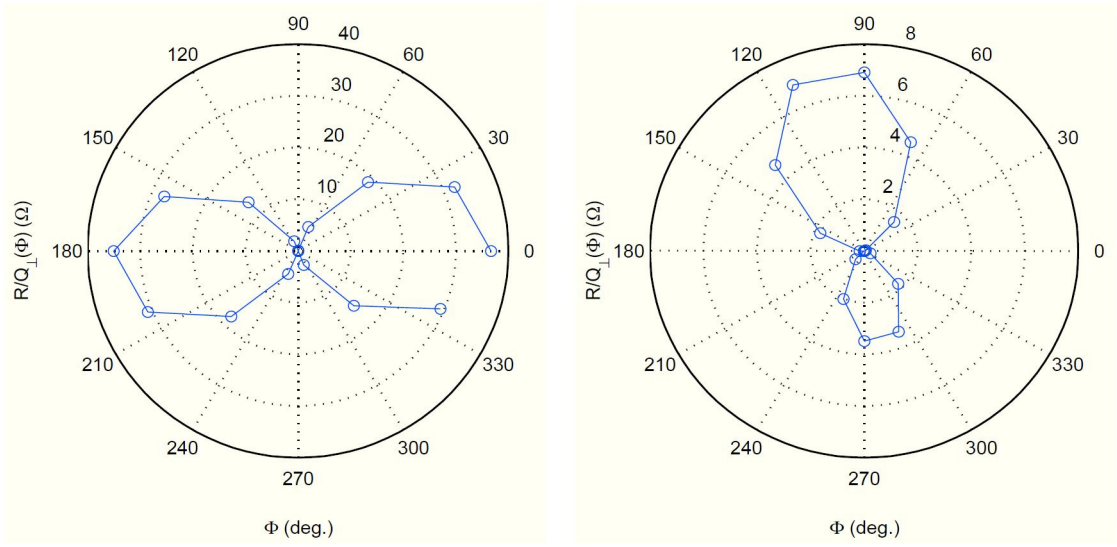

Figure 41: Polar maps of the transverse R/Q versus angle for two different polarizations of a TM_{110} type like dipole mode.

For BBU calculations the following parameters have to be extracted from 3D electro-magnetic field calculations: The mode's frequency, normalized shunt impedance, the external quality factor by the waveguide dampers and the polarization angle of the mode with respect to some given coordinate system.

The mode spectrum of Cornell cavity with 5 waveguides and one TTF-III FPC was determined by combined wide-band (6 GHz) off-axis beam excitation with a >500 m length

time domain wake iteration, followed by an Eigen mode analysis in preselected frequency ranges. Figure 42 shows the time domain data of the longitudinal and transverse shunt impedances versus frequency where the grey lines show modes determined by the Eigen mode analysis.

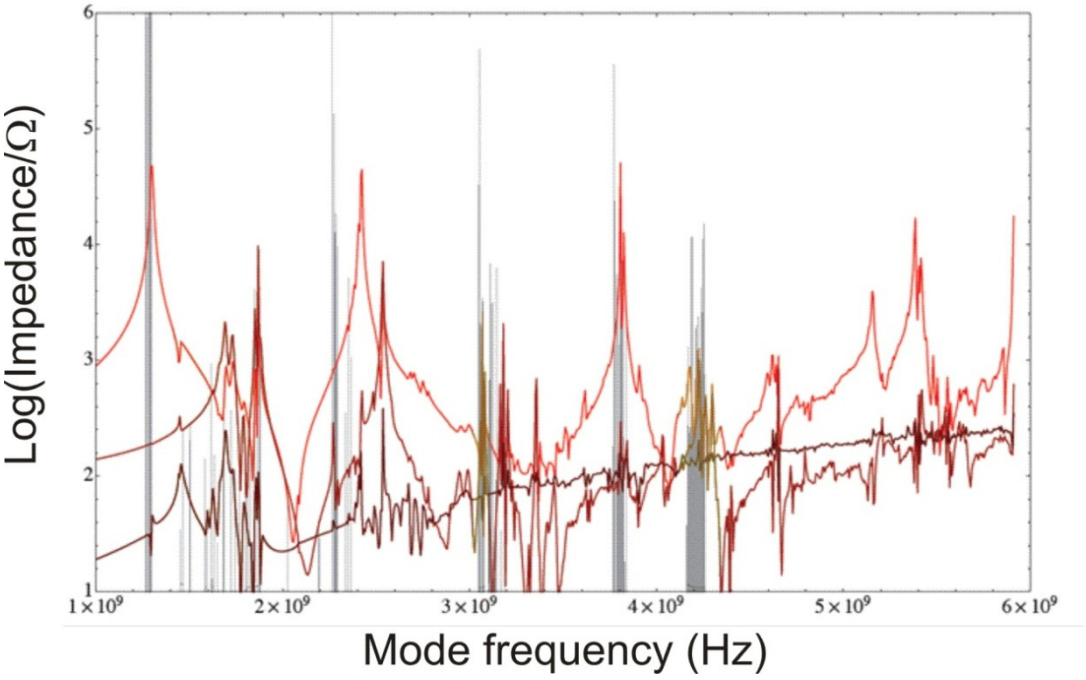

Figure 42: Time domain calculation of an impedance spectrum of a Cornell structure in the 5+1 coupler configuration
The red line shows the longitudinal impedance, the brown and dark brown lines the transverse impedance obtained by electron bunch tracking.

Figure 43 summarizes the obtained shunt impedance times external Q spectrum of the Cornell cavity with the 5+1 coupler configuration. Besides the dipole modes in the range of 1.7-1.9 GHz which intrinsically may couple strongly to a beam passing the cavity with a given offset to the center, there are strongly localized quadrupole modes with high $R/Q \cdot Q_{ext}$ values at 2.26 GHz and 3.77 GHz. It has to be analyzed further how far such modes may contribute to beam instabilities or increase of the beam's energy spread.

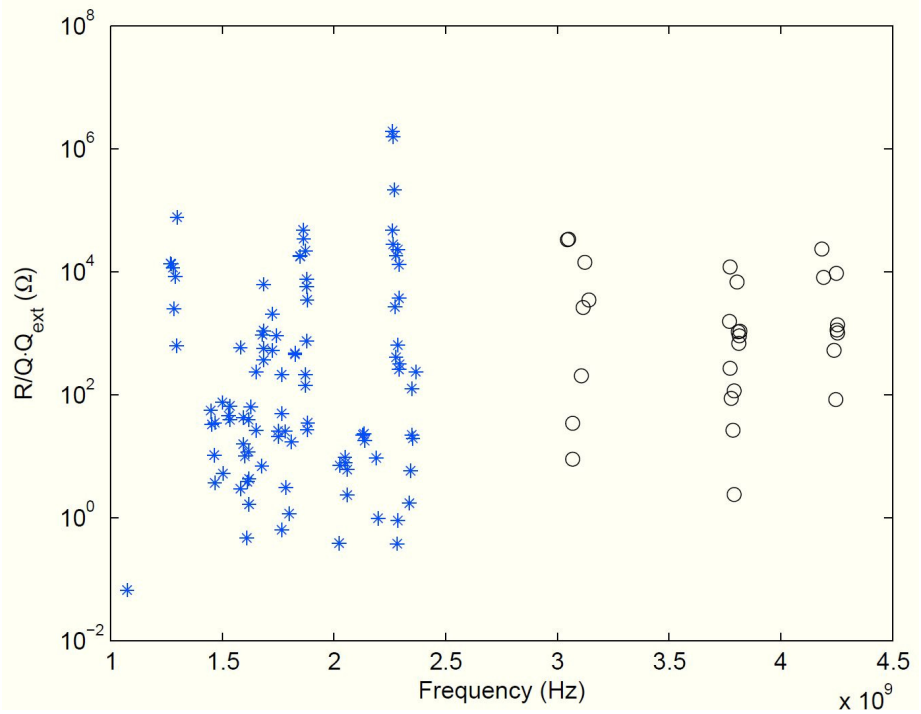

Figure 43: Transverse R/Q times external Q calculated for a Cornell type cavity with 5 waveguides and a TTF-III fundamental power coupler for frequencies up to 4.5 GHz.

Figure 44 shows an example of a strongly localized quadrupole mode with a very high external Q of $3.7 \cdot 10^7$ quasi trapped inside the 7-cell structure.

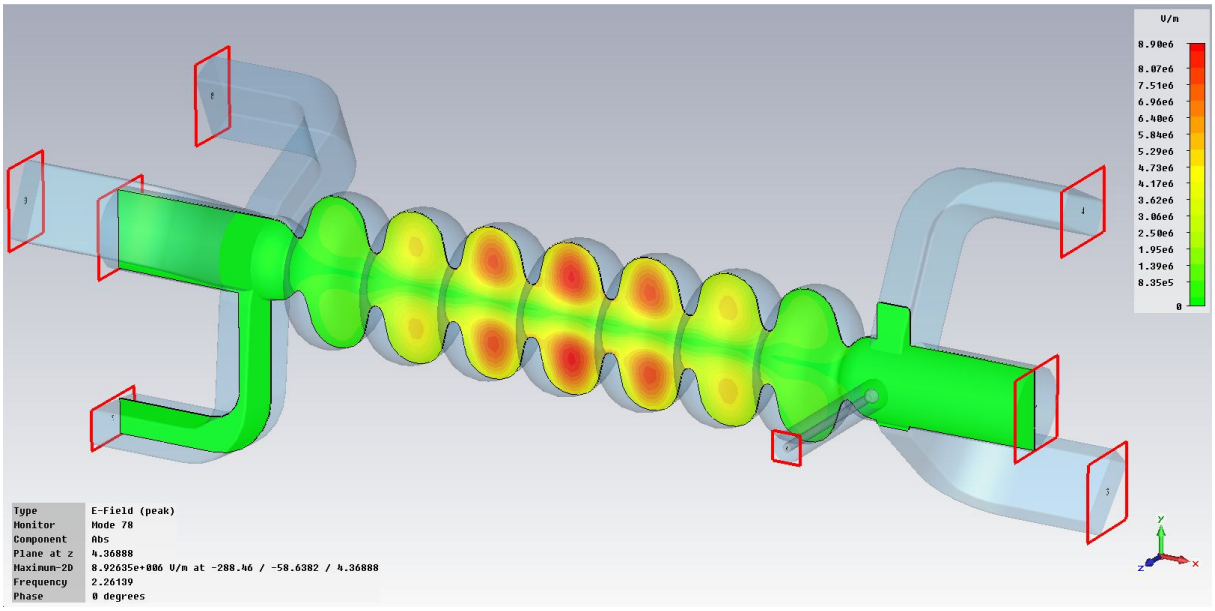

Figure 44: Electric field distribution of a strongly localized quadrupole mode at 2.26 GHz with $Q_{ext}=3.7 \cdot 10^7$ calculated by MWS^{TM} [10].

The design studies are ongoing in an iterative approach of combined beam breakup and Eigen mode calculations to identify dangerous modes for which the coupling needs to be changed.

Linac module

The linac module will house three waveguide HOM damped cavities. The waveguides will have thermal transition to room temperature, so the loads at the end of the waveguide dampers will be cooled by water. There will be temperature intercepts at 4.5 K and 80 K. The cavities including the water loads will be inside a vacuum vessel. A temperature radiation shield at 80 K is foreseen. The design of the module will start in 2013 when the final dimensions of the cavities are known. So parameters like the length and the cryogenic losses are preliminary. A total length of 5.1 m including ferrite beam pipe HOM dampers at the ends is estimated. The lengths of the module components are listed in Table 26 and the cryogenic losses based upon [11], [12], [13] and one-dimensional thermal calculations in Table 27.

Device	Length	Position
beam pipe HOM	300 mm	0 mm
transition incl. valve	350 mm	300 mm
cavity end group with WG	150 mm	650 mm
active cavity length 1	800 mm	800 mm
cavity end group with WG	150 mm	1600 mm
beam pipe, bellow	250 mm	1750 mm
cavity end group with WG	150 mm	2000 mm
active cavity length 2	800 mm	2150 mm
cavity end group with WG	150 mm	2950 mm
beam pipe, bellow	250 mm	3100 mm
cavity end group with WG	150 mm	3350 mm
active cavity length 3	800 mm	3500 mm
cavity end group with WG	150 mm	4300 mm
transition incl. valve	350 mm	4450 mm
beam pipe HOM	300 mm	4800 mm
total length linac module		**5100 mm**

Table 26: Preliminary length of the linac cryo module

		1.8 K		4.5 K		80 K	
Q_o = 1.5E10	Quan-tity	Static load	Dynamic load	Static load	Dynamic load	Static load	Dynamic load
Cavity V_{cav} = 14.5 MV	3	--	26 W	--	--	--	--
Coupler	3	0.15	0.2 W	1.5 W	2 W	2.5 W	10 W
HOM load	15	1 W	--	2 W	--	5 W	--
Subtotal		15.5 W	27 W	34.5 W	6 W	82.5 W	30 W
Beam pipe	2	<0.1W	--	2 W	--	10 W	--
Others	1	5 W	--	20 W	--	100 W	--
Module total		21 W	79 W	59 W	6 W	203 W	30 W

Table 27: Preliminary cryogenic losses of the linac cryo module

2.5.2.4. Cavity auxiliaries

Cavity tuners

The cavity tuner is a device to change the cavity length up to several millimeters and serves two purposes: To adjust the cavity resonance frequency after cool-down and to compensate frequency drifts or microphonics during operation. This is realized by two complementary techniques: Coarse and slow tuning of up to 1 MHz tuning range is done with a stepper motor attached to the cavity through adequate levers; fine tuning at up to 1 kHz is done by piezos integrated into the tuner support frame. From experience with TESLA cavities several frequency shifting mechanisms have to be coped with, as listed in Table 28. The resulting shifts were experimentally obtained with TESLA 9-cell cavities.

Procedure	**TESLA**	**Comment**
Evacuation of the cavity	+0.39 MHz	Cavity shrinks anisotropically
Cool-down from 300 K to 1.8 K	+1.95 MHz	Dominated by titanium tank; $\Delta l/l$ (300K->4K)=15E-4
Backlash pre-tuning	-0.6 MHz	Needs pre-stress on piezos
Sum	+1.74 MHz	Offset for cavity production

Table 28: Frequency changes relevant for pre-tuning

Because of differing space constraints each cavity type requires a different technical tuning solution, i.e. implementation of the coarse and the fine tuning mechanism. For the gun cavity it is envisioned to adapt the Rossendorf solution. The extent to which this can be done depends on the final design of the gun cavity, the choke filter and the cathode changing system. For the booster cavities, it is planned to use the Cornell adaptation of the coaxial blade tuner. Blade tuners are also envisioned to be used for the linac cavities.

These tuner types have been extensively tested at HoBiCaT [14], however, the B*ERL*inPro requirements pose an additional difficulty:

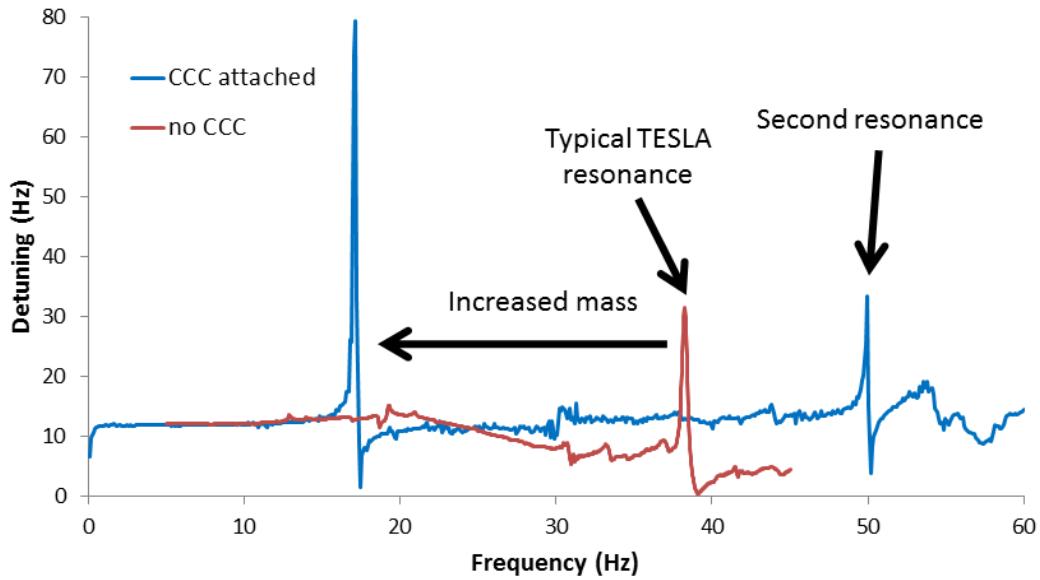

Figure 45: Transfer function of a cavity with increased moving mass attached

Since the linac cavities are equipped with large waveguide type HOM dampers, a significantly larger moving mass compared to the TESLA cavities is imposed on the tuner. This shifts the system's mechanical resonances towards lower frequencies, as has been demonstrated for a cavity that was equipped with a comparably heavy device at the moving end. The device is described in [15] and the resulting transfer function in Figure 45. The problem in this scenario is that the first resonance is approaching the cavity bandwidth which makes the cavity much more susceptible to microphonics.

It is planned to test the regular blade tuner with adequate mechanical loads and eventually modify the tuner design and the stiffness of the cavity.

Magnetic shielding of the cavities

A magnetic shielding is required to minimize the ambient magnetic field at the cavity location, which lead to a frozen flux in the cavity walls upon the superconducting transition. For example, a frozen external field of 55 µT (unshielded earth magnetic field) increases the cavity surface resistance R_s by 180 nΩ. Thus a cavity with a fairly high Q_0 value of 10^{10} would be downgraded to $Q_0=1.3*10^9$ when operated without any magnetic shielding which would increase the cryogenic needs by a factor of 7. To achieve a reduction of ambient magnetic fields to less than 1 µT at least two separate shielding are necessary. An inner shield made from cryoperm10 material is fitted around the Helium tank. Two different options are possible for the outer shield: (1) a dedicated µ-metal shield at the inside of the cryostat wall, as realized in HoBiCaT (2) manufacturing the cryostat from low-carbon steel with high magnetic permeability values and a facility to demagnetize the cryostat.

2.5.3. Cryogenics

All superconducting cavities are cooled with superfluid helium II to a temperature level of 1.8 K. The available Linde L700 liquefier provides saturated liquid helium at 4.2 K. The liquid helium is stored in a 10.000 l Dewar before it is piped through a system of transfer lines, valve boxes and heat-exchangers. Finally it is expanded to a pressure of 16 mbar and thus it cools down to 1.8 K transforming to the superfluid phase. The pressure of 16 mbar will be achieved by pumping the helium volume with a set of cold compressors and warm vacuum pumps connected upstream. The enthalpy of the returning cold gas will be recuperated in a heat exchanger and will contribute to the liquefaction process.

2.5.3.1. Existing Helium liquefier L700

In 2009 a Linde L700 liquefier has been installed in the extension building of the 'assembly hall'. The plant is under operation to supply the HoBiCaT-facility since then. A second TCF50 liquefier is running since 2003 to supply liquid helium to four SC magnets and a SC Landau cavity in the BESSY II storage ring. Both systems are connected for redundancy and mutual storage of helium.

The main parameters of the L700 liquefier are listed in Table 29 and the total system is shown in Figure 46.

Cold box	
Manufacturer/Type:	LINDE L700
Liquefaction with LN2 precooling:	710 l/h
Cycling Compressor	
Manufacturer/Type:	2x KAESER ESD441
Max. flow:	2x 77 g/s
Working pressure:	13 bar
Mains:	250 kW
Dewar	
Manufacturer/Type:	Cryotherm Helios 10.000
Capacity	10.000 l
Buffer Tank	
Capacity:	2 x 400m³

Table 29: Parameter of L700 Liquefier

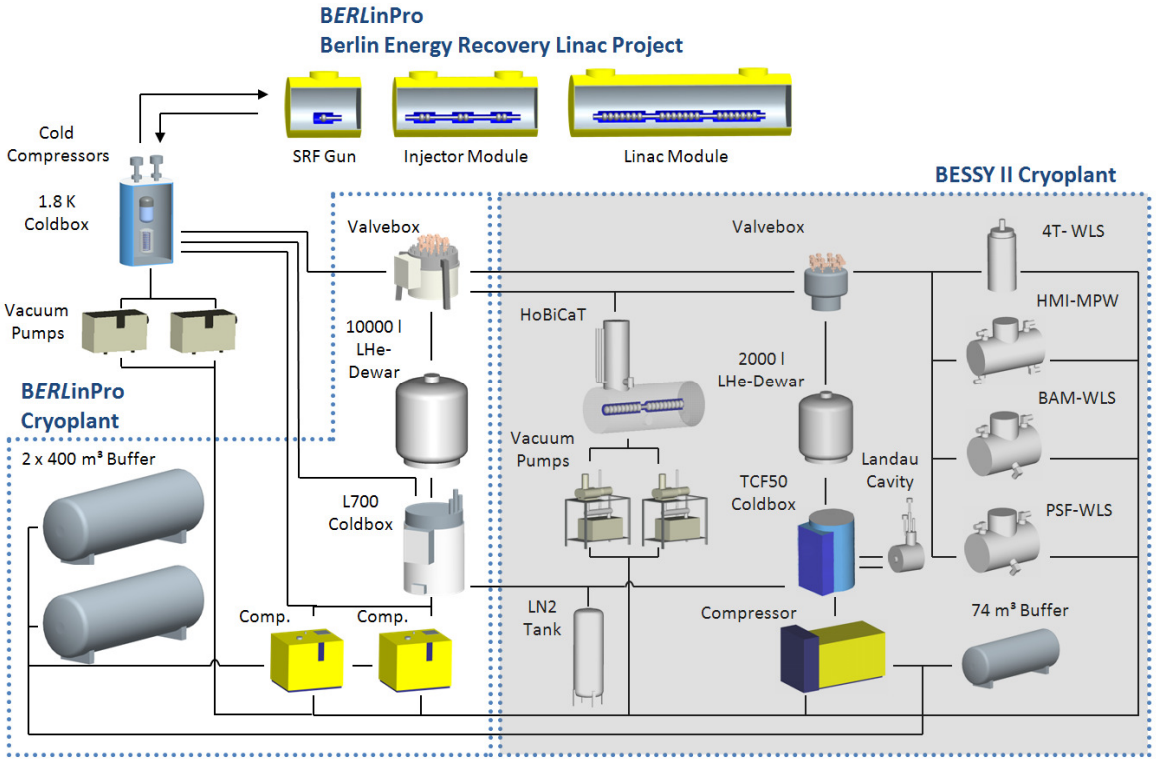

Figure 46: Schematic overview of the cryogenic system

2.5.3.2. Reconstruction of the L700 cryo plant

The cold box and the Dewar of the L700 plant will be moved to the new B*ERL*inPro-building. This step will avoid long distance transfer of saturated helium which would cause a two phase flow scenario. Such a scenario would be problematic because of the presence of a gas and a liquid phase in one pipeline. Alternating pressure drops and thus discontinuous flow can occur. With increasing length of the pipeline the proportion of the gaseous helium increases and dominates the pressure drop. This can lead to a plugging of the pipeline for the liquid helium phase and disable the steady flow.

Short transfer lines will reduce the technical risks and overall costs as well as simplify the calculations and the design.

Hence, the liquefier will be moved to a location close to the cryo modules and cold compressor box. The cycling compressors and the oil removal and gas management system will stay at their current position. Only warm pipelines and one comparatively simple transfer line between the assembly hall extension and the B*ERL*inPro-building have to be installed. This solution allows for an easy helium transfer to B*ERL*inPro while maintaining the supply for HoBiCaT and other experiments.

2.5.3.3. Cryogenic Loads

The cryogenic loads at B*ERL*inPro are dominated by the dynamic losses in the SC cavities. The total loads are listed in Table 30:

	1.8 K		4.5 K		80 K	
	Static load	Dynamic load	Static load	Dynamic load	Static load	Dynamic load
Gun module	7 W	16 W	34 W	8 W	130 W	75 W
Booster module	11W	39 W	62 W	24 W	180 W	270 W
Linac module	21 W	79 W	59 W	6 W	203 W	30 W
Subtotal	39 W	134 W	155 W	38 W	513 W	375 W
Cryo distribution	3 W	--	45 W	--	550 W	--
Total	42 W	134 W	200 W	38 W	1063 W	375 W

Table 30: Cryogenic load of B*ERL*inPro

2.5.3.4. Cold Compressor Cold Box

The Cold Compressor Cold Box will be one of the key components of the B*ERL*inPro cryogenic system. A schematic view is shown in Figure 47.

The main tasks of the CCCB are:

- Superinsulated housing of the cold compressors, heat exchangers and cryogenic valves
- Generation of sub-cooled liquid helium for 1.8 K system
- Enthalpy recovery of the compressed cold gas (recuperator)
- Generation of 80 K GHe
- Generation of supercritical LHe (4.5 K@ 3 bar)
- Phase separation of liquid nitrogen and liquid helium

Cold compressors provide the sub-atmospheric pressure of 16 mbar for the generation of 1.8 K superfluid helium for SC accelerator cavity cooling. At a mass flow rate > 10 g/s cold compressors can be used as a cost and energy efficient alternative to large scale warm pumping systems. The compression of the cold gas allows the use of very compact devices with small input power and less maintenance. Furthermore a recovery of the compressed cold gas enthalpy in relatively small sized heat exchangers can contribute to the liquefaction process.

High dynamic loads as expected due to the CW operation of the B*ERL*inPro accelerator will lead to high dynamics in the mass flow rate on the 1.8 K-system. A sophisticated controlling system with bypass and heater system is indispensable to provide a stable mass flow to the cold compressors for an operation within the load map.

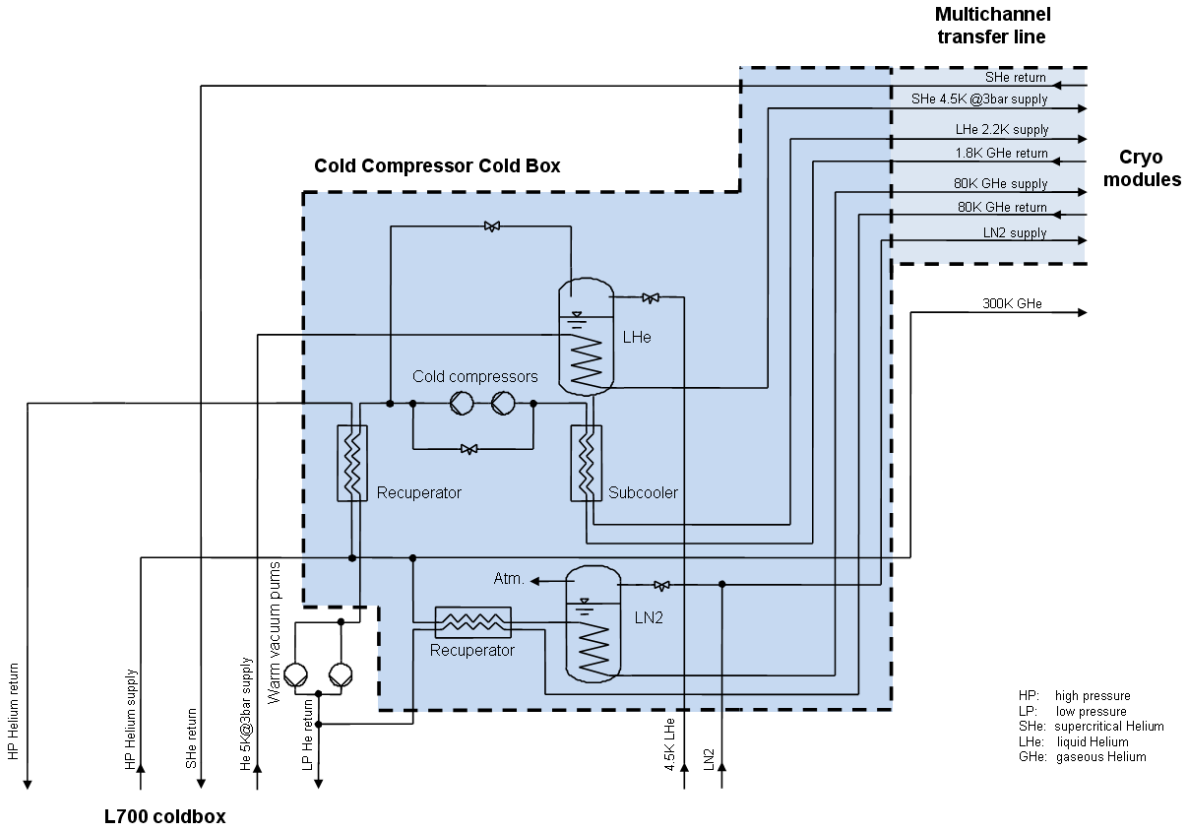

Figure 47: Cold Compressor Cold Box (CCCB)

2.5.3.5. Transfer system

The transfer system of the cryogenic plant will consist of a variety of different types of transfer lines and valve boxes. Flexible vacuum insulated transfer lines (NEXANS) will be used for a single stream transfer of liquid helium and liquid nitrogen (LN2). With LN2 shielded flexible transfer lines helium can be transferred with a minimum of radiation heat load over long distances. These types are successfully operated at the existing cryo plants for many years. The installation of these lines is comparatively easy because they are prefabricated and evacuated by the vendor. The only disadvantages are higher pressure drops compared to rigid lines due to the corrugation needed for stiffness and a very limited selection of available diameters.

In contrast to the easy handling of helium flexlines a multi-channel transfer line (MCTL) will be one of the most challenging cryogenic components. Due to the individual technical requirements the MCTL has to be designed for its special purpose and has to be assembled on site. It interconnects the CCCB with the cryo modules.

Several streams of helium with different temperatures and pressure levels pass through pipelines inside of a vacuum jacket. All internal lines are wrapped with multilayer superinsulation for protection against radiation heat transfer. Thermal loads as well as pressure and temperature differences lead to considerable mechanical stress. The multi-channel transfer line should be kept as simple and short as possible to minimize cryogenic loads, costs and technical risks. All these aspects will be considered from the very beginning of the B*ERL*inPro design process [16].

2.5.4. References

[1] S. Noguchi, E. Kako, M. Sato, T. Shishido, K. Watanabe, and Y. Yamamoto, "Present status of superconducting cavity system for CERL injector linac at KEK", in Proc. 2010 Int. Particle Accel. Conf. (2010).

[2] S. Noguchi, "Injector Cryomodule for cERL at KEK", presentation TTC meeting March 2011, Milano.

[3] M. Liepe, S. Belomestnykh, E. Chojnacki, V. Medjidzade, H. Padamsee, P. Quigley, J. Sears, V. Shemelin, V. Veshcherevich, "The Cornell ERL Superconducting 2-cell Injector Cavity String and Test Cryomodule", in Proc. 2007 Int. Particle Accel. Conf., Albuquerque (2010).

[4] M. Liepe , S. Belomestnykh, E. Chojnacki, Z. Conway, G. Hoffstaetter, R. Kaplan, S. Posen, P. Quigley, J. Sears, V. Shemelin, V. Veshcherevich, "Latest Results and Test Plans from the 100 ma Cornell ERL Injector SCRF Cryomodule", Proc. of IPAC'10, Kyoto, Japan (2010)

[5] F. Marhauser, "JLab High Current Cryomodule Development", in Proc. 2009 ERL Workshop, Ithaca, New York, USA (2009).

[6] N. Valles, M. Liepe, "Seven-Cell Cavity Optimization for Cornell's Energy Recovery Linac", in Proc. 2009 Workshop RF Superconductivity, Berlin (2009).

[7] James H. Billen and Lloyd M. Young, "SUPERFISH/Poisson Group Of Codes". Report LAUR-96-1834, Los Alamos, 1996. Revised 1999.

[8] B. Riemann, T. Weis, A. Neumann, W. Anders, J. Knobloch, H.-W. Glock, C. Potratz, U. van Rienen, F. Marhauser, "First Considerations Concerning an Optimized Cavity Design for the Main Linac of B*ERL*inPro", in Proc. IPAC 2011, San Sebastián, Spain (2011).

[9] A. Neumann , W. Anders, R. Goergen, J. Knobloch, O. Kugeler, S. Belomestnykh, J. Dobbins, R. Kaplan, M. Liepe, C. Strohman, "CW MEASUREMENTS OF CORNELL LLRF SYSTEM AT HOBICAT", in Proc. 2011 Conference RF Superconductivity, Chicago (2011).

[10] Microwave Studio™ ,CST AG, "CST Studio Suite", Darmstadt, Germany, 2011-2012.

[11] V. Veshcherevich, S. Belomestnykh, "Input coupler for main linac of Cornell ERL", in Proc. 2009 Workshop RF Superconductivity, Berlin (2009).

[12] C. E. Reece, E. F. Daly, G. K. Davis, M. Drury, W. R. Hicks, J. Preble, H. Wang, "Performance of the CEBAF Prototype Cryomodule *RENASCENCE*", in Proc. 2007 Workshop RF Superconductivity, Beijing (2007).

[13] E. Chojnacki, E. Smith, R. Ehrlich, V. Veshcherevich, S. Chapman, “Cryogenic Heat Load of the Cornell ERL Main Linac Cryomodule”, in Proc. 2009 Workshop RF Superconductivity, Berlin (2009).

[14] O. Kugeler, A. Neumann, W. Anders, and J. Knobloch, “Adapting TESLA technology for future cw light sources using HoBiCaT.,” *Review of Scientific Instruments*, vol. 81, no. 7, p. 074701, Jul. 2010.

[15] R. Geithner et al., “Dark Current Measurements on a Superconducting Cavity using a Cryogenic Current Comparator,” *Review of Scientific Instruments*, 2010.

[16] J. Fydrych, M. Chorowski, J.Polinski, J. Skrzypacz, "Design Methodology of Long Complex Helium Cryogenic Transfer Lines", in Transactions of the Cryogenic Engineering Conference-CEC: Advances in Cryogenic Engineering. AIP Conference Proceedings, Volume 1218, pp. 1103-1110 (2010).

2.6. Warm Systems

The tasks of the working area “Warm Systems“ are:

- The transfer of the scientific requirements to feasible technical concepts
- specification, purchase and commissioning of all normal conducting components of the accelerator including their infrastructural requirements

Being an experiment in accelerator physics, the performance requirements of B*ERL*inPro can change during the course of the project. Therefore, flexibility in the layout of the building, the infrastructure and all components is of high priority. It will facilitate to respond to scientific findings and to implement upgrades. Considering the tight budget, this is a special challenge in this work area.

Due to the high beam power, the handling of the radiation doses and the development of an adequate machine protection system (MPS) is another task of ‘Warm Systems’. It demands the close cooperation of all working groups. A first approach to all the questions that have to be discussed in this respect can be found in Appendix 3.2.

Special requests arising from commissioning needs might still impose changes to the layout of the warm components, especially for the diagnostics. The integration of superconducting technology in the machine might impose special procedures like particle free implementations.

2.6.1. Vacuum/Magnets

2.6.1.1. Magnets

An overview of the accelerator layout with the foreseen magnets is presented in Figure 48. The two return arcs consist of four dipoles, seven quadrupoles and four sextupoles each. Four matching quadrupoles are located in front and behind each arc. For the injection and extraction of the low energy beam two chicanes with three dipoles each are integrated in the linac straight. The last dipole of the injector chicane is shared with the merger, the first one of the extraction chicane is shared with the beam splitter, guiding into the dump line. 16 low energy quadrupoles focus the injected and extracted beam. Steering coils for the trajectory correction will be integrated into the main magnets wherever possible. In the present layout no space for separated steering coils is foreseen. A detailed design and layout of all magnets should start approximately two years before the machine is set up in the accelerator hall. The main parameters of the magnets can be found in 2.3.1.2-4.

Quadrupoles

Four of the 16 low energy quadrupoles are placed in front of the dogleg merger, two between the merger dipoles, four in front and four behind the linac and two in the extraction path. Their length is 150 mm. The full beam aperture is 40 mm for the injected, but 70 mm for the extracted beam. If possible, the quadrupole aperture should be set to

80 mm to serve both purposes. In order to ensure good reproducibility and symmetry the iron cores can be built by stacking isolated laminated iron layers of 1 mm thickness. The pole profile has to be optimized, to minimize the unwanted higher harmonic field in the central part of the magnet.

Seven of the high energy quadrupoles are placed in the arcs. The beam pipe in the arc is of elliptical shape, 40 x 70 mm. Four quadrupoles precede and follow each arc, here the beam pipe is round with a diameter of 40 mm. Also for the high energy quadrupoles an aperture of 80 mm could be used at all locations. The length of the high energy quadrupoles is 200 mm.

	Units	Low energy	High energy
Energy	MeV	< 10	50
Aperture	mm	80	80
Yoke length	mm	150	200
Number		16	30

Table 31: Quadrupole magnets for B*ERL*inPro

Dipole magnets

The two 180° arcs of B*ERL*inPro are composed of four dipoles which bend the beam by 45° each. The bending radius of 0.765 m corresponds to a magnetic length of 585 mm. The gap is set to 50 mm to host the 40 x 70 mm vacuum chamber in the C-shaped magnets. The good field region still has to be defined. 60 mm is the working assumption. One option to build equivalent dipoles is to cut and machine the yokes from 1 piece of iron to avoid differences in the material composition. The tolerances on the pole parallelism and flatness will be tightened to 10 µm, unless relaxed/tightened by tracking simulations. Each dipole winding will integrate a corrector coil, powered separately.

The design of the three dipoles in the merger is challenging, because the low energy beam of around 6 MeV is vulnerable. Due to the tight geometry, the coils have to be placed on the return yoke making it harder to achieve the required field flatness.

These limitations do not apply to the remaining dipoles. Their design has to meet the needs of the ‘spent’ beam.

The length of all merger, splitter and high energy chicane dipoles is 250 mm. The deflection angle is 18°. The chicane dipoles are run at the same field as the merger/splitter dipoles, except for the central chicane dipoles, where the field is doubled. The beam pipe is 40 mm for the injection, and 70mm for the extraction chicane. It has to be evaluated, if the field requirements are compatible with the larger aperture needed for the extraction dipoles for a common design.

Before the magnets can be designed in detail, the following information has to be gathered for all envisaged operational modes

- field strength
- field quality
- harmonic content
- good field area
- field stability
- gap height
- layout of magnet families

All corrector magnets will be integrated in dipoles, quadrupoles or sextupoles (2.3.1.8.).

Special care has to be taken in the design of the magnets in the dump line with respect to the varying energy spread and different loss scenarios.

The foreseen apertures of B*ERL*inPro are shown in Figure 48:

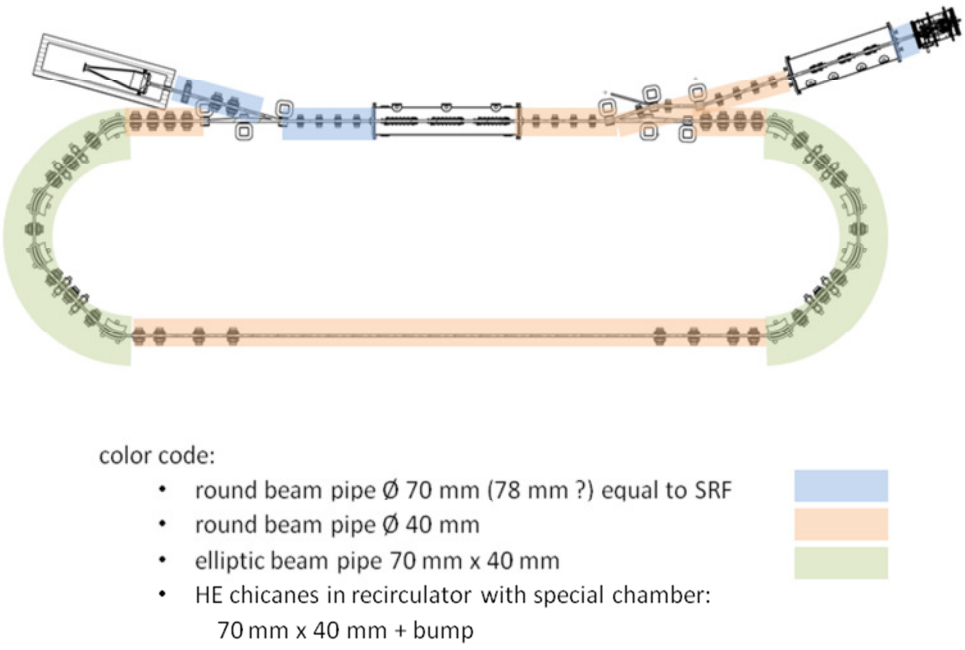

Figure 48: Different apertures of B*ERL*inPro

2.6.1.2. Vacuum system

It is assumed that for the successful operation of B*ERL*inPro average pressure values in the 10^{-9} mbar range are sufficient, but this has not yet been verified. Therefore, bake out to remove water partial pressure is assumed to be beneficial.

The vacuum scheme is shown in Figure 49. The machine is divided into ten vacuum sectors. For the separation of the vacuum sections, RF-shielded all-metal gate valves are

foreseen. For a 70 mm beam pipe the gate valves considered at present would have a flange size of 100 mm. These are very large and heavy valves, which requires large installation space and high investment costs. Each vacuum sector will be equipped with two cold cathode gauges for monitoring the vacuum pressure, which are connected to the vacuum interlock system.

32 ion sputter pumps will be installed at pumping ports. These pumping ports also allow the installation of vacuum gauges and all-metal cross-angle valves which are used for roughing and venting. To save costs, 16 sputter ion pumps will be connected to one controller. The necessity of additional NEG or TSP pumps in front of the cryo modules is under examination.

Dry turbo molecular pumps will be used for roughing and during bake-out. These pumps are installed in mobile pump carts, which in addition are equipped with dry and oil-free diaphragm pumps, a vacuum control and a venting system. The pump carts can be connected via flexible hoses to the cross angle valves which are installed in each vacuum sector.

For machine protection, fast closing shutter systems are foreseen. Shutters will be installed in front and behind of each cryo module as well as in front of the main beam dump. Aluminum (ACP5080) and Stainless Steel (316L) will be the vacuum chamber materials. The flanges are standard Stainless Steel (316LN). Conflate flanges and the flanges of the Aluminum chambers will be realized with Atlas Conflate Bi-Metal-Flanges. At the moment it is planned to only build Aluminum dipole chambers.

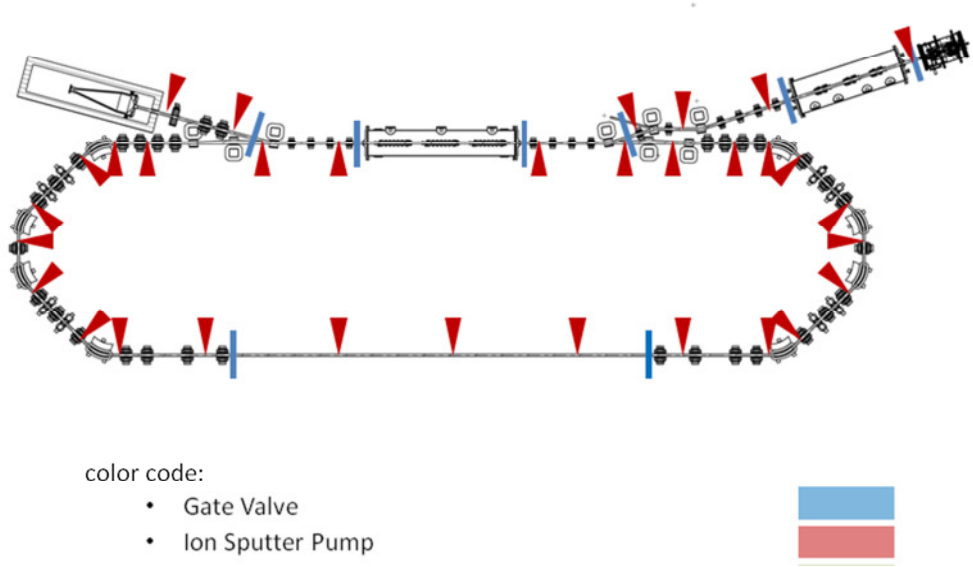

Figure 49: Valves and Pumps

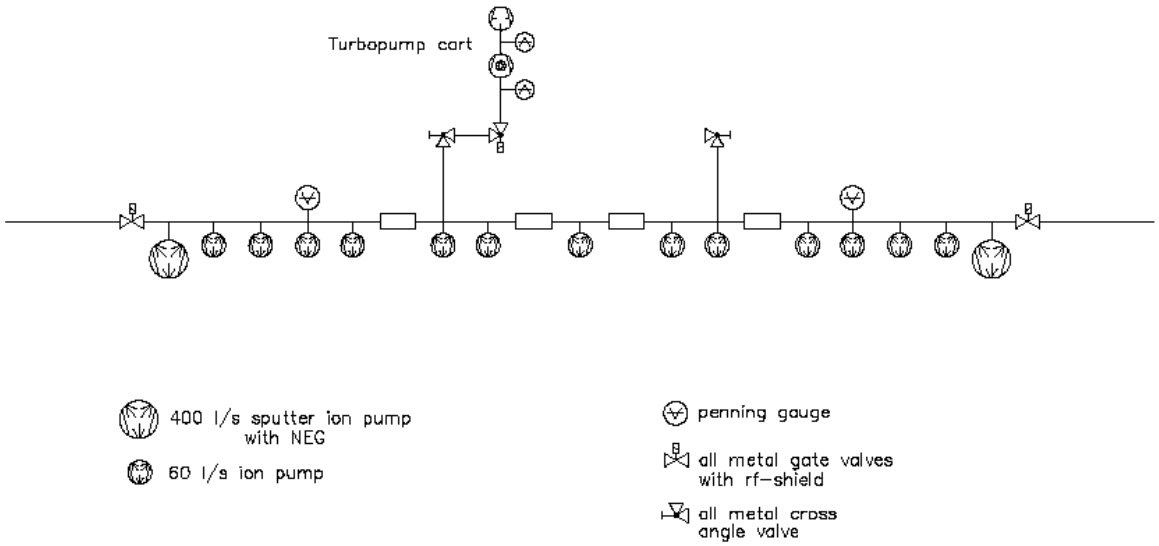

Figure 50: Arrangements of pumps, penning gauges and gate valves in one 180°arc.

				Energy required to heat up 1g to Δ T/K		
				100	500	melting
	Specific heat in 1/kg*J/K	Density in kg/m³	Melting Temp in °C	Energy /J	Energy /J	Energy /J
Copper	385	8930	1084	39	193	410
Graphite	711	2100	3823	71	356	2.704
Aluminum	910	2700	660	91	455	582
Stainless steel	500	7900	1510	50	250	745

Table 32: Thermal characteristics of some materials for beam dump and vacuum chambers

The design of the vacuum system is based on assumptions that yet have to be confirmed:

- transverse dimensions of the vacuum tube, as shown in Figure 48:
  The aperture strongly influences the layout of the magnets, the power supplies and their costs.

- material of the vacuum chamber:
  Stainless steel has been chosen due to cost aspects, but aluminium has advantages with respect to the specific heat and in case of activation.
- pressure level:
  10^{-9} mbar in the warm pathway is assumed so far, the pressure influences the ion accumulation, number and location of clearing electrodes and halo formation.

The following aspects have not yet been considered in detail:

- Impedance aspects have a mayor effect on the layout of the vacuum system especially with respect to machine protection.
- The expected CSR levels of several kW have to be considered, at least in the layout of the dipole chambers where CSR is a dominant effect.
- How does the integration of SRF technology influence known procedures? (Particle free installation for the complete machine?)
- Requirements for local beam dumps diagnostics have to be defined (amount / power rating)
- The diagnostic components depending on the requirements of the commissioning and operation concept.

2.6.1.3. Survey and alignment of machine- and components

To align the components of the machine and potentially the beam lines a geodetic network is required.

The coordinates of the components with reference to the electron path/photon path have to be transformed into the geodetic network coordinate system.

Therefore, the fiducials of the components have to be measured relative to the designed electron path.

Network

The fundamental geodetic network consists of magnetic nests for laser tracker targets with a typical diameter of 1.5".

They are placed on concrete walls, floors and ceilings of the accelerator hall and the equipment hall.

The network is measured using a laser tracker and a digital level.

To obtain final coordinates for the network points, all measurements are processed using least-square adjustment software.

Fiducial alignment

To adjust the components of the machine and the beam lines with respect to the geodetic network, all mechanical parts will be equipped with bore holes with a specific diameter, in which an adapter for the laser tracker targets is placed.

Equipment and accuracy

The available survey equipment consists of a Leica AT901-B laser tracker and a Leica DNA03 digital level. Under stable environmental conditions and a maximum distance of 40 m, the uncertainty of a coordinate measured with the laser tracker is ±15 µm + 6 µm/m. Within a volume of 2.5x5x10 m³ an accuracy of ±10 µm + 5 µm/m is achievable. These specifications are stated in units of maximum permissible error (MPE). Typical results are half of the MPE.

The digital level is specified with a standard deviation of 0.3 mm per km double leveling using an invar staff.

2.6.2. High power beam dump

The electron beam from an Energy Recovery Linac has to be dumped at its injection energy. With the specified beam current of 100 mA and the injection energy of 6 MeV, the dump needs to able to absorb 600 kW of beam power. The maximum beam energy, at reduced current, is 13 MeV.

In our first design, the dump consists of a cone-shaped copper block. Lots of water connectors and a stainless steel flange have to be brazed to the oxygen free copper body. To reduce the power density, the electron beam will be expanded by a combination of solenoid magnets to an opening angle of 150mrad. This guarantees that the power density in the OFHC copper will stay below 100 W/m^3 (see Figure 51) and the corresponding temperature below 200 °C (see Figure 52).

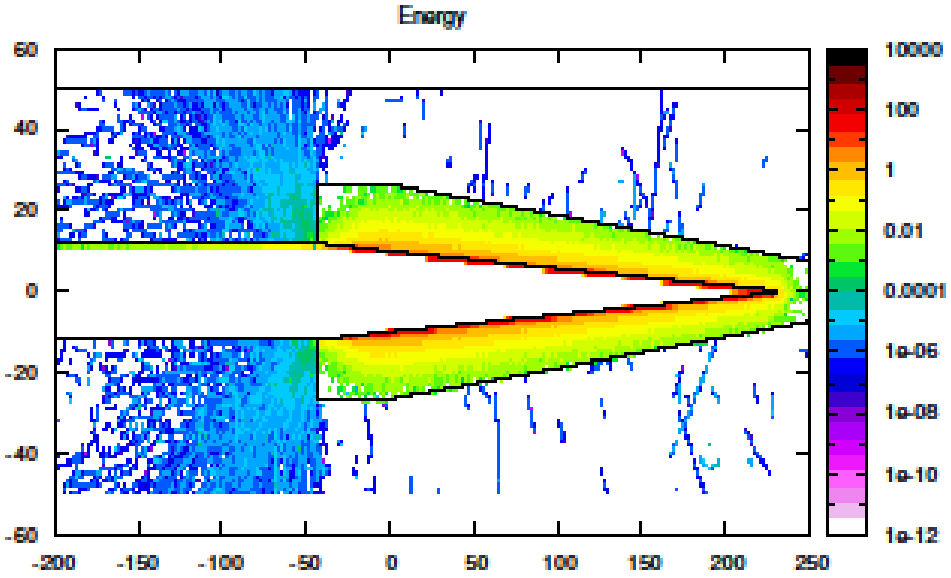

Figure 51: Power density distribution [W/m^3] in the beam dump (beam power 600 kW)..

The length of the cone-shaped copper tube has to be 3 m and the inner diameter at the entrance side is 400mm. The temperature of the cooling water will be 30°C and the heat transfer coefficient is calculated to be 5 W/m² K.

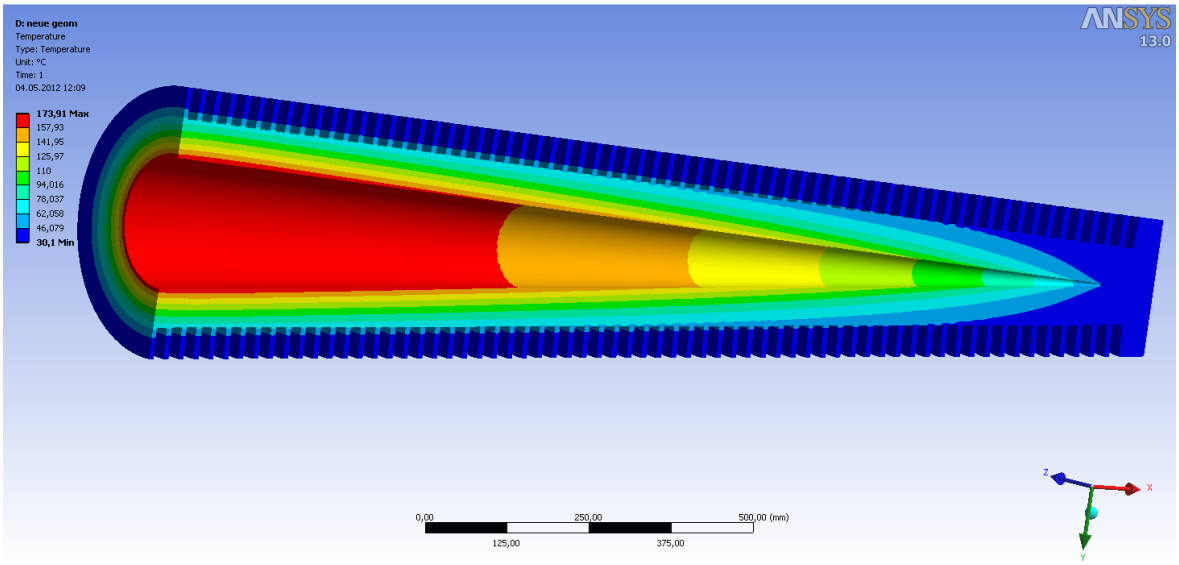

Figure 52: Temperature distribution in the beam dump (beam power 600 kW).

With this large entrance diameter of the dump cone, it will be possible to sweep the beam across the dump surface, increasing the safety margin for high power operation.

2.6.3. Power supplies

An ERL is a single pass device, a transfer line rather than a ring. Therefore, each part of the machine has its individual task, symmetry considerations do not apply and most of the magnets have to be equipped with independent power supplies. Furthermore, different operational modes will cause different magnet settings. Different potential machine settings are subject of further studies. Although matching quadrupoles are located in front of each arc simulation show the necessity to run the arcs asymmetrically under certain conditions. It is planned to make use of the spare BESSY II corrector power supplies where ever possible.

A family design is applicable only for the dipoles. All arc dipoles need to provide 45° deflection of the beam at all energies, special dump scenarios might need the possibility to switch of single dipoles, though the same applies for the 18° deflection of the three merger dipoles. The central dipole of the injection and extraction chicanes has to provide twice the field strength of the two outer dipoles in case of symmetric positioning and equal design.

The number of magnets and power supplies cover the major amount of independent subsystems possibly being involved in an undesired beam loss. So machine protection considerations set stringent demands on their reliability.

The necessary information for the specification of the power supplies include:

- number of magnets
- current rating / voltage rating including safety margins
- magnet families design
- dynamic requirements
- unipolar or bipolar operation
- required stability (in relation to nominal current I_{max}) in terms of
    - ripple (DC to 10 kHz)
    - long term stability (8 h)
    - reproducibility

Based on the magnet field and gradient requirements the layout of the magnets and the magnet families will be designed such that standard power supplies can be used. This will help to decrease the costs.

Table 33 lists the parameters of available standard power supplies.

Power rating of magnets and families	**≤10 kW**	**≤1 kW**	**≤100 W**
Nominal Current (I_{max}):	100 A (unipolar)	± 8 A (bipolar)	± 3 A (bipolar)
Nominal Voltage (V_{max}):	< 90 V (unipolar)	< ± 40 V (bipolar)	< ± 40 V (bipolar)
Ripple related to I_{max}	≤ ± 10^{-5}	≤ ± 10^{-3}	≤ ± 10^{-3}
Stability (8 h) related to I_{max}	≤± 10^{-5}	≤± 10^{-4}	≤± 10^{-4}

Table 33: Standard power supplies

2.6.4. Beam diagnostics and instrumentation

The task of beam diagnostics and instrumentation is to support and aid as much as possible to reach the project goals, i.e. to demonstrate that an ERL is a candidate for a future light source in terms of stability and reliability. It has to assure that the primary target parameters, like current, emittance and beam stability, can be measured

accurately. Other and less important beam parameters like the bunch length will be determined with simpler and less accurate techniques. At this stage of the project the planned distribution of diagnostic components around the facility is shown in Figure 53.

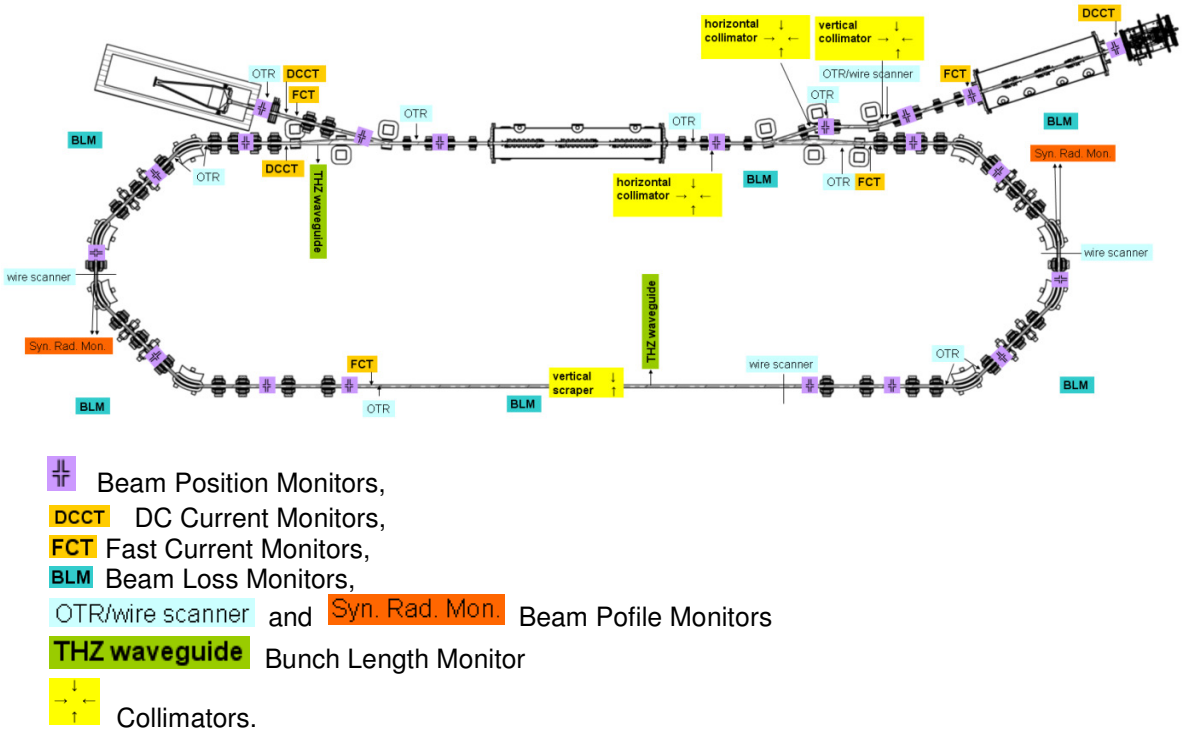

Figure 53: Distribution of diagnostic components in B*ERL*inPro

Beam position monitors

There are twenty beam position monitors (BPM) evenly spread along the injector, around the recirculator and towards the beam dump. The monitors consist of either simple circular pick-up electrodes or strip line ensembles similar to the ones in use at BESSY II and developed for the earlier BESSY-FEL project. The signals will be analyzed by digital electronics. A very flexible solution would be the use of fast digital oscilloscopes. In this case the analysis software is running together with a soft-IOC for the communication with the EPICS control system on these scopes. Such a BPM system has been developed for the Top-Up-project at BESSY II. The analog input band width is most demanding for the two monitors adjacent to the main linac structure where one ideally would like to determine the position of the two co-propagating beams with time displaced bunches. In this case a bandwidth of 2.6 GHz is required.

Beam size monitors

The preservation of the small emittance of the beam is one of the project's challenges. Therefore, up to fourteen beam size monitors will be installed. Primarily well established

but destructive techniques will be employed: Detection of optical transition radiation (or fluorescence) which is emitted by the electron beam traversing a thin metallic target (or hitting a fluorescent screen or crystal). The radiation is imaged and viewed by a CCD-camera.

Four wire scanners in combination with the beam loss monitors capable of detecting the small number of scattered halo electrons will allow for the analysis of beam tails and their formation. The wire scanners in the bends are supplemented by non-destructive synchrotron radiation monitors. The imaged beam has to be viewed by intensified CCD-cameras because of the low energy of the emitting electrons. With suitable optics and apertures blocking the beam core a direct and on-line measurement of the beam halo seems to be feasible.

The location of the beam size monitors has been chosen adequate to determine transverse emittances from quadrupole scans. The energy spread can be measured with monitors located in dispersive regions and where contributions from the transverse planes are small. The longitudinally sliced transverse emittance can be determined from a quadrupole scan with zero-phasing the accelerating voltage and observing the beam size of the energy chirped beam in a dispersive region. The final positions of some of the monitors is likely to change and will not only depend on the actual electron beam optics but also on the position of a transverse deflecting cavity which might be installed.

Current monitors

It is planned to install three DC-current transformers (DCCT) because of their accuracy and stability. With carefully selected transformers a high resolution paired with low noise and small thermal drifts can be achieved. The monitors will have a resolution of at least 1 μA with a 1 s integration time. At a beam current of 100 mA this would allow to determine and eventually optimize the efficiency at the 10^{-5} level. In addition there will be four fast current transformers (FCT) which are less sensitive, however, will measure the charge of a single 77 pC bunch with a resolution at the percent level.

Beam loss monitors

Particle losses have to be minimized further. This can be done with the help of six very sensitive beam loss monitors (BLM) strategically distributed around the facility. We plan to use photomultiplier tubes (PMT) connected to plastic scintillators. The monitors can detect single lost electrons and are ideal for the delicate final adjustment of the efficiency. Detection of many particles lost simultaneously demands more sophisticated electronics and data analysis. The spatial resolution of the monitor for localizing losses is sufficient in comparison with the small size of the facility. After some kind of calibration these monitors can be used to trigger a (laser) beam abort system in order to protect components against excessive electron beam bombardment.

Collimators

In the design three horizontal and vertical collimators are foreseen in order to scrape-off some of the halo electrons. Their location was chosen according to the value of the beta function. The vertical mechanical scraper in the long straight section opposite to the linac

structure is intended to simulate a small gap undulator. The location and number of the collimators will be determined finally based on more refined calculations and estimates for the dark current and the distribution of halo particles.

Bunch length monitor

In the initial phase of the project the bunch length is not a very critical parameter. Two relative bunch length monitors based on the detection of μ-wave power are planned to be installed after the main linac and after the first 180° bend where the bunches can be further compressed. With a suitable set of μ-wave diodes the spectral range of up to a few hundreds of GHz can be covered. Thus the length of bunches in the ps to sub-ps region can be observed.

A streak camera viewing the emitted synchrotron radiation would allow for an absolute bunch length measurement with a resolution of 1 to 2 ps. The front ends for the synchrotron radiation monitors should be designed such that the streak camera can easily be installed later.

2.6.5. Application programs

Generic applications

The existing generic applications within the EPICS [http://www.aps.anl.gov/epics] toolkit and the Control System Studio (CSS) suite [http://cs-studio.sourceforge.net] are well suited to cover all requirements during device test, device installation, and facility commissioning.

A choice of display managers (CSS/BOY, edm) will provide engineering screens for device control, synoptic views for navigation, status, alarm and trending for supervisory tasks.

Alarms (warnings and faults of devices or device groups) can be managed using the alarm application CSS/BEAST. Tree structured navigation guides operators to the problem and provides appropriate device control displays.

For ‘slow’ trends and correlations (< 1Hz) an archive and retrieval environment is available, capable of collecting data from several thousand channels, covering years of data with second resolution. A universal strip tool application (CSS/DataBrowser) is able to plot live and archived data in the same plot.

Application and infrastructure logs are collected in databases (syslog-ng, Splunk). They provide valuable clues for analysis of failures and system performance.

The powerful MMLT (Matlab Middle Layer Toolkit) embeds modeling, procedural and evaluation capabilities. During commissioning these tools provide a framework for ad-hoc measurement tasks as well as for rapid prototyping and test of control mechanisms.

Model based Set-up and Analysis

For physics applications requiring online modelling (e.g. dispersion free steering), MMLT and its modelling engine AT (Accelerator Toolkit) are the first and possibly sufficient choice. At a later stage embedding a specific modelling approach might be preferable.

Performance Optimization and Tuning tools

For B*ERL*inPro performance tuning, smooth operation and minimal beam loss, feedback loops of very different qualities will be required. These will range from local beam optimization to complex schemes that allow to feedback signal quality and coincidence levels to the various sources of drift and jitter.

For the crucial low level feed forward and feedback systems needed for the linac cavities, existing control hardware from Cornell University has been installed, studied and tuned at the HoBiCat test facility. It still has to be determined if this solution fits all requirements. For operations, the LLRF control system must be properly integrated into the global EPICS environment to allow for status supervision, parameter adjustment, and external control.

2.6.6. Control system

EPICS framework

Experience and in-house expertise gained through construction, commissioning, and operation of BESSY-II and the MLS clearly advise the use of the EPICS toolkit for B*ERL*inPro controls.

In the past, EPICS has been constantly improved with respect to cleaner software interfaces, platform independence, and functionality. In the future, the developments for EPICS V4 will extend its robustness and performance to high level physics applications and data acquisition.

Architecture: Vertical structure

File-, data base-, and application servers based on Linux will be deployed for control room services and consoles. Virtualization technology will provide high flexibility, robustness, and scalability. Switched GigaBit Ethernet will comprise the backbone of the B*ERL*inPro controls network. PPC based single board front-end computers (IOCs) in VME crates will house VME I/O boards and connect to field bus segments, “soft” (Linux-based) IOCs will be directly communicating to Ethernet attached devices, embedded controllers inside devices will combine ease of installation with signal conditioning capabilities.

Commercial solutions, unique components or devices with high diagnostic requirements will be integrated using adequate interfaces from the EPICS toolkit (OPCgateway, VXI-11, LabCA). Examples for such “smart” subsystems are the local Windows-PC based controls of the photo cathode laser systems, PLC controllers in the RF transmitter, or diagnostic set-ups based on National Instruments devices with LabView-only interface.

For controls transparency the EPICS Channel Access protocol has to be common to all subsystems. Additional network services might be provided as needed. Troubleshooting and maintenance in general will be supported by mobile consoles and wireless LAN, providing integration of all kinds of mobile devices.

Common naming convention

For the major BESSY facilities, a collision-free naming convention scheme has been defined (see *http://www.helmholtz-berlin.de/media/media/grossgeraete/betrieb_b/docs/naming_convention_for_bessy_mls_berlinpro_..._components.html* for details).
B*ERL*inPro will share this convention, to allow operation by a common crew from a central control room, and to ensure portability of applications between the facilities.

Every reference to a component of the control system should be made by a symbolic name. `Component' in this sense can refer to a piece of equipment (device), a predefined group of such components or a processor connected to the networks (symbolic or virtual device).

Device names have to be unique and short. Nevertheless they have to convey information about the location (facility, domain and subdomain), the functionality (family representing device class or type), and also the specifics (member) and multiplicity (counter).

All B*ERL*inPro devices belong to the “facility” F (‘Future Projects’). The major functional units constitute the “domains”: **I**, the injector including the gun, booster and merger, **R** the recirculator, **D** for the splitter and beam dump, potentially L for beam lines and E for experimental stations (Figure 54). Ancillary systems are C-control room, G-gallery and V-Virtual) as well as H - the preparatory and test facility HoBiCat. For reasons of unambiguousness every B*ERL*inPro component has to belong to a subdomain like L, the linac section.

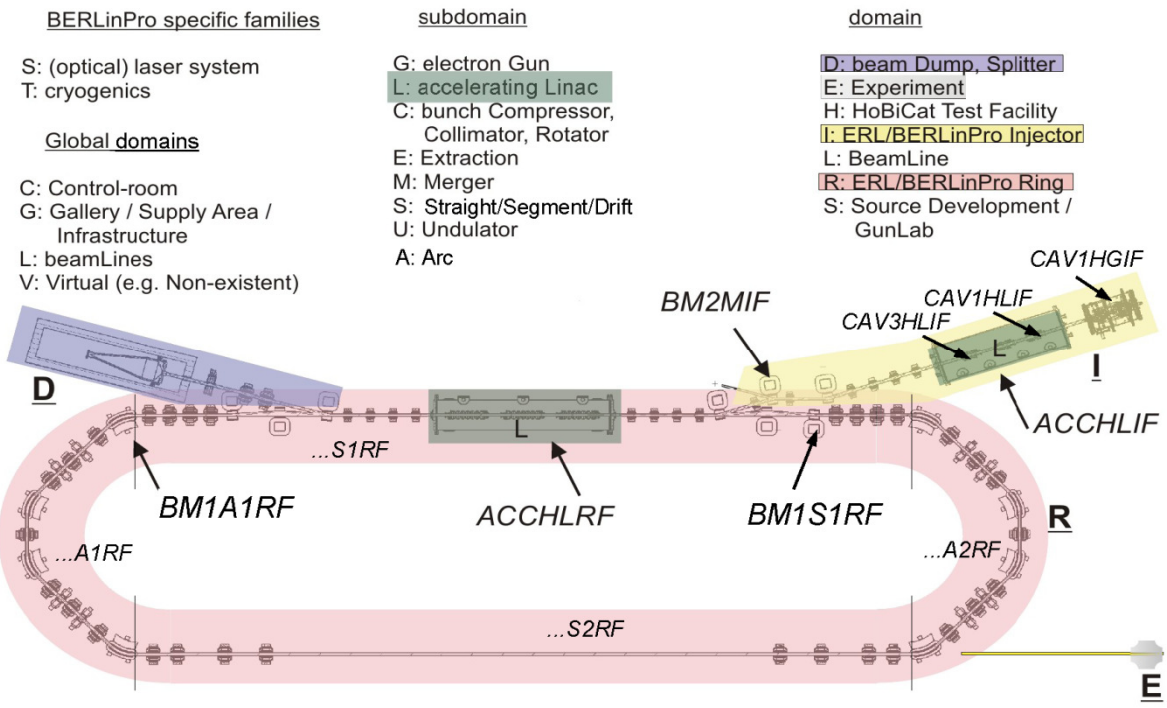

Figure 54: Unified Naming Convention for B*ERL*inPro, BESSY and MLS
Names have to be formally composed of mandatory and optional elements. These elements are named and concatenated in the following way: member family [counter] subdomain domain facility

Data model: Devices

The common data model within the accelerator controls community consists of ‘devices’, grouped into ‘classes’ with certain ‘behavior’, ‘attributes’ and ‘events’. Identification of a specific device is usually done by geographical hierarchy. This core data model is contained in the naming convention. Device names serve as a bootstrap pointing into a relational database holding all required configuration data.

I/O requirements: Device classes

Hardware implementations of beam accelerating and guiding elements share many properties. Within the EPICS collaboration, a large repository of various hardware drivers exists. Most devices needed for B*ERL*inPro are very similar to those already installed at BESSY II, MLS, or other facilities.

Sub-Systems

Specific requirements like speed or precision, existing in-house expertise, vendor constraints, savings in implementation effort, minimizing the pool of spare parts, etc.: there are many reasons for solving certain controls aspects with more localized sub-units and integrate these sub-systems as a whole into the global control system. For B*ERL*inPro, expected controls sub-systems include ‘photo cathode lasers’, ‘LLRF’, and ‘cryo system’.

Machine protection

In view of the very high electron beam intensities machine protection systems (MPS) play an important role for B*ERL*inPro, because improper operation of the accelerator could lead to serious damages of the machine (Appendix 3.2.).

According to the operation mode of B*ERLi*nPro the MPS must analyze adequate input signals from diagnostic systems (e.g. beam position monitors or beam loss monitors) and be able to inhibit the operation of certain sub-systems to ensure safe operation. Wherever possible, the design of the safety systems should be in accordance with commonly accepted international standards like EN-ISO-13489 or EN-IEC-62061 to ensure the needed functional safety.

Diagnostics

Profile and screen monitors have high requirements on data burst transmission or local pre-processing capabilities. Meaningful shot-by-shot analysis and correlation depend on novel techniques for data storage and retrieval of huge data sets. The expected high data throughput may require performance optimized databases (e.g. SciDB, Hypertable).

Within the EPICS context, AreaDetector, the most common package for image acquisition and analysis, supports a wide variety of Firewire and GigE cameras from all major vendors.

Slow timing

A general timing framework, providing a powerful infrastructure for timing fiducial generation and distribution is required

Within the EPICS users, the modular system provided by Micro Research Finland Oy, is the well supported de-facto standard, providing typical jitter down to < 5 ps rms.

3. Appendix

3.1. Appendix to 2.3 Optics / Theory / Modelling

Effects leading to emittance growth in the injector

Transverse space charge: Space charge effects influence the particle motion in beams with relatively low energy and high peak current. We can neglect space charge only if [1]:

$$\frac{\varepsilon_y^2}{y^3} >> \frac{I}{I_0(\beta\gamma)^3}\frac{1}{x+y} << \frac{\varepsilon_x^2}{x^3}, \quad and$$
$$\frac{5}{16}\frac{I}{\varepsilon_{x,y} I_0(\beta\gamma)^3} L << 1$$

with $\varepsilon_{x,y}$ - transverse emittance, x, y – rms beam sizes, I – peak current, $I_0 \approx 17$ kA – the Alfven current, $\beta = \frac{v}{c}$, L – typical path length. In the opposite case space charge effects will lead to emittance growth.

Assuming a recirculator path length of 20 m, where the pulses are compressed to 2 ps in the standard mode, and a peak current of 15 A we can neglect space charge effects for $\gamma \gg 75$, i.e. behind the linac.

To counteract the emittance growth due to transverse space charge an emittance compensation scheme can be applied.

Longitudinal inhomogeneity of space charge density: If the bunch is long in its reference frame, it can be divided into slices, the interaction between the slices can be neglected and the motion of the slices is regarded independent of each other. The equations of the motion of one slice in a space charge dominated beam are (Kapchinsky-Vladimirsky equations):

$$x'' + \frac{(\beta\gamma)'}{\beta\gamma}x' = \frac{j}{x+y} - gx$$
$$y'' + \frac{(\beta\gamma)'}{\beta\gamma}y' = \frac{j}{x+y} - hy$$

where x, y are the rms sizes of the slice, $j = \frac{I}{I_0(\beta\gamma)^3}$ is the normalized current, $g = \frac{eG_x}{p}$ and $h = \frac{eG_y}{p}$, with *G* is the focusing field gradient.

The slices start at the cathode with the same radii but different current density. Therefore, the motion of the slices in phase space is different. In projection on the *x* or *y* plane, this leads to an increase of the phase space area filled by particles. As a result the emittance grows.

The equations for the differences Δx and Δy between the rms slice size and "reference" slice size are given by:

$$\Delta x'' + \frac{(\beta\gamma)'}{\beta\gamma}\Delta x' = -\frac{j(\Delta x + \Delta y)}{(x+y)^2} - g\Delta x$$
$$\Delta y'' + \frac{(\beta\gamma)'}{\beta\gamma}\Delta y' = -\frac{j(\Delta x + \Delta y)}{(x+y)^2} - h\Delta y$$

These are the equations of two coupled oscillators (with damping, if $\beta\gamma$ changes due to acceleration). Therefore, each slice size oscillates around the reference sizes and the frequency of the oscillation (coupled pendulum with two Eigen modes) does not depend on the amplitude if the difference is small [1]. After half a period of the oscillation the slice size coincides again with the reference value. At this point the emittance will be also minimal ("emittance compensation").

In an axisymmetric system a solenoid is used to compensate the emittance at a certain point, usually in the booster. As the beam in the merger of B*ERL*inPro is still space charge dominated it is necessary to aim at an emittance compensation point behind the main linac. For a system like a merger, without axial symmetry the emittance compensation technique [2] should be used to make both x- and y-emittances minimal at the center of the linac. Quadrupoles are used to adjust the beam sizes for this purpose.

Energy change due to longitudinal space charge: ASTRA simulations of the injector calculate the maximal longitudinal electrical field behind the booster for the standard mode as:

$$E_z \approx 5\,keV/m\,.$$

The main impact of longitudinal electrical space charge fields on the beam dynamics is a variation of the particle energy, δ_{sc}:

$$\delta_{sc} = \frac{\int E_z dz}{E_0} \approx \frac{E_z \cdot L}{E_0}\,,$$

where L is the length of the dispersive section and E_0 the particle energy.

Mismatch of slice centers due to energy changes in a dispersive section: Due to the energy dependence of the particles' x-coordinate behind a dogleg merger any energy variation leads to emittance growth. The particle offset δx and angle $\delta x'$ at the end of the merger can be estimated by:

$$\delta x = \int \frac{\partial \delta_{sc}}{\partial s} \cdot D ds \approx \delta_{sc}\overline{D}$$
$$\delta x' = \int \frac{\partial \delta_{sc}}{\partial s} \cdot D' ds \approx \delta_{sc}\overline{D'}\,,$$

Where D and $D'$are the dispersion function and its derivative,. $\overline{D}$ and $\overline{D'}$ are the averaged value over the dispersive section. The linear offset of slice centers at the end of the merger can be partially compensated by adjusting the dispersion at the end of the merger

(in this case the merger is not exactly achromatic). If the correlated energy spread in the bunch is high, only small corrections of the D and D‘ are needed to bring the slices on-axis again. But the change of particle energy due to longitudinal space charge fields is mainly non-linear. The estimation of this effect is given by:

$$\Delta\varepsilon^2 = \delta x^2 \left\langle x'^2 \right\rangle + \delta x'^2 \left\langle x^2 \right\rangle - \delta x \delta x' \left\langle x' x \right\rangle$$

Neglecting possible correlation between particle coordinates and angles, we can simplify

$$\frac{\Delta\varepsilon}{\varepsilon} \approx \sqrt{\frac{\delta x^2}{x_{rms}^2} + \frac{\delta x'^2}{x'^2_{rms}}} \approx \sqrt{\left(\frac{\delta_{sc} \cdot D}{x_{rms}}\right)^2 + \left(\frac{\delta_{sc} \cdot D'}{x'_{rms}}\right)^2} \approx \frac{E_z L}{E_0} \sqrt{\left(\frac{D}{x_{rms}}\right)^2 + \left(\frac{D'}{x'_{rms}}\right)^2}$$

where x_{rms} is the bunch size, and x'_{rms} the angle. This effect is minimized for a small dispersion function, a short merger and high particle energy.

Aberration in the solenoid: The beam naturally has a large angular spread behind the gun (about 8 mrad). A strong solenoid is necessary to focus the beam. The aberrations in the solenoid can be estimated using the equation of motion in a solenoid to 3rd order terms:

$$r'' = -Kr + (K\frac{B''}{2B} - K^2)r^3 + Kr^2 r' \frac{B'}{B} - Krr'^2,$$
$$K = \frac{e^2 B^2}{4p^2 c^2}.$$

Here r is the particle radius and B is the solenoid field. In approximation of a thin solenoid the kick angle experienced by the particle is given by integration:

$$\Delta r' = -r \cdot \int K ds + r^3 \cdot \int (K\frac{B''}{2B} - K^2) ds + r^2 r' \cdot \int K \frac{B'}{B} ds - rr'^2 \cdot \int K ds,$$

The first term on the right hand side describes the linear focusing. The strongest of non-linear terms is r^3 and the corresponding emittance growth is:

$$\Delta\varepsilon \approx r_{rms}^4 \int \left(\frac{e^2 B B''}{8p^2 c^2} - \left(\frac{eB}{2pc}\right)^4 \right) ds$$

.

By increasing the solenoid’s length we can decrease the aberration. The (normalized) emittance growth for the currently used solenoid field profile with a magnetic length of 0.21 m and beam size of r_{rms}=2.5 mm is 0.15 mm·mrad. Such a slice emittance growth seems to be acceptable. The field profile is technically feasible.

Over-compression due to RF non-linearity: This effect might lead to a significant growth of the current in over-compressed slices. As a result their motion becomes totally different from the rest of the beam, which might result in halo or particle loss.

$E(ct)$ is energy distribution in a bunch after the booster. For our estimation we assume that:

$$E(ct) \approx \tilde{E}\cos(ct\frac{2\pi}{\lambda}+\varphi_0)\,.$$

where φ_0 is the phase of the bunch center, $\tilde{E}$ is an effective sum of gun and booster energy gain.

Considering the longitudinal motion of two particles in the bunch, we can estimate local and global compression factors n_l and n_g. Goal of the following calculation is to find values for R56 and φ_0, which delivers the requested bunch length but does not lead to global or locale over compression. Since the larger chirps occur in the local compression frame it gives the upper limit for R56. The compression factors are defined by:

$$n_g = \frac{1}{1-R_{56}\frac{2\pi}{\lambda}\frac{\sin(\Delta\varphi)}{\Delta\varphi}tg(\varphi_0)}$$

$$n_l = \frac{1}{1-R_{56}\frac{2\pi}{\lambda}\frac{\sin(\varphi_0+\Delta\overline{\varphi})}{\cos(\varphi_0)}}\,,$$

Here $\Delta\varphi$ is the half of the bunch length, $\Delta\overline{\varphi}$ is the distance from the bunch center to the two particles, R_{56} is the longitudinal dispersion. For small angles $\Delta\varphi$ and φ_0 we get an estimation

$$n_g = \frac{\lambda}{2\pi R_{56}\Delta\varphi}$$

If $n_l=\infty$ over-compression occurs (ideally, no particles with larger phases should be in the beam).

$$\Delta\overline{\varphi}_{ovb} = \arcsin\left(\frac{\cos(\varphi_0)}{R_{56}}\frac{\lambda}{2\pi}\right)-\varphi_0$$

The maximal possible value of R_{56} at which over-compression does not happen is.

$$R_{56} = \frac{\cos(\varphi_0)}{\sin(\varphi_0+\Delta\overline{\varphi})}\frac{\lambda}{2\pi}$$

The full energy spread in the bunch is δ:

$$\delta = 2\sin(\Delta\varphi)\cdot tg\,\varphi_0\,,$$

where $\Delta\varphi$ is half of the full bunch length.

In the case of a Gaussian longitudinal bunch profile the value of the “full bunch length” should be chosen appropriately (e.g. we take $t_{full}=6t_{rms}$). Since there is no limit for a Gaussian distribution, particles in the bunch head can be over-compressed and do not take part in the emittance compensation. Since there are only about 0.1% of electrons out

of 3σ, we consider this to be acceptable. Caution should be taken in order to prevent these particles forming halo.

We limit the rms energy spread with 10^{-2}, to control higher order effects:

$$\delta_{rms} = \sin(\Delta\varphi_{rms}) \cdot tg\,\varphi_0 = 10^{-2}$$

For a Gaussian laser pulse of 5 ps rms length, the bunch rms length after the gun is 1.8 mm. Therefore, φ_0=12˚ and R_{56}=10 cm are optimal values.

Conclusion: without longitudinal bunch profiling it is more difficult to compress bunches due to long bunch tales. Higher compression will produce over-compression in the bunch head, which can be one of the sources of beam halo.

References

[1] S.V. Miginsky. Space charge effects, coherence of charge oscillation, and emittance. Technical Physics, 2008, Vol. 53, №9, pp. 1197-1208.

[2] S.V. Miginsky. Emittance compensation of elliptical beam. NIM A 603 (2009), pp 32-34.

3.2. Appendix to 2.6 Warm Systems

Machine Protection System (MPS)

The handling of the high radiation doses and the development of an adequate machine protection system (MPS) is one task of 'Warm Systems'. It demands the close cooperation of all working groups. A first approach to the upcoming questions can be found here.

Beam power at different places of the machine	**E_{Max} /MeV**	**I_{Max} /mA**	**P_{Max} /kW**	**Interlock reaction time /µs**	**Energy deposition in the machine /J**
BESSY II Injection: 10 Hz, 360 ns bunch train, CW, duty cycle: 1/277.778	1700	1	1.700	1,E+06	6
Storage Ring: 800 ns revolution time	1700	300	510.000	8,E-01	408
B*ERL*inPro				1,E+01	2
gun to booster	2	100	200	1,E+03	200
CW				1,E+04	2.000
booster through				1,E+01	7
merger to linac	6,0	100	650	1,E+03	650
CW				1,E+04	6.500
linac through				1,E+01	7
extraction	6,0	100	650	1,E+03	650
to dump				1,E+04	6.500
CW					
recirculator 200 ns revolution time	50	100	5.000	2,E-01	1
recirculator	50	0.6	30	1,E+03	30
CW					

Table 34: Energy deposition in the machine for different interlock reaction times; for comparison, the BESSY II numbers are also listed

The main challenges for the MPS arise from the radiation doses, high enough to activate the equipment and destroy electronic units and organic materials. During regular operation up to 650 kW of beam power are expected along the low energy path between the gun and the beam dump. Due to unwanted beam loss up to 30kW of CW beam power

(limit here is available RF-power) and 5 MW of peak beam power (only 200ns) can be lost in the recirculator along the high energy path.

Therefore it is necessary to identify possible loss scenarios and to estimate the expected hazards. Suitable sensors to detect the different loss scenarios and actuators fast enough to avoid damages have to be integrated into the system.

The development of the MPS involves contributions from all work packages:

Optics / Theory / Modelling

- quantification of expected beam losses, due to dark current, halo, Coulomb or Touschek scattering or BBU limits,
- description of unexpected beam loss scenarios due to malfunction of systems, like magnets or RF-trips
- definition of limits on intended beam parameters for different operation modes, like beam size or offsets

Cold Systems

Analysis of the behaviour of the SRF systems in case of

- beam loss in the recirculator (stored energy in the SRF structures)
- dark current from gun, booster and main linac
- full or partial shutdown due to internal interlocks

It should be studied in how far the

- energy spread of the spent beam is affected by the efficiency of the energy recovery process
- the SRF systems can be used as part of the actuator pool for the MPS and the personal safety interlock PSI

Laser & Synchronization

The laser will be the main actuator for a fast beam inhibit mode within the MPS. Different solutions for an interrupt of the laser have to be developed for different time scales and must be incorporated in different procedures.

Vacuum/Magnets

- implementation of passive protection precautions for vacuum chambers
- evaluation of the impact of heat dissipation on the components
- realization of locations for controlled beam dump
    1. main beam dump for P= 650 kW CW
    2. collimators for halo and machine protection

Power Supplies

- review of the standard interlock circuits with respect to the challenging new demands
- review of the reliability of the power supplies with respect to the expected damage

Diagnostics

- sensor systems for emergency stop of the gun
- diagnostic tools to detect unexpected formations prior to beam loss
- control of actuators in the fast timing region (sub-ms)

Control System and Electrical Installation

- development and installation of interlock systems for signal analysis of the sensor systems and control of actuators in the slow timing region (above ms)
- archiving and visualization of the errors and sensors

Application Programs

- state machines have to be developed to restrict high power operation to secure conditions
- online beam data analysis to inhibit dangerous regions of beam operation